Spring 5-16-2020

Space and Depth-Resolved Naturally Occurring Toxic Groundwater Species in Bangladesh and Rwanda: Origination and Risk Analysis

Kenneth Hamilton
khamilton@smu.edu

Space and Depth-Resolved Naturally Occurring Toxic Groundwater Species in Bangladesh and Rwanda: Origination and Risk Analysis

Approved by:

_____

Prof. Andrew Quicksall
Associate Professor of Civil & Environmental Engineering

_____

Prof. John Easton
Senior Lecturer of Civil & Environmental Engineering

_____

Prof. Jaewook Myung
Assistant Professor of Civil & Environmental Engineering

_____

Prof. Wenjie Sun
Assistant Professor of Civil & Environmental Engineering

_____

Dean James Quick
Associate Vice President for Research
Dean of Graduate Studies
Professor of Earth Sciences

Space and Depth-Resolved Naturally Occurring Toxic Groundwater Species in Bangladesh and Rwanda: Origination and Risk Analysis

A Dissertation Presented to the Graduate Faculty of

Lyle School of Engineering

Southern Methodist University

in

Partial Fulfillment of the Requirements

for the degree of

Doctor of Philosophy

with a

Major in Civil & Environmental Engineering

by

Kenneth M. Hamilton II

(B.S., Environmental Engineering, Southern Methodist University)

(M.S., Environmental Engineering, Southern Methodist University)

May 16, 2020

ACKNOWLEDGMENTS

This work could not have been accomplished by the wisdom of my brilliant advisor, Dr. Andrew Quicksall, along with his many colleagues in the Department of Civil and Environmental Engineering here at SMU. I'm also forever grateful for everyone involved in this process. Expressly my Mum and Dad for remaining patient with me through this long intellectual development. My friends, for always making sure I knew good times were ahead, Mrs. Salcedo for making sure I was fed, Mr. Salcedo for the Sunday soccer lessons and, Monica for always cheering me on.

Hamilton, Kenneth B.S., Environmental Engineering, Southern Methodist University, 2012
M.S., Environmental Engineering, Southern Methodist University, 2013

Space and Depth-Resolved Naturally Occurring Toxic Groundwater Species in Bangladesh and Rwanda: Origination and Risk Analysis

Advisor: Andrew N. Quicksall
Doctor of Philosophy conferred May 16, 2020
Dissertation completed April 17, 2020

Access to safe potable water is a necessity for all. Groundwater is a commonly relied upon drinking water source for many areas around the world. This is especially true for communities in high density, rural settings. Such is the case for populations near Cox's Bazaar, Bangladesh, and in the Bugesera region of Rwanda. Sediment and groundwater contamination, through toxic dissolved species, represents a significant public health risk to exposed populations. Tropical soils, such as the soil profiles in Bangladesh and Rwanda, often contain higher concentrations of heavy metals (Rieuwerts, 2007). Additionally, nitrate from fertilizers, are widely used on the soils in these regions. While hazardous risk will never be alleviated in its entirety, it is the goal to diminish the threat as much as possible. To accomplish this task, a complete and fundamental understanding of contaminant solid-solution partitioning mechanisms is required. It is also important to note that contaminant distribution over space and depth is a contributing factor to potential exposure. The outcome of this dissertation combines spatial- and depth-resolved sampling to quantify contamination risk posed by heavy metals and other toxic

species. In finding and evaluating these hazardous risks, potential solutions to alleviate and manage public health exposure are offered.

The first chapter involved groundwater sampling at Kutupalong settlement camp near Cox's Bazaar, Bangladesh. Sponsored by the United Nations High Commissioner for Refugees (UNHCR), thorough sampling of the community's potable groundwater, took place throughout the entire settlement. Sampling uncovered subsurface biogeochemical processes that ultimately govern the release of Pb and NO_3^-. Pb concentrations were found as elevated as 150µg/L, well above the World Health Organization's guideline of 10µg/L Pb in drinking water. Further investigation indicated nitrogen dynamics regulate pH in the subsurface. Changes in pH control the solubility of Fe and Mn oxides and, therefore, their associated sorption and desorption of Pb. Contaminant release is spatially heterogeneous within the resettlement's groundwater. This would make *in situ* remediation a tedious and possibly ineffective solution. To compensate, geochemical data in combination with GIS spatial analysis generated risk assessment maps. The maps illustrate the heterogeneity of risk associated with distinct contaminants throughout Kutupalong. In doing so, risk maps provide a mitigation strategy of avoidance for contaminated well sites, strategic guidance for currently safe wells, the closure of high-risk wells, and the placement of future ones.

The second study in this dissertation looked at naturally occurring metal contamination in groundwater from a tropical region. Water quality mapping in Bugesera, Rwanda, highlighted multiple metal contaminations throughout the region. Multiple in-use boreholes contained Mn exceeding the former WHO guideline of 400µg/L. Several sites also contained U exceeding the WHO guideline of 30µg/L. U was found to be over 50µg/L in some cases and over 400µg/L in one extreme circumstance. Sediment sampling in 2016 and 2017 helped verify that multiple

areas within Bugesera contain elevated solid-phase concentrations of various metals with very different mechanisms of potential release into the environment. Three different sites were sampled and assessed for concentrations of multiple heavy and trace metals. Among the metals evaluated, Mn, U, and V presented the highest levels of sediment concentrations. Depth-resolved sampling uncovered subsurface characteristics unique to each locale. Depth to groundwater table and associated redox changes varied by locale. A location with seasonally persistent vadose conditions is contrasted with locations showing redox changes induced by seasonally fluctuation pore saturation via groundwater table oscillation.

Sequential extraction experiments were completed to identify the metal speciation. Loss on ignition (LOI), calcination, and soil acidity measurements further characterize the sediment chemical systems and provide depth to interpretation as to the mobility of the metals. This research aims to characterize the elevated metal concentrations in the subsurface as well as determine the mechanisms of release for potential exposure to the environment and the public health. Ultimately, this will permit communities within Bugesera to develop without risk of exposure to toxic metals.

The final phase of research looked beyond the soil-water interface and studies contamination exposure through fine sediment particles. Small size airborne particles are well-known pathways for chemical exposure, including exposure to heavy metals. Though metals concentrations are important, they alone do not verify the complete exposure sediments or sediment particles present. Hakanson (1980) and Tomlinson et al. (1980) describe ecological risk indices that give a more accurate assessment of contamination risk. By using contamination factors (C_f), pollution load index (PLI), and potential ecological risk index (RI), an accurate assessment of the toxicity and exposure by fine sediment particles can be calculated. In this

study, two different locations in Bugesera are examined. It is found that sub 75μm particles present a far greater level of potential exposure risk than larger particle sizes. The greatest potential hazard comes from a region with constant redox cycling. Metals of most concern, at this location, are Cu and Pb. The other studied site is a region with a yearly constant vadose zone. At this location most concerning metals are Pb, Cd, and Cu.

Through understanding the biogeochemical processes, their independent release mechanisms, and potential exposure risk, informed, adequate, and necessary management judgments can be determined. Whether decisions are made for strategic avoidance or direct mitigation, responsible parties cannot do so without the pertinent information from in-depth examination. The complete aim of this dissertation looks to gather all necessary information to make sound decisions in keeping the public health at large protected from toxic metal exposure, specifically metal exposure from tropical soils.

TABLE OF CONTENTS

LIST OF FIGURES

LIST OF TABLES

CHAPTER 1

Introduction

1.1 Background

Soil-groundwater chemical interactions are part of a unique and complex relationship. Understanding this association, its consequences on the environment, and its further impacts on the human population, is imperative for public health and safety. Subsurface biogeochemical reactions can result in the sequestration and/or release of toxic elements. Many trace and heavy metals are concerning considering their inherent health risks posed to the public. While geogenic toxic hydrated metal cations and oxyanions are hazardous worldwide, developing nations have a particular vulnerability (Nriagu, 1992). Geopolitics and global economics are forces that bridge public health to the environment. The work studied groundwater, sediments, and soil groundwater interactions in susceptible areas of developing nations of interest. The Bugesera district in Rwanda and a Rohingya refugee resettlement near Cox's Bazaar, Bangladesh were identified as areas of interest.

In 2011 and 2013, sampling trips to the Kutupalong settlement, was sponsored by the United Nations High Commissioner for Refugees (UNHCR). Map 1 below, details the location of Bangladesh and the Kutupalong settlement. It is a settlement for Rohingya refugees escaping persecution in Myanmar. Kutupalong is located near the city of Cox's Bazaar in Bangladesh's

hill tracts region. The shallow depth to bedrock hill tracts region in Bangladesh differs from the more well known deep deltaic regions of the country associated with contamination of arsenic. Geologically, the hill tracts have varied bedrock instead of the uniform Holocene sediment found in the deltaic zone.

Rwanda is a small, inland, equatorial, east-central African nation and is geologically part of the East African Rift Zone as shown in Map 2. The country is surrounded by the neighboring rift valley nations Uganda, Democratic Republic of Congo, Tanzania, and Burundi. Rwanda contains a variety of differing geologies and environmental systems. The Bugesera district in Rwanda is a unique area directly south of the nation's capital Kigali. The district is a drier region than neighboring regions to the north and west yet it contains more surface water than the other regions. Its geomorphology leads to numerous lakes and wetlands not seen elsewhere in the region. Bugesera is the eastern province's westernmost district. It borders the southern district to the west, Kigali to the north, and Burundi to the south. Bugesera's location is illustrated in Map 2.

1.2 Metals & Toxic Species

1.2.1 Heavy Metals

Uranium is a heavy metal, mostly associated with fuel for nuclear fission power (Domingo, 2001; Winde et al., 2017). The public, therefore, commonly thinks of uranium risk as its radioactivity. It is also, however, a highly toxic element when biologically absorbed in plants and animals, including humans. Its absorption can lead to numerous toxicological human health

effects as well as deleterious effects on ecological systems (Selvakumar et al., 2018). In humans, uranium accumulates most commonly in the liver, kidneys, and bones (Bajwa et al., 2017). Uranium ingestion is mostly known as a nephrotoxin targeting proper kidney function (Kurttio et al., 2005). Kurttio and others have studied natural uranium uptake, via drinking water, and its affliction on human bone turnover (Kurttio et al., 2005). However, uranium is now also seen as toxic to the human reproductive system (Shuang Wang et al., 2019). Naturally occurring uranium is a toxic element and, therefore, of interest when it is found in aquifers and sediments. Uranium is also frequently linked to other environmentally relevant geochemical cycles (Zavodska et al., 2008).

Lead and manganese are both metals of environmental concern. In the case of lead, it is a heavy metal with numerous health concerns (Flora et al., 2012; Roy and Edwards, 2019; Trueman et al., 2019), including being expected as a human carcinogen (National Toxicology Program, 2011; Rehman et al., 2018). Lead carcinogenicity is of immense concern due to notable lead exposure globally (Silbergeld, 2003). Lead is widely documented as a neurotoxin, contributing to neurophysiological damage and function decline (Mason et al., 2014). The decline of nervous system functionality is associated with chronic exposure (Mason et al., 2014). Experimental findings suggest lead's neurological effects extend to intellectual deficiencies, especially among children (Lanphear et al., 2005; Redmon et al., 2018; Slikker et al., 2018).

Manganese is a transition metal involved in environmentally important processes (Herndon et al., 2018). It is essential for the proper biological function of living organisms (Santamaria and Sulsky, 2010). It does not have the same health effects as many heavy metals, but, at concentrations studied, is toxic with overexposure and can lead to numerous organ failures (Crossgrove and Zheng, 2004). Manganese overexposure is correlated with decreased

fertility and other reproductive issues (Crossgrove and Zheng, 2004). In trace concentrations, manganese is essential for brain development but overexposure will cause manganese to be a toxicant to the brain (Takeda, 2003). In many instances, the exposure of either element is governed by their geochemical intrarelationship in an environmental system (Dong et al., 2003, O'Reilly and Hochella, 2003). The geochemistry of lead and manganese and their toxicological impacts are described in more depth below.

1.2.2 Oxyanions

Oxyanions are anions attached to an oxygen atom and are similarly hydrated in solution. Unlike hydrated cations, oxyanions can include metals, metalloids, and non-metals. Vanadium and nitrate are typical examples of oxyanions.

Vanadium is a redox driven, transition metal, similar to chromium. Vanadium is a well know geochemical constituent; however, studies into its environmental and health impacts have lagged (Huang et al., 2015). There are numerous health effects associated with vanadium (Guagliardi et al., 2018). Health implications due to vanadium exposure include poisoning of the respiratory, circulatory, and nervous system as well as the kidneys and digestive organs (Venkataraman and Sudha, 2005). Vanadium geochemistry is also an identifier for redox changes (Huang et al., 2015). It has several oxidation states, but V(IV) & V(V) are the most prevalent species in aqueous environments (Pourret et al., 2012). Understanding vanadium speciation relationships will help yield a complete geochemical picture of the subsurface environment.

Nitrogen dynamics strongly influence subsurface chemistry.

To fully comprehend certain geochemical trends, nitrate and other nitrogen species must be understood to discern their environmental significance. Nitrate is a dietary nutrient important for proper biological functions (Larsen et al., 2011); however, ingesting drinking water contaminated with elevated nitrate can lead to methemoglobinemia, especially in newborns (McCasland, 1985). Methemoglobinemia is the inability of the hemoglobin molecule to transport oxygen and carbon dioxide. Resulting in tissue hypoxemia and, in some cases, death (Wright et al., 1999). Nitrate is thus a significant anion for its environmental functions and its hazard to public health(Szalińska et al., 2018).

1.3 Distribution Mapping

Distribution mapping is an efficient and effective means to fully understand spatial trends of analytes of interest. This provides researchers a tool to explore geochemical relationships and the public a tool more fully for visualizing the risk of contaminated areas. Combining known spatial and biogeochemical data can spatially quantify risk in map form. Such maps graphically illustrate concentrations of metal contamination in a region. The maps feature geochemical data loaded into layers to depict not only the hazardous metal concentrations exposed, but also to provide insight into areas that are at risk for exposure. Exposure risk as described by Stamatis Kalogirou and Christos Chalkias are hazards from the environment affecting humans and hazards sourced from humans affecting the environment resulting in human health implications (Stamatis Kalogirou & Christos Chalkias, 2014)

1.4 Ecological Risk Assessment

It is vital to know the concentrations of heavy metals in an environmental system, to access information regarding soil, water, and the sediment-water interface. However, concentrations alone do not output the complete environmental impact that metals assert on a surrounding environment. For a more comprehensive assessment of potential ecological risk, statistical indices are employed. Several statistical ecological risk indices are used to account for the potential impact metal contaminants pose on the adjacent sediment (Zhu et al., 2012), as well as to determine the nature of contamination and its potential sourcing (Jiang et al., 2014; Rabee et al., 2011).

1.5 Research

After identifying the geo-constituents in the subsurface and groundwater of Bangladesh and Rwanda, several questions were raised forming the bases of the hypotheses studied in this dissertation:

- Iron, manganese, lead, and nitrate, are spatially co-expressed in Kutupalong groundwater
    - Multiple interlinked biogeochemical processes are controlling the concentrations of lead and nitrate in Kutupalong groundwater
    - A drinking water risk assessment tool can be produced from the spatially integrated data
- Near-surface Bugesera, Rwanda sediment expresses depth-resolved changes in partitioning of heavy metal cations & oxyanions

  Toxic metal concentrations are disproportionally elevated in fine particles of near-surface sediments in Bugesera, Rwanda

- Potential exposure is a function of particle size. surface sediment particles

As an environmental engineer, solutions to questions faced are resolved using the best available practice according to the situation. The questions studied are not just to enhance the fundamental understanding of subsurface interactions in each location. Environmental problems are well known in some instances, so it is necessary to thoroughly evaluate and fully define each issue. While not the focus of the study, providing recommendations is the duty of an engineer and preliminary recommendations will be given here. Ultimate recommendations will administer the most effective, efficient, and economical mitigation techniques to help resolve toxic metal exposure. Future work conducted will involve applying best practices to prevent and or remediate metal contaminants. Laboratory-scale and pilot-scale experiments will actively engage in mitigation techniques to optimize the best available solutions. It is also important to consider that there exist multiple solutions for any remediation issue. A mitigation strategy should not only optimize the best available technology, but it should also correspond to the socioeconomic values of the principal clients. While preliminary recommendations will be offered here, the major result of these fundamental research questions will provide an essential practical guide to the complex engineering solutions that will follow.

1.6 Figures

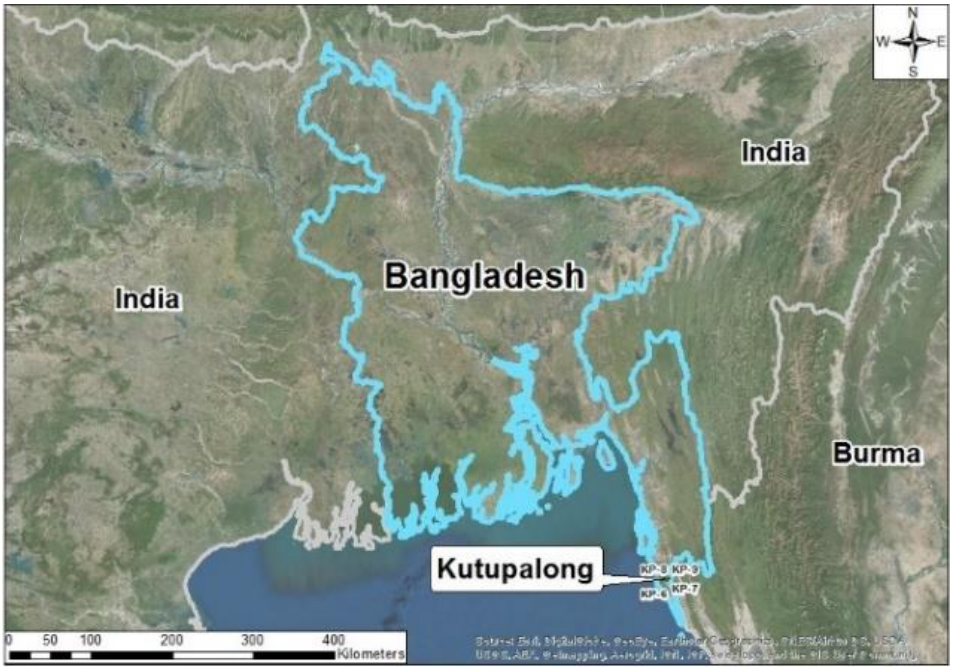

Figure 1.1) Location of Kutupalong Resettlement Camp in Bangladesh.

Figure 1. 2) Map of Rwanda and the Bugesera District

CHAPTER 2

Groundwater Lead and Nitrate Mapping for Origination and Risk Assessment in Kutupalong, Bangladesh

Submitted to the *Journal of Environmental Pollution*

Abstract

Kutupalong is a refugee settlement sponsored by the United Nations High Commissioner for Refugees (UNHCR). It is located southeast of Cox's Bazaar, Bangladesh near the border of Myanmar. The settlement is a densely populated Rohingya community with an expanding number of resettled people. The Rohingya people are escaping targeted violence in Myanmar (World Health Organisation, 2017). A 2018 UNHCR report estimated roughly 688,000 Rohingya have fled Myanmar for Bangladesh since August 2017. Although, from the end of 2017 to the beginning of 2018, Rohingya refugees arrivals to Bangladesh have slowed (Hosoi and Sharhan, 2018). This intense population increase strains available resources, especially drinking water.

The population sources water from shallow aquifers via hand pump wells. Sampling groundwater in the Kutupalong settlement revealed biogeochemical co-expression connected to the release of Pb and NO_3^- as well as other contaminants, including Mn and Fe, throughout the settlement's drinking water systems. Subsurface nitrogen dynamics are regulating pH. Changes in pH are controlling the dissolution of Fe and Mn hydroxides and the sorption and desorption of associated Pb. There is significant lead contamination in Kutupalong, where Pb concentrations exceed 150µg/L, ten times the World Health Organization's health guideline.

The nature and distribution of these geochemical expressions are varied throughout the settlement, making it difficult to provide effective mitigation strategies. However, sampling documentation combined with spatial referencing can yield non-traditional tools, such as risk

assessment mapping, that can be used to address heterogeneous contaminants. Risk assessment maps detail the region's areas of contamination and potential areas of concern. Spatial assessment maps provide key guidance for determining if current water-bearing sources are safe for use and help to strategically plan future well placement.

2.1 Introduction

In 2012, the Kutupalong settlement near Cox's Bazaar, Bangladesh was home to a slowly increasing number of Rohingya refugees. As of 2018, almost 1 million Rohingya people fled Myanmar into neighboring Bangladesh to avoid genocide. The settlement is supported by the United Nations High Commissioner for Refugees (UNHCR), which provides emergency care to Kutupalong inhabitants, including access to potable water. The majority of water is accessed through hand-pumped groundwater wells, which are a typical mode of delivery for communal water sources for much of the developing world (Carter et al., 1996). These water sources are monitored by the UNHCR for immediate, biological causes of contamination. Additional testing is limited because of time and financial resources. For emergency response situations,-securing potable water for short-term relief is paramount. However, the Rohingya people settled in Kutupalong are no longer in a temporary relief situation, the camp has been in existence for decades, in some cases with three generations living there. The importance of regular biological monitoring is obvious, however, the need for heavy metal monitoring is necessary as consumption of low-level contaminated water for an extended period can lead to chronic conditions, even without the immediate appearance of symptoms. It is therefore imperative to examine the chemical composition of these aquifer sources.

2011 and 2013 sampling trips to the Kutupalong settlement, sponsored by the United Nations High Commissioner for Refugees (UNHCR), revealed not only elevated levels of lead (Pb), nitrate (NO_3^-), iron (Fe), and manganese (Mn) but also highlighted potential geochemical trends pertaining to the co-expression of these contaminants in the system. It is important to assess the concentrations of these contaminants considering their significant concerns to public

health. Moreover, recognizing the geo-spatial distribution of contaminants provides communities with a greater understanding of how these contaminants are sourced and related to external activities, which can lead to the preservation and improvement of community well-being.

Lead is a dangerous heavy metal contaminant to humans. Even extremely low levels of lead in the human body can cause negative health effects (Needleman and Bellinger, 1991). Lead exposure is connected to many health-related issues including reproduction concerns and carcinogenicity (Flora et al., 2012) (Steenland and Boffetta, 2000). Lead has no function within the body and as such when it is consumed by children especially, as it is a neurotoxin causing severe childhood neurological development (Gidlow, 2004). Nitrate though commonly used in natural systems as a fertilizer, at increased exposure is also linked to developmental and reproductive health abnormalities. Methemoglobinemia is the most concerning complication of excessive nitrate exposure (Fan et al., 1987). Nitrate induced Methemoglobinemia, affects infants mostly. However, nitrate induced methemoglobinemia can occur in those older than infancy. Individuals with reduced stomach acidity, and those with a lack of the enzyme to revert methemoglobin to hemoglobin can experience methemoglobinemia (Waskom, 1991). Iron, while not a hazardous contaminant to human health, is an aesthetically unpleasing impurity and at certain levels can render groundwater unusable (Das et al., 2007). Manganese on the other hand, while similar in its geochemistry to Fe, is toxic with overexposure. The World Health Organization (WHO) previously recommended an aesthetic standard of 100 µg/L and a health standard of 400 µg/L. Dietary Mn toxicity can lead to decay of the nervous system and associated problems with the lungs, heart, liver, and other organs (Crossgrove and Zheng, 2004).

Iron and manganese oxides are found in many natural systems and are associated with heavy metals. In both natural and synthetic systems, Fe and Mn oxides sorb heavy metals, such

as Pb to their surfaces in both soil and aqueous environments(O'Reilly and Hochella, 2003). Although Fe-oxides are often favored for the sorption of Pb, due to their abundance and high surface areas making the case for Fe oxides to be optimal for Pb sorption (Dong et al., 2003). However, many studies have shown a preferential sorption of Pb to Mn oxides (McKenzie, 1980; Schroth et al., 2008; Villalobos et al., 2005). Additional environmental studies have recorded Pb uptake by certain plants to be impeded by manganese oxides (McKenzie, 1978; Villalobos et al., 2005). Chen studied the phytoavailability of Pb in soils and concluded Mn retarded the uptake of Pb (Chen et al., 2000). Gadde performed studies detailing Pb sorption to hydrous ferric oxides and hydrous manganese oxides (Gadde and Laitinen, 1974). Sorption and desorption processes are driven by pH changes in the environment. The pH sensitivity and reversible nature of heavy metal adsorption are of great significance (Gadde and Laitinen, 1974).

Groundwater sources of Kutupalong are heavily impacted by nitrogen processes ensuing during nitrogen cycling. Nitrogen as nitrate is a groundwater pollutant and is typically sourced anthropogenically through agricultural means. However, population density is a major aspect of nitrate contamination as well. Pit latrines and domesticated animals pose a danger to groundwater quality because of waste discharge without any pretreatment. Therefore, exemplifying the role a high population density plays in the impact of groundwater quality (Wakida and Lerner, 2005).

This study assessed the chemical constituents and the spatial geochemical trends pertaining to Kutupalong's groundwater quality. Shifting pH is caused by nitrogen cycling from nitrate. Change in pH induces Pb sorption and desorption from Mn and Fe oxides. Ultimately, the paired processes result in the release of a significant amount of available Pb into the groundwater system. However, spatial expressions of soluble Pb are heterogeneous and thus, Pb

concentrations are varied throughout the total groundwater system. Using spatial mapping tools, a view of overlaying trends describes an area heavily afflicted with chemical contamination. Furthermore, these spatial maps can be used as a guidance tool for future groundwater well placement.

2.2 Methods

Trace elemental and ionic concentrations were collected through a series of groundwater samples, covering an extended range in the Kutupalong resettlement camp. Aqueous species analysis of both sample sets was completed using inductively coupled plasma- mass spectrometry (ICP-MS) for cations and ion chromatography (IC) for anions.

2.2.1 Field Sampling

Sampling was conducted during two trips in 2011 and 2013 to the Kutupalong settlement located southeast of Cox's Bazaar, Bangladesh. The missions involved identifying suitable drinking sources, most notably from shallow groundwater aquifers, then collecting an adequate representable sample from the source, followed by chemical analysis of the sample. Sampling consisted of taking simple water quality parameters and prepping aliquots of samples for instrumental analysis. A YSI 556 MPS meter and probe were used for *in situ* measuring the conductivity, oxidation-reduction potential (ORP), pH, and temperature. A Garmin GPS eTrex 20 establish latitude, longitude, and elevation at each site location. Kutapalong has a total of 108 (97 functioning) tube wells distributed throughout the camp. In 2011, 38 wells were sampled with a 39% coverage area. Wells are generally clustered by 2-7 wells throughout the camp allowing for efficient sampling, but also allowing for *de facto* repeat samples to get an idea of the

aquifer and spatial heterogeneity. Wells were located in areas of intense populations, and generally close to latrines. This allowed us to see any temporal changes in the water table, however, due to the timing of sampling we were unable to catch any seasonal variation. Water samples were collected for metal and anion analysis, where concentrated HNO_3 was used to preserve metals, while anion samples were left un-acidified. A 10-mL sample was passed through a .45 µm Whatman filter into each prepped micro-centrifuge tube. Samples were sealed in transfer containers for shipping back to the US. In the laboratory, samples were stored at 4˚C.

2.2.2 Analytical Techniques

2.2.2.1 Inductively Coupled Plasma Mass Spectrometry

Solution phase metal concentrations were analyzed using a Thermo Fisher Scientific, Thermo X-Series 2 ICP-MS. The instrument used a 5% HNO_3 matrix, prepared from trace metal grade concentrated 65-70% nitric acid and 18.2 mΩ Nanopure water. All measurements were completed in collision cell technology-kinetic exclusion discrimination (CCT-KED) mode. Samples were diluted with 18.2 mΩ Nanopure water and 5% HNO_3 to accommodate a calibration concentration range of 0.5 µg/L to 100 µg/L. A blank sample, composed of 5% HNO_3, was measured every ten to fifteen samples. Blanks were used to verify sufficient washout time between sample runs and to monitor drifting during instrumental analysis. Instrument calibration used standards ranging from a concentration of 0 to 100 µg/L. High-quality standards were prepared from SPEX CertiPrep Multi-Element Solution 2A diluted into 5% HNO_3. Sample concentrations were processed in excel spreadsheets. Mass uncorrected results from the instrument were calibrated with uncorrected instrument values of known standard concentrations. Calibration curves with an R^2 of .9999 or higher were used in combination with

blank subtraction and dilution factors to convert uncorrected instrumental values to concentrations.

2.2.2.2 Ion Chromatography

Analytical measurements of anion concentrations in the samples were accomplished using a Dionex Ion Chromatography (IC) System, ICS-1100. Samples were measured on the Dionex IonPac® column AS23 and the corresponding AS23 guard column. Nitrate, and sulfate, were analyzed. A required eluent of 4.5 mM $Na2CO_3$/ 0.8 mM $NaHCO_3$ was prepared and plumbed through the instrument. The pump on the instrument was run at 1 mL/min and the suppressor at 25 mA. Samples were prepared by diluting 1 mL of sample into 4 mL of 18.2 mΩ Nanopure water in IC-specific vials with filter caps. Standards were prepared by diluting anion specific standards into 18.2 mΩ Nanopure water to make solutions of concentrations of .1 to 75 mg/L. Blanks used 5 mL of 18.2 mΩ Nanopure water. Peak area results from the instrument were calibrated with instrumental peak area values of known standard concentrations. Calibration curves with an R^2 of .999 or higher were used in combination with blank subtraction and dilution factors to convert sample instrumental values to concentrations.

2.2.3 Chemical Mapping and Digital Extrapolation ArcGIS

Generation of choropleth interpolation maps was performed using ESRI ArcMap 10.1, licensed through Southern Methodist University. GPS points were collected on sampling trips using a Garmin eTrex 20. They were gathered in an excel spreadsheet in decimal degree format. Any relevant chemical data associated with each sampled wellpoint was loaded into the excel

spreadsheet with their associated site name and GPS points, such as pH, temperature and ORP, as well as data collected from the IC and ICP-MS. The GPS data from the excel spreadsheet and associated chemical data were loaded into the map using the WGS 1984 Geographic Coordinate System.

With the Spatial Analyst Extension in ArcGIS, the Natural Neighbor interpolation method was used to generate interpolated choropleth maps. The method uses an algorithm that takes the closest points near a query point and applies weights to the area based on proportionate areas to interpolate a value. Within the software, Voronoi polygons are drawn around the input points. Next, at each interpolation point, a new Voronoi polygon is drawn and the percentage of overlap between the new polygon and the original polygons are used as the weights. This is in contrast with the Inverse Distance Weighted (IDW) method which applies similar weights to points at similar distances to the interpolation point. The Natural Neighbor method was selected over other methods because when using the default settings, the interpolated areas matched the actual value of the input points. When using the default IDW settings, the subset interpolation area surrounding an input point would not always equal the value of the input point.

The tool is located within the Spatial Analyst portion of Arc Toolbox under the Interpolation tab. The data was loaded with the input point features. The default cell size was used. Upon generation of the natural neighbor layer, the layer class breaks were changed to be generally evenly divided among the data points and the layer colors are modified to be used for risk assessment. One of the class breaks was set at the selected guideline for the chemical parameter, such as a WHO or EPA guideline. Interpolated areas that contain wells that were below the selected guidelines are assigned different shades of blue, used in this context as a safe color. This is to indicate interpolated areas that contain safe drinking water concerning the

selected chemical parameter. Interpolated areas that exceed guidelines were assigned different shades of orange, red, and purple. This was to indicate varying levels of exceedance of the selected chemical parameter in the interpolated areas. Lighter shades of orange exceed the least. It is recommended that the drinking water in these interpolated areas be avoided when possible. Darker shades of red and purple indicate areas that exceed the most. Generally, the recommendation is to close wells within these interpolated areas.

While the output from this method can supply an excellent tool for decision making, yet there are limitations. The approach uses a two-dimensional method applied to what is a three-dimensional aquifer. Variation in sediments with depth could produce associated variations in the third dimension that is not accounted for here. To counteract this, only wells of similar depth were used in the interpolation in an attempt to represent a single depth of the aquifer. This is appropriate as most wells are drilled to nearly the same depth. Additionally, those utilizing the output data for future risk planning should be aware that a single interpolated value may not represent the exact chemical data at that location. Interpolated data should be used as indicators of general trends and not considered as exact predicted values at given locations.

2.3 Chemical Analysis and Correlation

Chemical analysis of samples displays several geochemical tendencies involving key groundwater constituents. Figure 2.1a depicts a pH drop corresponding to a significant lead release. Elevated lead levels are exhibited throughout groundwaters at acidic pH ranges, while levels decrease and subside as the pH rises from 4.5, shown in Figure 2.1a.

The system's nitrate concentration decreases with increasing pH (Figure 2.1b). A system such as the observed cannot remove nitrate non-biologically. This indicates a microbially

mediated nitrate reduction process is yielding an ORP drop while raising the pH of the system. Figure 2.1b points to high nitrate observed at a pH of 4 and nitrate nearly absent in most samples as the pH rises above 5. This multi-step dissimilatory nitrate reduction mechanism converts nitrate to a secondary N species while consuming H^+ and oxidizing organic material to CO_2 (Drever, 2002).

$$5C_{organic} + 4NO_3^- + 4H^+ \leftrightarrow 2N_2 + 5CO_2 + 2H_2O$$

Karanasios gives the minimal ORP value for denitrification as – 50 mV. Indicating that any ORP value at or above -50 mV would likely limit sulfate-reducing and methanogens because the presence of nitrate would be the optimal terminal electron acceptor (2010). Measured ORP values range from 205 to -101 mV. Figure 2 a and b graphically illustrate Mn and Fe against ORP, rendering a view of high transition metal concentration in suboxic to anoxic waters. Mn and Fe concentrations against ORP indicate redox potential environments dominantly preferable for nitrate and metal reduction (Brettar et al., 2002; Salazar et al., 2013) heavily suggesting microbially mediated processes controlling these key groundwater constituents.

Figure 2.3 a and b illustrate Mn and Fe concentrations that are most abundant just below neutral pH values and significantly decline at both high and low pH. Mn exhibits a slightly higher soluble concentration than Fe at decreasing pH, as is to be expected. It is well documented that iron oxides are far less soluble than manganese oxides, thus, it is natural to find higher Mn concentrations in solution e.g. (HEM, 1972). This suggests lead removal is instigated by sorption processes pertaining to Mn and Fe particles. Studies performed by O'Reilly (2003) and Trivedi (2003) indicate preferred Pb sorption to Mn oxides and Fe oxides as a function of pH. Pb sorption curve, given by Drever, describes Pb adsorption to Fe hydrous oxides (2002). A fundamental key to adsorption is pH and Pb's optimal adsorption pH value is 5.5 (Drever, 2002).

Microbial rate reactions of Pb sorption to Fe and Mn exceeds the rate of Pb dissolution during Fe and Mn reduction. Indicating the reason behind Pb's continued sorption under reducing conditions.

Sulfate concentrations are spread throughout pH ranges of sampled water as shown in Figure 2.4. Concentrations are noticeably absent above pH 7. Slightly below neutral pH, however, Mn, Fe, and SO_4^{2-} concentrations are all seen declining, coincidentally at the lowest ORP values in the region. Sulfur reduction processes are likely occurring given the low ORP values. Sulfide scavenging of Fe and Mn ions via sulfide minerals is therefore possible. Ramamoorthy (2009) showed that Fe is easily retained in the mineral phase under anoxic sulfidic conditions. Jones (2011) discusses Mn reactivity in the presence of sulfide is like that of Fe and Mn. Sulfide minerals are therefore possible in bottom waters with present concentrations of sulfide. In reduced waters, sulfide minerals are also known to collect heavy metals through adsorption processes (Jean and Bancroft, 1986). Precipitation of PbS is kinetically faster than their pyritization into Fe sulfide minerals (Morse and Luther, 1999). The exact sequestration mechanism (adsorption or coprecipitation) of heavy metals via sulfide minerals in most natural systems is questionable (Huerta-Diaz et al., 1998). Heavy mineral appropriation by sulfide minerals is most likely occurring at high pH values. The determining mechanism is unknown and is the subject of future research.

2.4 Spatial Analysis of Co-expression

Contour map constructs, modeled from analytical data and GPS coordinates, give a comprehensive view of Kutupalong subsurface chemical interactions. The contour maps show the spatial extent of selected constituents and their varying concentrations seen throughout the

settlement. Figure 2.5 shows Mn concentrations meet or exceed world health organization (WHO) aesthetic guidelines and established health parameters in nearly every region of Kutupalong. Concentrations in the range of 100 µg/L to 400 µg/L are observed in the center of the settlement spread through the southern and southwestern portion of the camp. Even higher concentrations are observed throughout the rest of Kutupalong with a couple extreme levels revealed in the northwest (Figure 2.5). Similarly, elevated iron concentration, are widespread in Kutupalong simultaneously as well. Figure 6 illustrates the elevated iron spread in the settlement. Every sampled water groundwater source exhibited iron levels above the WHO aesthetic guideline of 300 µg/L.

The map of Pb also shows values to be dominantly above the WHO health limit. Figure 2.7 gives the spread of Pb concentration in Kutupalong. Showing that Pb contamination is heavily present in the camp's subsurface. Figure 2.8 details nitrate concentration. Interestingly, nitrate for the most part is not present in concerning levels. A few regions in Kutupalong do exhibit levels of concern, however. In Figure 2.8 four regions are above the US Environmental Protection Agency's (US EPA) limit for nitrate.

Spatial analysis vividly highlights the relationships of Mn, Fe, and midrange pH in regions of Kutupalong. Comparing Figure 2.2 to spatial Figures of 2.6, 2.7, and 2.9 not only graphically is a trend seen between Fe and Mn at (5-7) pH, but spatial mapping further enhances this bias. Figure 2.9 features pH resolution in Kutupalong and highlights the regions of sub neutral pH. Thorough inspection of Figures 2.5 and 2.6, it is now spatially known that elevated concentrations of Fe and Mn correspond to areas of (pH range 5-6.5) pH. Further solidifying the graphical argument of an elevated pH generated by the reduction of Fe and Mn. The microbial

processes cause a rise in pH through the consumption of H^+ while reducing Fe and Mn oxides into solution.

In conjunction, spatial maps of NO_3^- and pH reveal overlaps of low pH with elevated NO_3^- concentrations. Figures 2.8 and 2.9 show the spatial expression of nitrate and pH respectively. While there is spatial variance in correlation, most of the high nitrate zones demonstrated in Figure 2.8 do correspond to low zones of pH shown in Figure 2.9. Similarly, spatially resolved aqueous lead concentrations (Figure 2.7) correlate well to spatially resolved pH values (Figure 2.9). Nitrogen cycling is the controlling process in this pH - ORP zone. Also, Pb follows this pH trend. Figure 2.7 illustrates Pb expressions resonate with NO_3^-, Fe, and Mn zones. Indicating Pb sorption to Fe and Mn are dictated by pH changes caused by nitrogen cycling.

The spatial correlation between Pb and NO_3^- is beneficial for public health developmental management. Summation of spatial concentrations can be synthesized into spatial resolutions of both elements depicting a net impact of concentrations in Kutupalong. Producing a spatial net impact modeling elevated subsurface concentration as well as predicting areas of concern for contaminant release. Risk assessment mapping can model overlapping concentrations of multiple contaminants to predict subsurface areas for optimal use. Figure 2.10 depicts the combined Pb and NO_3^- spatial coverage. This combined map can be used as a guidance tool to optimize the geolocations of water points for sound usage.

2.5 Conclusion

Kutupalong settlement provides potable water for an increasing population of displaced people. It is thus a public health concern and needs to recognize the quality of water being

delivered to the settlement's population. Analyses revealed co-expression that ultimately explains the release of contaminants into the drinking water system. Nitrogen cycling yielding the formation of nitrate is shown to control pH by the release of paired hydrogen ion. Nitrogen mediated pH levels control the surface charge of iron and manganese oxyhydroxide minerals and thereby the sorption and desorption of surface-bound contaminants. Desorption of Pb from Mn and Fe hydroxides leads to Pb availability in Kutupalong's drinking water. While Pb concentrations are well correlated with low pH and high nitrate, the observed co-expression is spatially heterogeneous.

Non-point source contamination problems are challenges that require unique mitigation strategies. Chemical sampling in Kutupalong has shown that not just Pb, but other contaminants of concern are intermittently widespread throughout the settlement. While contaminations are widespread, solutions are possible. Proper management of source contamination for nitrate is possible and would greatly influence the subsurface chemistry. Limiting nitrogen input, such as fertilizer runoff and animal waste, would help reduce nitrogen cycling driven pH drops in the groundwater. This cuts the risk posed by direct contamination of NO_3^-, the pH driven dissolution of available Mn, and the pH-controlled desorption of Pb from oxyhydroxides. Risk assessment maps are an alternative strategy capable of identifying, accounting for, and avoiding contaminated areas. Interpolated spatial models give users the ability to identify current and potentially hazardous areas allowing a more complete examination of assessed contaminants. If needed, spatial referencing can help strategically determine if existing wells should be closed and avoided as well as a tool for determination of future well placement to accommodate incoming populations. The developed spatial technique is a valuable method to assist in solving the crisis in Bangladesh. Not only would using spatial techniques regionally help mitigate local issues but

using on a global scale would help facilitate proper responses to current and future environmental and public health crises.

2.6 Figures and Tables

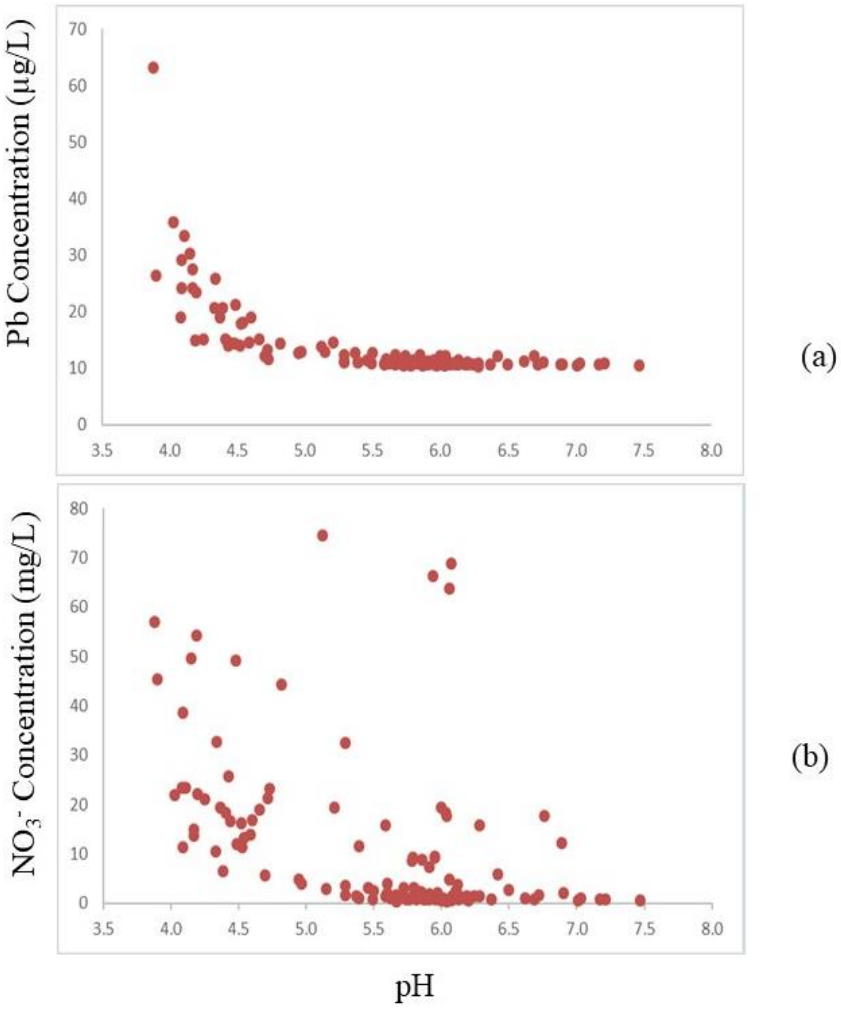

Figure 2. 1) Pb & NO_3^- concentration with pH. Measured concentration of soluble lead and nitrate sampled in Kutupalong. (a) Elevated lead levels are uniformly released at pH values around 4 and decrease as the pH rises to circumneutral where soluble lead levels are nearly absent. (b) High nitrate levels are most noticeable at pH values slightly above 4. Nitrate concentrations decrease as the pH rises barring a few outliers.

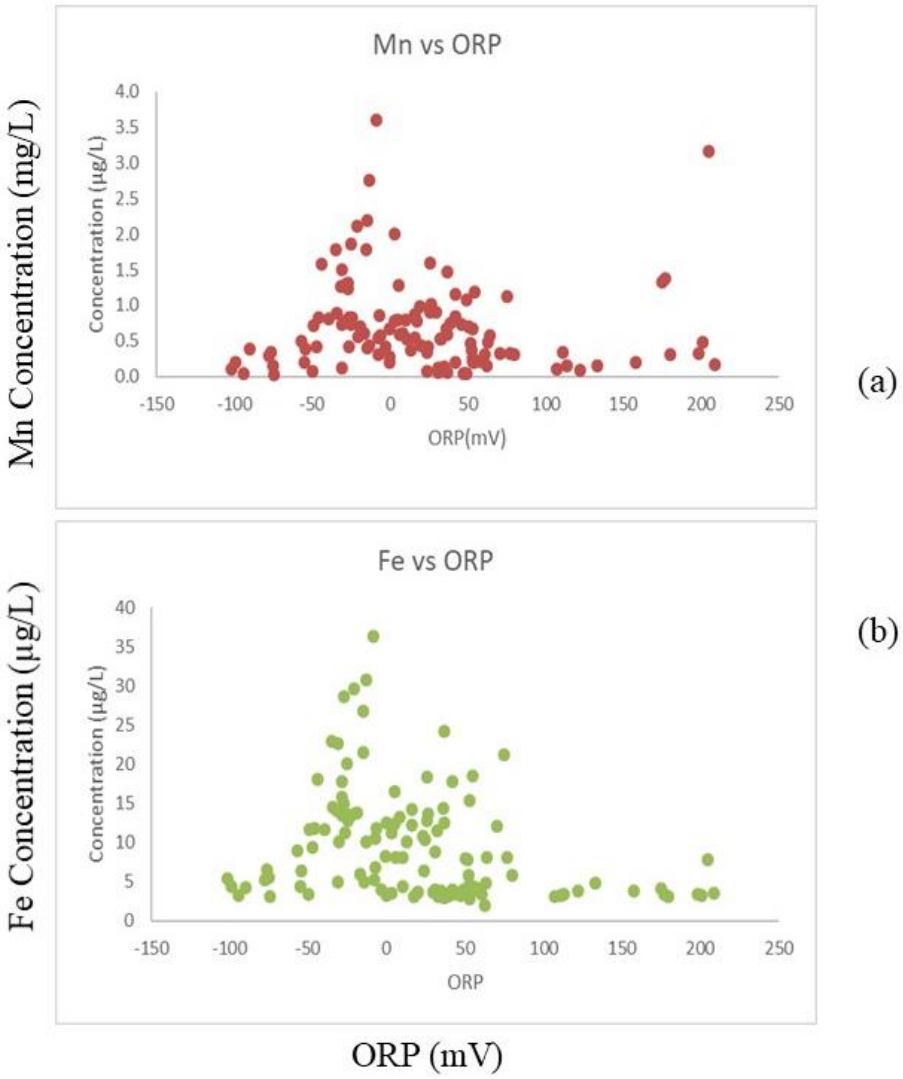

Figure 2. 2) Mn & Fe concentrations with ORP. (a) & (b) Iron and manganese concentrations from field samples versus measured ORP showing similar patterns of concentration.

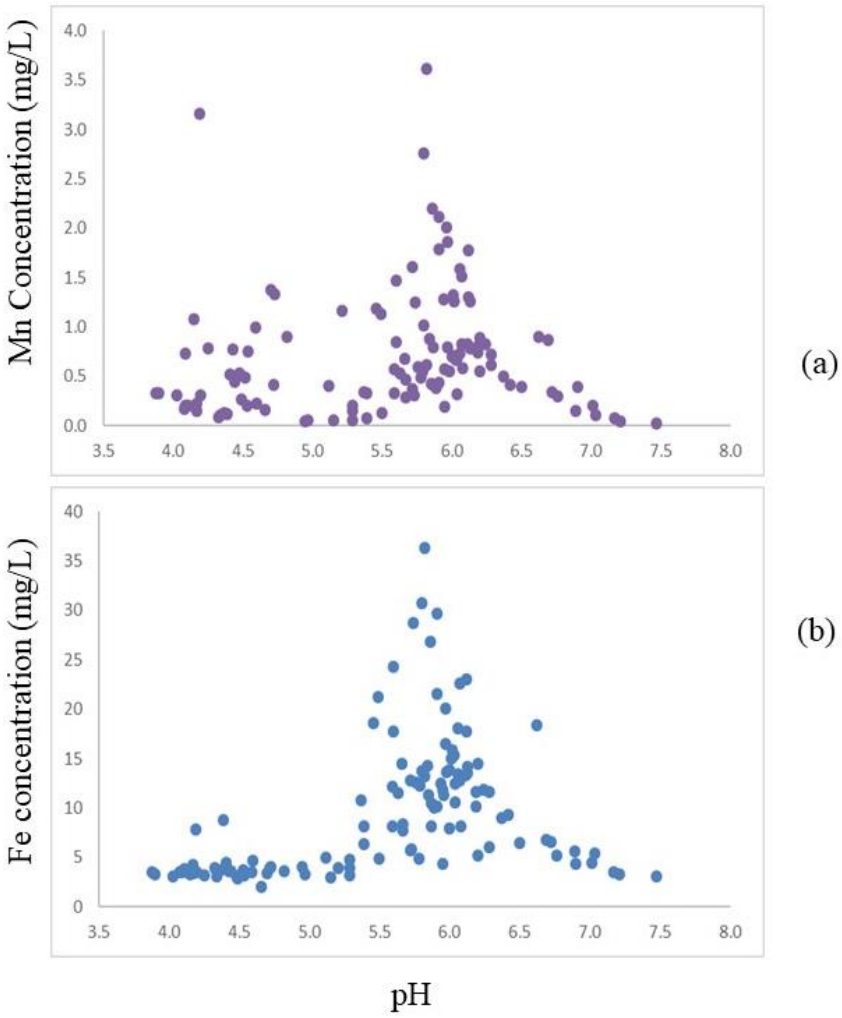

Figure 2. 3) Mn & Fe concentrations with shifting pH. (a) & (b) Measured soluble manganese and iron concentrations. Both elements mimic each other in terms of their highest concentrations are optimal near a pH of 6. Iron and manganese levels subside at pH values on either side of 6.

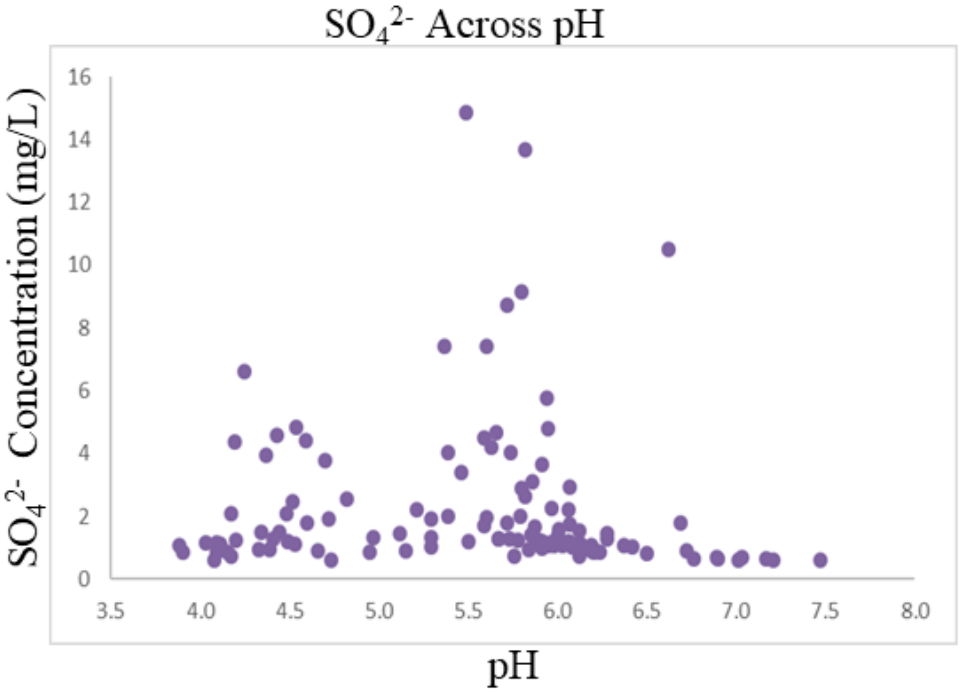

Figure 2. 4)SO_4^{2-} concentration with shifting pH. Measured concentrations of sulfate at respective pH values. Sulfate values are noticeably lower above pH 6. Low levels are demonstrated throughout the pH range. However, several outliers do exist, but do not exceed 16 mg/L

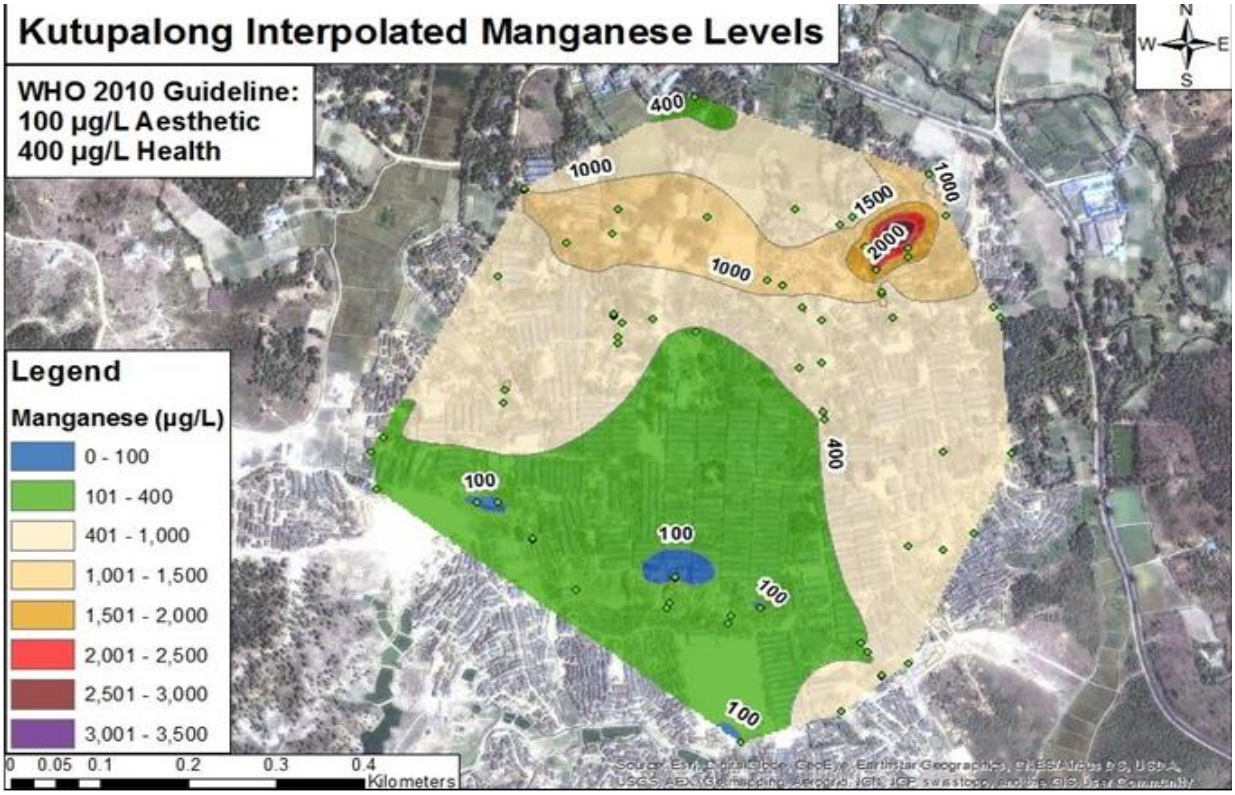

Figure 2. 5) Interpolated Map of Mn. Interpolated spatial coverage of manganese in Kutupalong shallow groundwater sources. Spatial imaging describes over half the camp exceeding the 2010 WHO health guidelines for manganese. A substantial portion of the settlement's sources exceed the WHO aesthetic guideline.

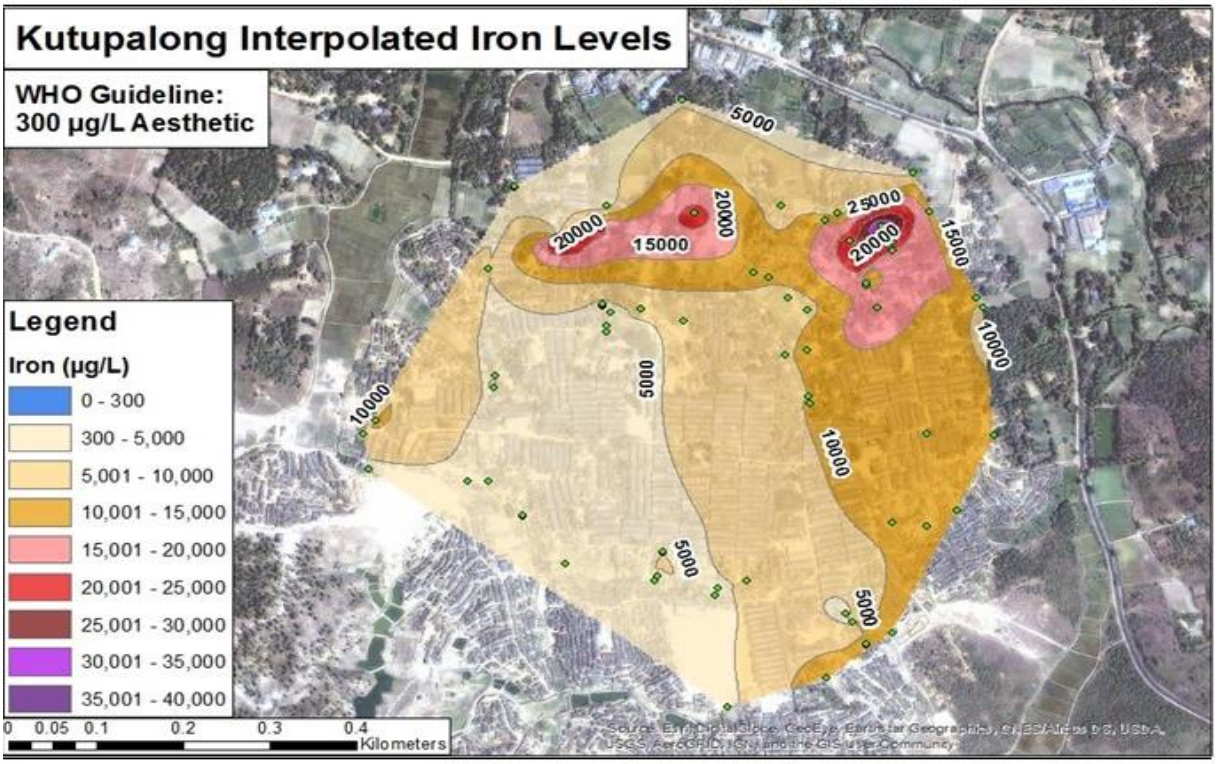

Figure 2. 6) Interpolated Map of Fe Interpolated spatial coverage of Iron across shallow groundwater sources in Kutupalong. Spatially, the entire Kutupalong camp shows iron levels above the WHO aesthetic guideline.

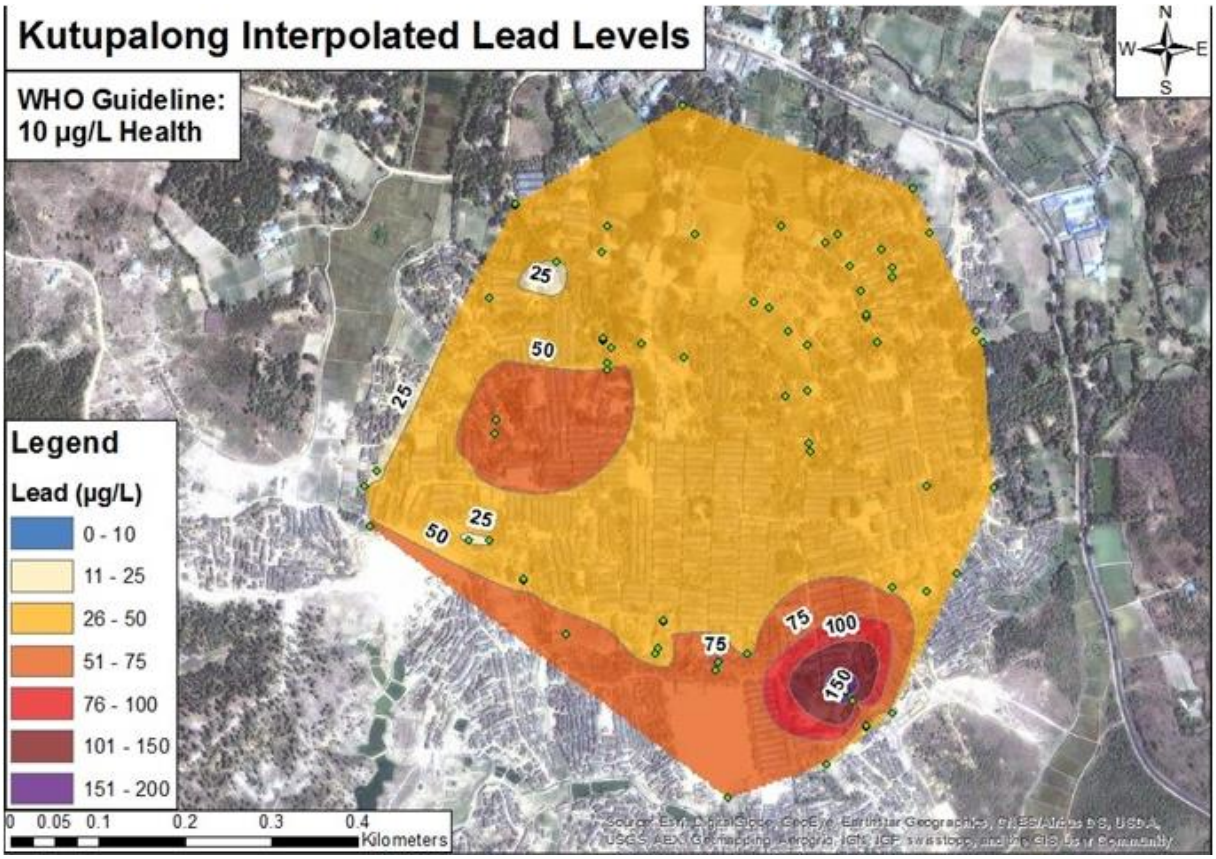

Figure 2. 7) Interpolated Map of Pb. Interpolated spatial coverage of lead concentrations in Kutupalong shallow groundwater sources. Lead is shown to be concentrated in the southeastern portion of the settlement.

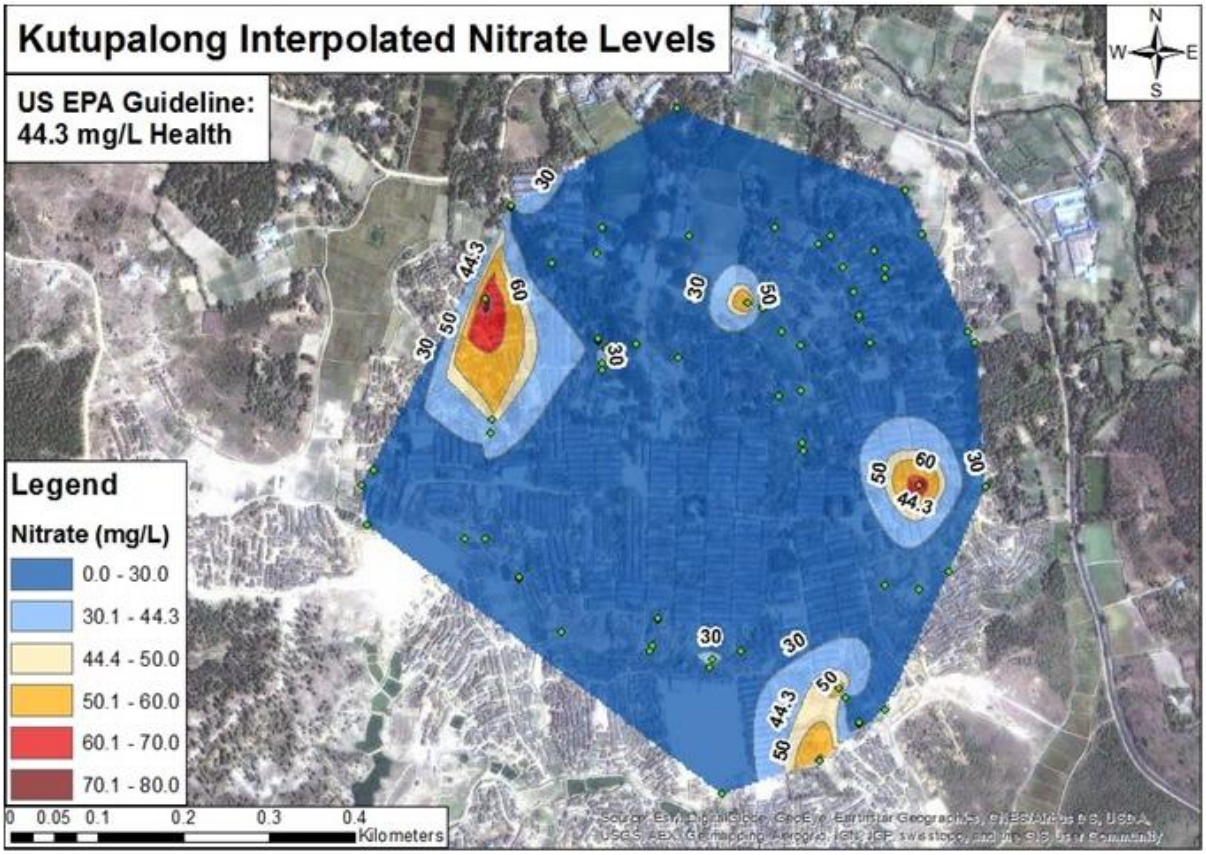

Figure 2. 8) Interpolated Map of NO_3^-. Interpolated spatial coverage of nitrate levels in Kutupalong shallow groundwater sources. Imaging depicts concentrated areas of elevated nitrate contamination.

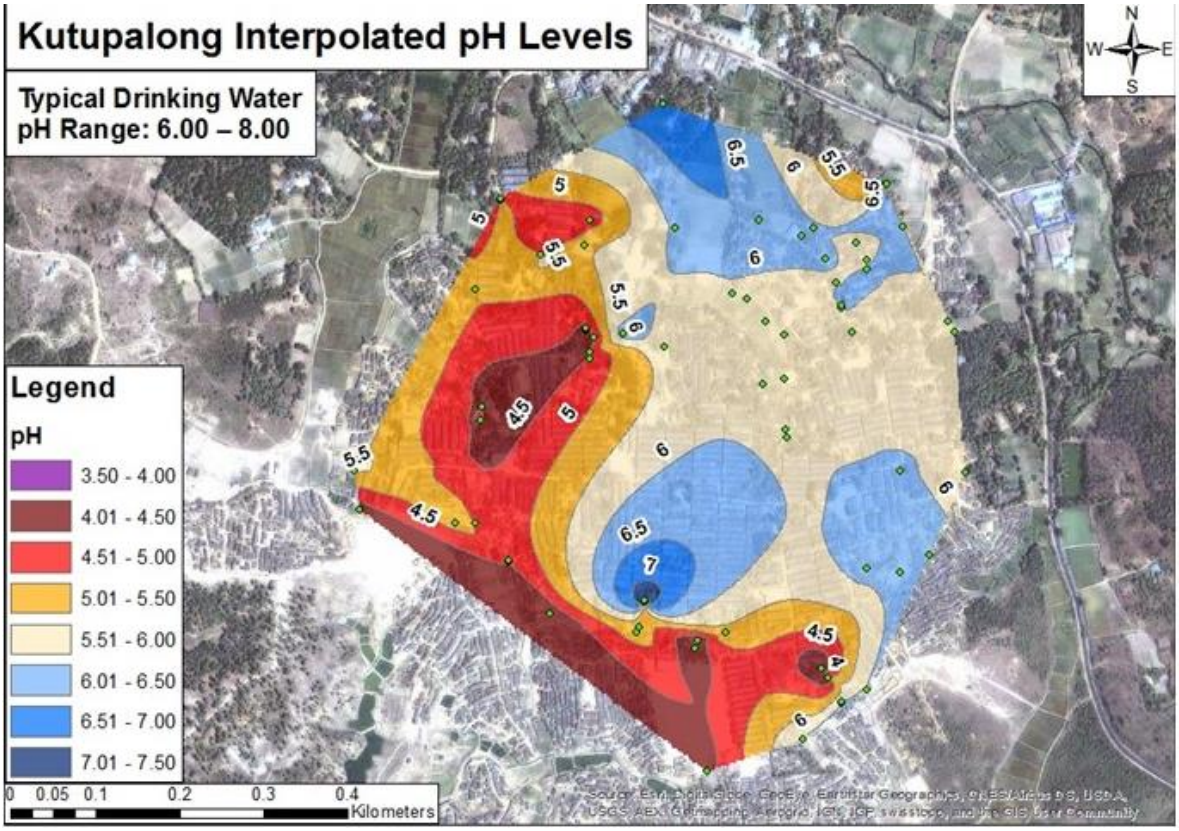

Figure 2. 9) Interpolated Map of pH. Interpolated spatial imaging of pH levels in Kutupalong. Much of the settlement is outside the typical pH range for drinking water.

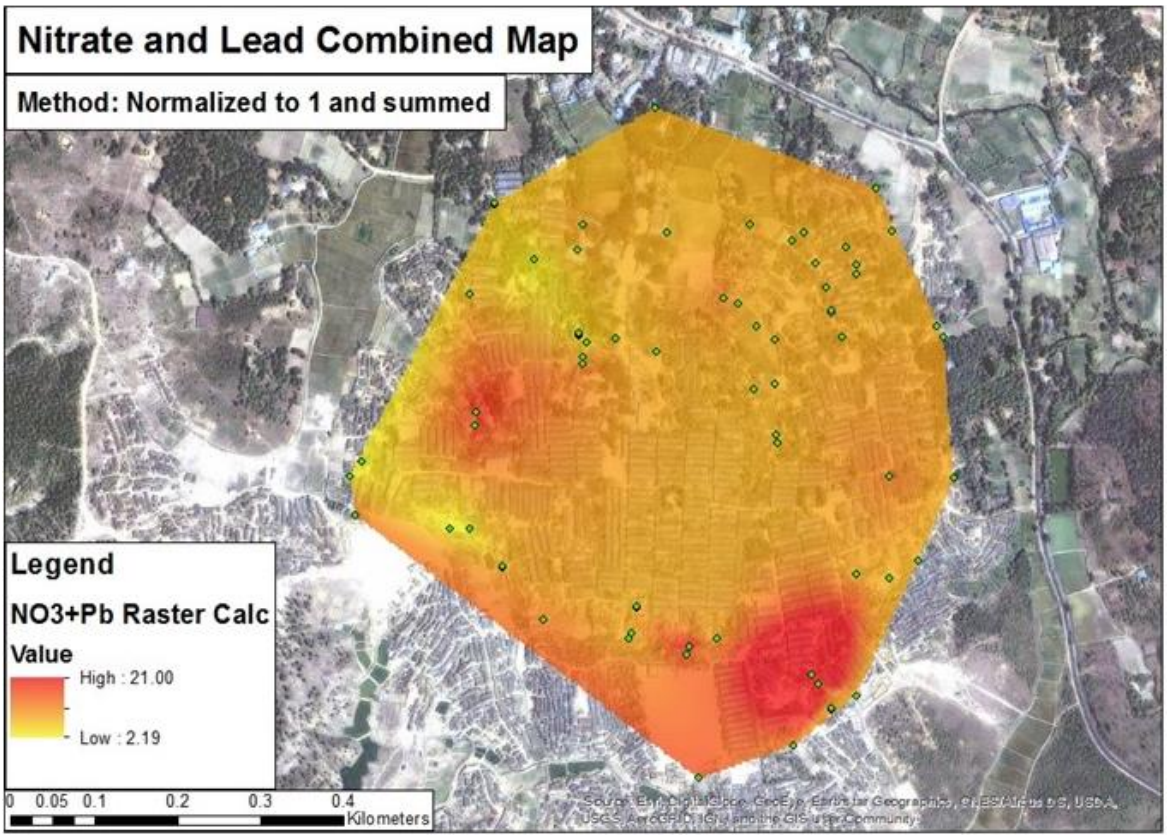

Figure 2. 10) Risk Map. Spatial raster portraying areas in Kutupalong where concentrations of both nitrate and lead are present.

CHAPTER 3

Impact of Local Groundwater Conditions on Solid Speciation and Associated Soil-Water Partitioning of Toxic Trace Metals in Bugesera, Rwanda

To be submitted to *Applied Geochemistry*

Abstract

Rwanda's Bugesera district is a semiarid region in the country's southeast. The district possesses numerous lakes and other surface water bodies, but local populations in remote areas rely primarily on hand-pumped shallow groundwater. Water quality monitoring in 2012 and 2014 lead to the discovery of several elevated metals in the region's groundwaters. The potential release or exposure of these heavy metals is a concerning issue for much of the population, especially in the remote sectors of the district. It is well known that changes in soil-water partitioning can lead to the subsurface release of heavy metals such as, in this case, manganese, uranium, and vanadium. Here, mechanisms of spatially heterogeneous release are explored via solid-phase speciation analysis of locales with varying groundwater dynamics.

2016 and 2017 sediment sampling determined that various regions in Bugesera experience diverse levels of elevated metal concentrations leading to very different potential mechanisms of release into the environment. Three handpump sites, within Bugesera, are sampled and evaluated for solid concentrations of manganese, uranium, and vanadium. Depth-resolved solid-phase sampling from each location revealed subsurface characteristics unique to each site. Site1 shows a redox shift at the water table. Samples from Site2 are completely collected from the vadose zone. While Site3 also reveals a redox shift, at the water table, but with differing subsurface results from Site1. Sequential extraction experiments were completed

on each sample to understand metal solid speciation. Loss on ignition, calcination, and soil acidity are techniques used to quantify associated soil components that can impact metal speciation. These data combined can guide the biological availability and mobility of the metals in question. This study aims to examine elevated metal concentrations in the subsurface and to determine the mechanisms of potential release into the environment via solid-phase speciation. Understanding these geochemical processes will allow for Bugesera to safely develop and expand its economic potential by addressing metals risks before and during development as opposed to reacting to future problems.

3.1 Introduction

Bugesera is a region within Rwanda's eastern province, containing a geomorphology leading to numerous lakes and wetlands. Though containing more surface water than regions to the west and north, the region is semiarid and has been known to be impaired by drought (Rwanyiziri and Rugema, 2013). For all the surface water present in Bugesera, many communities historically rely on shallow, groundwater sources. Groundwater sources provide a natural barrier to microbial contamination. Surface water, however plentiful, is nominally not suitable for human consumption without treatment rendering groundwater sources even more valuable to local communities.

2012 and 2014 water quality monitoring in Bugesera, Rwanda, uncovered toxic metals in shallow aquifer drinking water systems. Uranium, and especially manganese, were established at toxic levels in several drinking water sites across the district. These findings prompted further investigation into the soil-water interface throughout the region. Excursions in 2016 and 2017 provided sediment samples, from select Bugesera groundwater sites, further highlighting the presence of potentially harmful elements.

Manganese is a transition metal associated with numerous environmental processes in the subsurface. Geochemically, it is an important element that, even at elevated concentrations, is nominally seen as a harmless environmental pollutant. Previous World Health Organization (WHO) guidelines, however, recommended manganese levels under 400 μg/L. These guidelines have since been discontinued, on the insistence that manganese is only a health concern at and above 400 μg/L and is rarely available in drinking water at such concentrations (World Health Organization, 2011). 2012 and 2014 water quality monitoring in Bugesera, Rwanda noted in-use drinking water boreholes containing significant amounts of manganese. Several sites far

exceeding the 400 μg/L guideline. High manganese concentrations are not unique to the East African Rift Valley. Globally, numerous drinking water sources exceed 400 μg/L leading manganese to be of a public health concern (Frisbie et al., 2012) with heightened exposure leading to manganese toxicity, despite the shift in stance of WHO.

Concerns with uranium, as an environmental pollutant, are mostly owed to its radioactive nature. Historically, uranium has been considered a major component of nuclear power (Domingo, 2001). Uranium, though, is a toxic heavy metal with numerous ecological and public health concerns separate from any radioactivity concerns (Selvakumar et al., 2018). Elevated concentrations were found in Bugesera's drinking water sources. It is therefore important to investigate the dynamics in the subsurface of naturally occurring uranium.

Vanadium is an understudied, transitional metal of growing importance. It is used in many industrial services such as petroleum refining, steel processing, and as a catalyst for the reduction of NOx gasses (Bredberg et al., 2004; Imtiaz et al., 2015). From an environmental standpoint, vanadium is becoming increasingly more important (Imtiaz et al., 2015). There is debate on the toxicity risk vanadium poses, but vanadium contamination is a concern and should be studied and assessed.

Essential to understanding the release dynamics for manganese, uranium, and other potentially toxic metals, is their solid-solution partitioning. Metal bioavailability is not solely determined through the sheer abundance of metallic concentrations in contaminated soil (Sauvé et al., 2000). Potential environmental and public exposure, by metal availability, is thus a determinant of multiple subsurface factors including soil acidity, soil organic matter, and soil redox potential)(McBride et al., 1997; Roychoudhury and Starke, 2006).

This study aims to examine the chemical constituents controlling soil-water partitioning to categorize and determine the potential release mechanisms of toxic metals in the region. It also looks to investigate the bioavailability and mobility of constituents that are variably expressed in the region.

3.2 Methods

3.2.1 Soil Coring

Soil core samples were collected using a 30 cm stainless steel push corer. Standard soil sampling method was applied. Following site determination, the corer was pushed into the sediment as far as it could via hand and rubber mallet. Samples were taken from softer sites where the corer could be fully extended into the sediment. After the initial sample was collected, a 30 cm length is added to extend the corer's reach. Multiple lengths were added until core depth exceeded the groundwater table, or all lengths were used. For a sample core, each core length denotes a depth fraction for that sample. Each depth fraction is further subdivided. The top inch to 5 in and the bottom 5 in of the fraction was discarded. The remaining sediment was removed, intact from the corer's barrel by a stainless-steel spatula, and homogenized on aluminum foil. The depth fractionated homogenized sample was then collected in a 50 ml centrifuge tube.

3.2.2 Sequential Extractions

A sequential extraction procedure modified from Tessier and coauthors was used to quantify speciation of elements of interest in the collected sediment core depth fractions (Tessier et al., 1979). Species from the four most environmentally relevant fractionation phases were

measured. Phase 1 determined the exchangeable cations from the sampled sediment. 0.5 grams of dried sample is placed in a 50 ml centrifuge tube. 8 ml of 1 mol/L $MgCl_2$, at pH 7, solution was then added to the centrifuge tube. The sample was extracted for one hour on rotators. Following the extraction, and each following extraction, the mixture was centrifuged at 4000 rpm for 5-10 minutes to compact the remaining sediment. The extractant is poured off and prepped for ICP-MS analysis.

Phase 2 obtained analytes bound to the carbonate fraction of the sediment. 8ml of 0.1 mol/L sodium acetate, adjusted to pH 5 with HNO_3, was added to the residual of phase one. Phase 2 is extracted for 5 hours on rotators. Following extraction, the sample is centrifuged at 4000 rpm for 5-10 min. The extricated solution is poured off and prepped of ICP-MS analysis.

Phase 3 was intended to target analytes bound to the poorly crystalline iron and manganese oxides. 20 ml of 0.1 mol/L hydroxylamine hydrochloride, adjusted to pH 2 via HNO3, was added to the residue from phase 2. The reaction ensued for 16 hours, while on rotators. Next, centrifugation at 4000 rpm occurred and the extracted solution was poured off for ICP-MS preparation.

The final extraction, phase 4, targeted analytes bound to organic matter. The residual from phase 3 was combined with 3 ml of 0.02 mol/L HNO_3 and 5 ml of 30% H_2O_2 at pH 2. The mixture was extracted for 1 hour on rotators. The mixture was then placed in a preheated hot block at 85 °C for 1 hour. This phase 4 process was repeated once more. The extracted material was diluted with 5ml of 1 mol/L HNO_3, and finally poured off and prepared for ICP-MS analysis.

3.2.3 Loss on Ignition

A loss on ignition (LOI) analysis determined the organic matter content in the sediment core samples. Representative depth-resolved samples, from each core, were dried in an oven around 100°C for 1 hour, driving off any water. The sample was then massed, to gain the weight of dry mass, and placed in a pre-massed ceramic crucible. Following measurement, each sample was placed in the furnace at a temperature of 550 °C for 1 hour to oxidize organic matter to CO_2. Each crucible was then removed and allowed to cool in a desiccator until room temperature was reached. Once cooled, the crucible containing the sample was massed again. The differential mass loss can be attributed to the amount of organic material in each sample (Walter E. Dean, Jr., 1974). An equation for LOI is given by (Heiri et al., 2001):

$$\mathrm{LOI_{SOM}} = \frac{(M_{dry} - M_{550})}{M_{dry}} \times 100$$

Where,

LOI_{SOM} = the mass differential of organic material.

M_{dry} = the mass of the dried solid at 100°C

M_{550} = the mass of the solid at 550 °C

3.2.4 Calcination

Calcination is a continuation of LOI. A modified calcination analysis was used to determine the carbonate fraction. Samples previously measured in LOI analysis were then placed

in the furnace at temperatures of 1000 °C for one hour. After ignition, the crucibles were cooled to room temperature in a desiccator. Once ambient temperature was reached the samples were massed again. Mass loss from 550-1000°C is considered mass loss attributed to carbonate conversion to CO_2 (Walter E. Dean, Jr., 1974). Modified equations for calculating calcination are given by (Heiri et al., 2001):

$$\mathrm{LOI_{Carb}} = \frac{(M_{1000} - M_{550})}{M_{dry}} \times 100$$

$$\text{Carbonate \%} = \mathrm{LOI_{Carb}} \times 1.36$$

Where,

LOI_{Carb} = The mass differential due to the loss of carbonate material.

$M_{1,000}$ = The mass of solid at 1000°C.

M_{550} = The mass of solid at 550°C.

M_{dry} = The mass of solid at 100°C.

3.2.5 Soil Acidity

A modified method for soil pH determination is taken from *Methods of Soil Analysis part 3- Chemical Methods*(*Methods Soil Anal. Part 3—Chemical Methods*, 1996). Soil acidity analysis determined pH using a 1M KCL solution. 2 g of sample, from each sampled depth, was

massed out and placed in a 15ml centrifuge tube. 2 ml of 1M KCL is added and mixed to the sample. The mixture is rested for ten-minutes, then measured with a pH meter and probe. The pH is recorded as pH_{KCl} (*Methods Soil Anal. Part 3—Chemical Methods*, 1996).

3.2.6 Inductively Coupled Plasma Mass Spectrometry

Solution phase metal concentrations were analyzed using a Thermo Fisher Scientific, Thermo X-Series 2 ICP-MS. The instrument used a 5% HNO_3 matrix, prepared from trace metal grade concentrated 65-70% nitric acid and 18.2 mΩ Nanopure water. Analytical measurements were completed using collision cell technology with kinetic exclusion discrimination (CCT-KED) mode. Samples were diluted with and the same 5% HNO_3 matrix described above to adjust to the calibration concentration range of 0.5 µg/L to 100 µg/L. A blank sample, composed of the 5% HNO_3 matrix, was measured every ten to fifteen samples. Blanks were used to verify sufficient washout time between sample runs and to monitor drift during instrumental analysis. Instrument calibration used standards ranging from a concentration of 0 to 100 µg/L. High-quality standards were prepared from SPEX CertiPrep Multi-Element Solution 2A diluted into 5% HNO_3. Calibration curves with an R^2 of .999 or higher were used in combination with blank subtraction and dilution factors to convert uncorrected instrumental values to concentrations.

3.3 Results

The results of this study are divided into three locations where each sediment core was sampled. Each sample site is located near a groundwater handpump and within an area of use by

a local community. Each analyte at every location was summarized into individual five-number summaries. Each one found in the appendix.

3.3.1 Lowland Swamp

Samples cored from the initial Site1 location were cored from a lowland swamp, where previously sampled groundwater showed elevated manganese in solution. Groundwater sampling characterized soluble manganese well above, at the time, WHO Guidelines for manganese in drinking water. Manganese was found to be 622μg/L in the pore water. The site was thought to be potentially comprised of an abundance of manganese minerals due to the high manganese concentrations in the pore water. Table 3.1 characterizes the soil acidity. The soil pH trends to acidic levels with depth. Near-surface pH values are circumneutral while values at depth reach pH values of 4.6. Figure 1 describes the SOM with descending depth. A visible trend that shows the percentage of organic matter gradually increases with depth, even as depth descends past groundwater. Figure 3.2 graphically describes the five-number summary for SOM above and below groundwater. Relating an increase of SOM below the groundwater. The sediments' carbonate material is shown not to have a clear trend with Figure 3.1. Though Figure 3.2 uses the five-number summary to show that there is a higher average percent of carbonate material below the water table.

Figure 3.6 demonstrates the abundance of various species of manganese sampled from Site1's sampled core. The figure shows manganese is present in large quantities in various solid species, with the most prevalent speciation occurring as manganese oxides. Organic matter and carbonates phase species are also at noticeably high concentrations. At near-surface,

concentrations decrease steadily with depth. Below groundwater (45-50 cm), concentrations rapidly decline to near zero. Figure 3.7 depicts manganese absolute concentration and concentration per phase, by depth, in each core. While the lower plot of Figure 3.7 illustrates the fractional percentage of manganese concentration by phase. Analysis shows manganese exist in high levels in the surrounding soil, but unlike the other analytes, it is not concentrated in the organics. Manganese exists heavily in its oxide form (MnIV) but also as an exchangeable divalent cation (Mn^{2+}).

Figure 3.8 indicates uranium speciation and depicts solid uranium concentrations that are most viable in the carbonate phase along with the soil organic matter. Figure 3.8 shows an increasing trend with depth. Surface concentrations are near zero and gradually increase until groundwater is reached. At a saturated depth, uranium values take a significant jump in solid concentrations. The upper plots of Figure 3.9 illustrate the absolute concentrations of uranium observed at the lowland marsh. The plots further illustrate the mineral phase speciation of uranium obtained from sequential extraction experiments. The lower plots describe the uranium percentages found in each of these extracted phases confirming the analysis of Figure 3.9 that solid uranium concentration is mostly found in the organic and carbonate phases.

Vanadium speciation at the sampled site is described in Figure 3.10. Vanadium is mostly present while bonded to SOM showing a trend of decreasing concentration with depth. Absolute abundance and vanadium speciation percentage are both described in Figure 3.11. Vanadium concentrations are at significant levels throughout the soil profile; however, they are focused in the SOM.

3.3.2 Mining Hill

The sample cored near a mining hill, Site2, was done so at a decommissioned borehole. Groundwater previously sampled near location was found to have excessive levels of metals, most noticeably uranium. Previous studies characterized uranium at 420μg/L. The WHO guideline is 30 μg/L. The well was decommissioned due to poor quality. The entire set of lengths were added to the instrument during sampling of this core (266cm). Notably, groundwater was never reached. Soil acidity, as shown in Table 3.1, is maintained around pH 6 with near-surface depths hitting slightly acidic pH values. Figure 3.1 shows the percentage of SOM and carbonate material. While Figure 3.3 illustrates the five-number summary of SOM and carbonate material. Depth correlations with organic matter and mineral carbonate are not observed.

Manganese is shown to be elevated at this location, though not at the same concentrations observed from the previous site. Figure 3.12 indicates significant amounts of manganese in the oxide form relative to other species. The depth-resolved absolute concentrations and speciation of manganese are given in Figure 3.13.

What little uranium found on the solid is focused on the organic and carbonate phases. Figure 3.14 illustrates the uranium speciation and concentration for site Site2. Figure 3.15 describes the absolute concentration and percentage of uranium speciation further describing what is seen in Figure 3.14.

Figure 16 reveals vanadium trending with depth. Vanadium is mostly bound to the organics but also with the oxides. Figure 3.17 further breaks down vanadium concentration and speciation with depth.

3.3.3 Agricultural Field

The sample taken from an agricultural field was cored from a setting without prior data. Not much was known about this site. Water produced at this site is described as having a salty taste and aesthetically unpleasing appeal. A 67 cm core was sampled, where groundwater was reached at depths of 33-40cm. Table 1 shows the inclination of the soil pH to increase with depth. Depths above the groundwater contain acidic soils while neutral soils persist below. Figure 3.4 details the SOM and carbonate material at this site. Further illustrated by Figure 3.5, The boxplot of the five-number summary shows the sediments above groundwaters as having higher percentages than those below groundwater. SOM and carbonates decrease with depth with some outliers observed at groundwater.

Manganese observed at this site is far lower in solid concentrations than in the previously examined locations. Figure 3.18 illustrates the perceived manganese solid concentrations found in the agricultural field. Figure 3.19 outlines manganese speciation with depth also recording that most manganese is found in the oxides. Uranium, at this location, is also present at low values on the solid; however, it does decrease with depth as shown in Figure 3.20. Figure 3.21 shows uranium movement with depth as absolute concentrations and uranium speciation. Solid vanadium behaves similarly with depth as described in Figure 3.22. Vanadium is only observed

in two phases at this location. From Figure 3.23, vanadium is associated with the oxides and is bound to the organic fraction.

3.4 Discussion

Chemical analyses define several geochemical trends within the Bugesera subsurface. Many relationships are consistent with the known geochemistry of individualized analytes. However, results are not constant across all sites for each subsurface expression. The three sites, examined in this study, each express the variability of concerning elements' bioavailability in a manner unique to the localized subsurface area. Five-number summaries of each analyte from all three locations are given in the appendix.

3.4.1 Manganese

Site1, the lowland swamp, is overwhelmed with manganese in the soil and groundwater. Solid manganese is mostly observed as an oxide with concentrations steadily decreasing with depth. At groundwater, (45-50 cm), solid manganese levels descend rapidly. Soil pH levels above groundwater are 6 and above. At these pH levels, under oxidizing conditions, manganese is known to form solids. Accordingly, Figures 3.6 & 3.7 show heavy manganese presence in oxides and organic matter. In acidic and or reducing soils manganese is highly soluble, this being observed in Figures 3.6 & 3.7 also. At and below groundwater, soil pH turns acidic simultaneously with manganese solid concentrations nearing zero. This transition most likely records solid MnO_2 reducing to soluble $Mn^{2+}$with depth. The difference in solid Mn found above and below the groundwater was tested to be statistically significantly different with 95% confidence according to t-Test Appendix Table 11-14.

At the mining hill location, manganese is present and found mostly in the oxides, (Figures 3.12 & 3.13) but not in the solid concentrations seen previously at the manganese inundated swamp. Soil acidity hovers around a pH 6, Table 3.1, optimal pH for manganese to form solid complexes. The carbonate and organic matter at this location are low which is why manganese oxides are the most abundant solid complex (Figures 3.1 & 3.3). In this sample, the reduction of MnO_2 to Mn^{2+} is not observed though it is likely the reducing process is taking place at deeper depths once groundwater is reached.

The manganese interactions at and around the water-table denote a groundwater barrier for a redox shift in the subsurface environment. Depths above groundwater are an oxidizing environment, while the saturated zone presents reducing conditions. The groundwater table is observed at both the lowland swamp and the agricultural field (Figures 3.6 & 3.18). Though the sediment core obtained from the Site3 location was sampled past the groundwater table, similar geochemical tendencies as the lowland sample are not recorded. Solid manganese is present at far lower concentrations than previously examined. High levels of near-surface SOM would indicate plenty of organic complexes for manganese to bind with at surface. The soil pH above groundwater in the oxic zone, however, is too acidic for manganese complexation promotion. Thus, manganese is far more soluble in this area and is not found in mineral form at the same levels in preceding regions. It is likely, therefore, that Mn is soluble above the water table due to acidity and below the water table due to the redox condition.

3.4.2 Uranium

Figures 3.8 & 3.9 describes uranium concentration, at the marshland, with depth. Noting that solid uranium is not heavily present until groundwater. Uranium is soluble under oxic conditions and highly insoluble in reducing ones. There is a change of uranium (VI) to uranium (IV) in the reducing environment. This redox driven solubility shift is shown through the significant uptake in uranium concentration with depth observed in Figures 3.8 & 3.9. With 95% confidence it is concluded that there is a statistically significant difference between U above and below the groundwater (Appendix Table 15-18).

The core taken from the mining hill was appropriated in a region where previous analysis noted substantial groundwater uranium. It is believed that this region sits atop parent granite rock, a potential source of considerable amounts of subsurface uranium. Given that the core, sampled at this location, did not reach groundwater, it was not expected to see a redox shift in the subsurface environment. Figure 3.14 depicts a near absence of solid uranium. Uranium being highly soluble under oxidizing conditions is consistent with a lack of observed solid-phase uranium. It is highly likely that the uranium here is present in the pore water and as U(IV) in the deeper reducing environment.

Unlike the first locations sampled; uranium is nearly completely absent from the reducing environment found in the agricultural field subsurface. As noted in Figures 3.20 & 3.21. This is most likely due to this region not sitting atop granite parent material (Dewaele et al., 2010; Ghehi et al., 2012)

3.4.3 Vanadium

Vanadium throughout the marshland region is found bound to organic matter. Solid vanadium concentrations decrease with depth, even past groundwater (Figure 3.10). The reducing conditions and the increase of SOM, at depth, does not change the declination of solid vanadium. Vanadium's solubility seems to be more affected by the increasingly acidic soil pH, (Table 3.1 & Figure 3.11). Reducing conditions promote a reduction of vanadate V(V) to vanadyl V(IV), increasing the ion's solubility (Bredberg et al., 2004). Further, V (V) reduction to (IV) increases the ions sorption propensity to SOM (Reijonen et al., 2016). Both trends are supported by the low solid concentrations and the percentage of V in SOM shown in Figures 3.10 & 3.11. These trends are tested and proven with 95% confidence to be statistically significant according to t-Test (Appendix Table 19-21).

In the subsurface of the mining hill region, vanadium is complexed on organic matter, and found in lesser concentrations on the oxides. With depth, levels are decreasing on SOM and increasing on the oxides, Figures 3.16 and 3.17. This is most likely because of the decrease in organic material with depth. Figure 3.1 depicts a slight decrease with depth for SOM at this location.

In the agricultural field, solid vanadium is seen declining in both SOM and oxides. The declination can be attributed to the depth of diminishing organic material and the increase in soil pH. A neutral to high pH means vanadium is more soluble, which is likely happening with vanadium downturn at depth. It is also likely that a reduction of vanadate to vanadyl is taking place after the environmental redox shift. Figure 3.22 displays this noticeable subsurface activity.

The collected samples demonstrate the diverse sediment and soil profiles within Bugesera. The hypotheses of unique and significant trends, with depth, per elemental speciation, were tested using a t-test with unequal variances. T-test indicates that there are statistically

differing spatial trends, with depth per heavy metal, from each sampled location. These t-tests are completed with 95% confidence and can be found in Appendix A (Appendix Table 10-21). It is expected to see differences in elemental expressions between saturated sediment samples where groundwater is reached in one and a completely dry sample in the other. However, the dissimilarities between saturated sediments collected in redox changing environments were visible. This hypothesis was also proven using the t-test (Appendix Table 22-32). Differentials in elemental expressions by these sediments are caused most notably by the changing soil acidity and other physicochemical parameters. The changing soil pH combined with the depth varying presence of SOM, carbonate material and redox shifting environments are controlling factors for the highly differing elemental expressions in a relatively small spatial setting. Figure 3.1 describes SOM increasing in concentration with depth for the lowland swamp and the mining hill regions. This trend, however, is not observed in the agricultural region as shown in Figure 3.4. From the topsoil down, there is a decrease in the SOM in the agricultural subsurface. Other notable reasons to the differing subsurface expressions are, the absolute abundance of elements and physiochemical material in the subsurface as well as parent rock material. Shale is a predominant parent rock material in the subsurface of the agricultural field (Ghehi et al., 2012).

3.6 Conclusion

Rwanda's Bugesera region uniquely differs from the country's more tropical climate regions. It, however, is no less important to Rwanda's future economic development. Construction is already underway for a second international airport in Bugesera making regional development the next step for Rwanda's progress as an East African hub. With land development comes public health and safety concerns. Transitioning Bugesera from an agrarian municipality to a land developed region means potential for the environmental release of toxic bioavailable

chemicals. Bugesera development is a necessary progressive step, especially considering its exceptional place in recent Rwandan history. Nevertheless, precautions must be taken with future development. The interpretations of subsurface geochemical expressions described in this study will go a long way into future land development in Bugesera.

3.7 Figures and Tables

Table 3. 1) Location Soil Acidity. The sampled depth at each investigated site and the associated measured soil pH.

Soil Acidity					
Site1		Site2		Site3	
Depth(cm)	**pH_{kcl}**	**Depth(cm)**	**pH_{kcl}**	**Depth(cm)**	**pH_{kcl}**
5-10	7.2	**3-28**	6.3	**3-8**	5.4
10-15	6.3	**33-58**	5.7	**9-13**	5.0
15-20	6.3	**64-88**	5.9	**13-20**	5.2
20-25	6.2	**88-116**	6.0	**20-27**	5.4
25-30	6.1	**121-146**	5.9	**27-33**	5.5
30-35	5.8	**151-176**	6.1	**33-40**	6.1
40-45	6.2	**181-206**	6.0	**43-53**	6.3
45-50	6.0	**211-236**	6.0	**53-63**	6.4
50-55	5.8	**236-266**	6.1	**63-67**	6.4
55-60	5.6				
62-67	5.6				
67-72	5.4				
72-77	5.0				
77-82	4.7				
82-87	4.7				

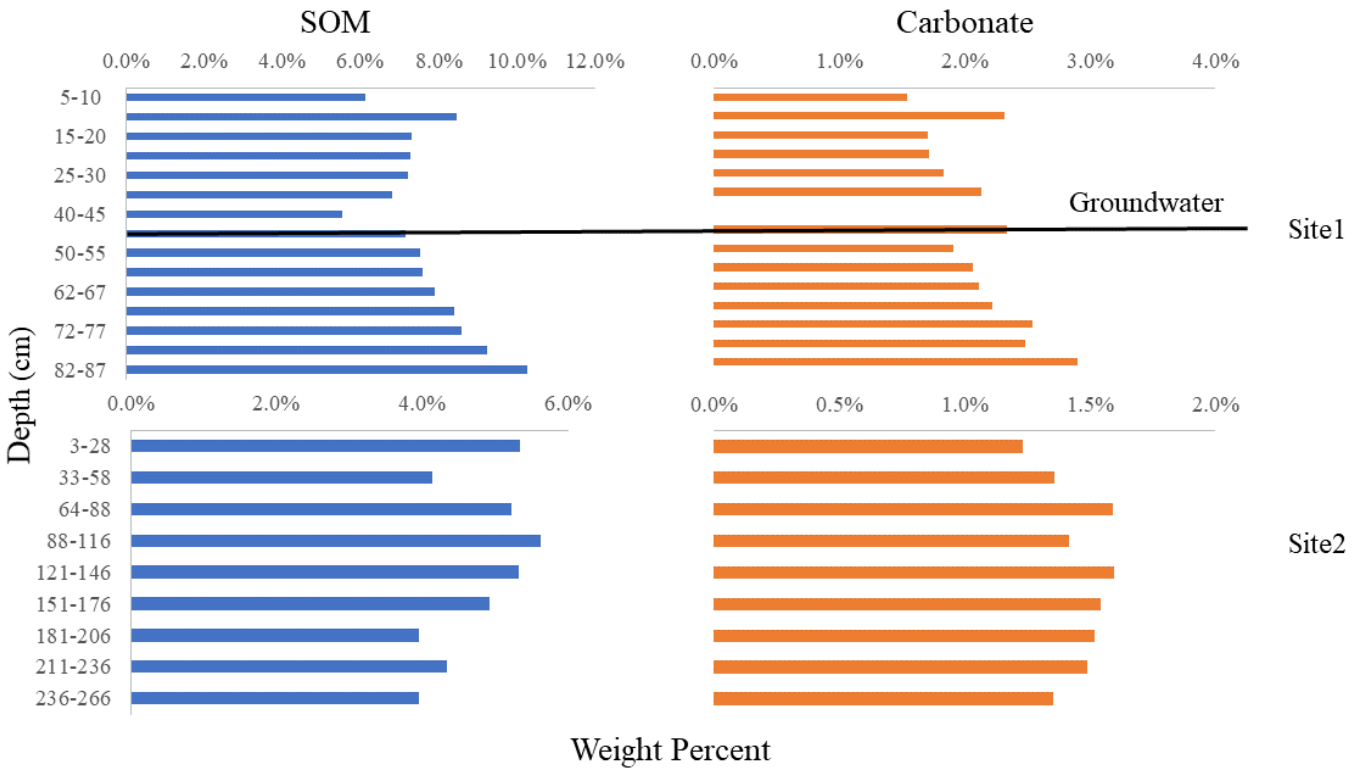

Figure 3. 1) SOM & Carbonate Material at Site1 and Site2. Depth-resolved organic and carbonate fractions of sample Sites1 & 2. At Site1, groundwater was reached at a depth of 45-50 cm and is indicated with the black horizontal bar. Groundwater was not obtained at measurable depths for Site2.

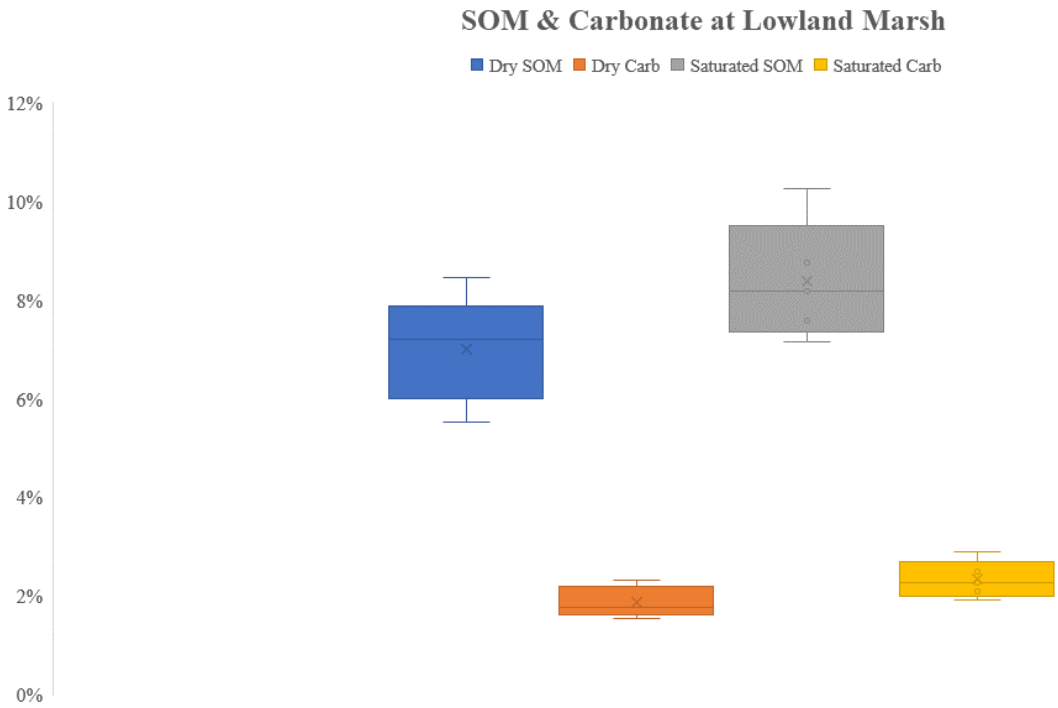

Figure 3. 2) Error of SOM and Carbonate Material at Lowland Marsh. The boxplot gives the five-number summary for SOM and carbonate material. The separation of data points is determined by SOM and carbonate material above and below groundwater

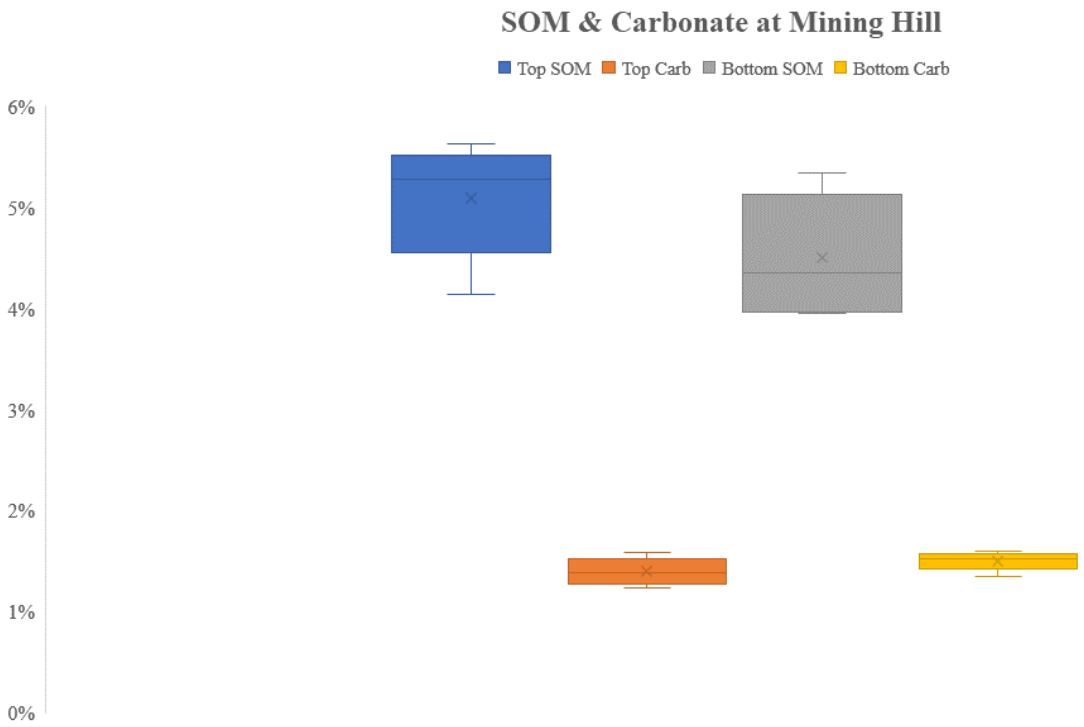

Figure 3. 3) Error of SOM and Carbonate Material at Mining Hill. The boxplot gives the five-number summary for SOM and carbonate material. The boxplot gives the five-number summary for SOM and carbonate material. Groundwater was not reached at this location. Data is separated by the top 116cm being the top half of the sample. The remaining 150cm being the bottom half.

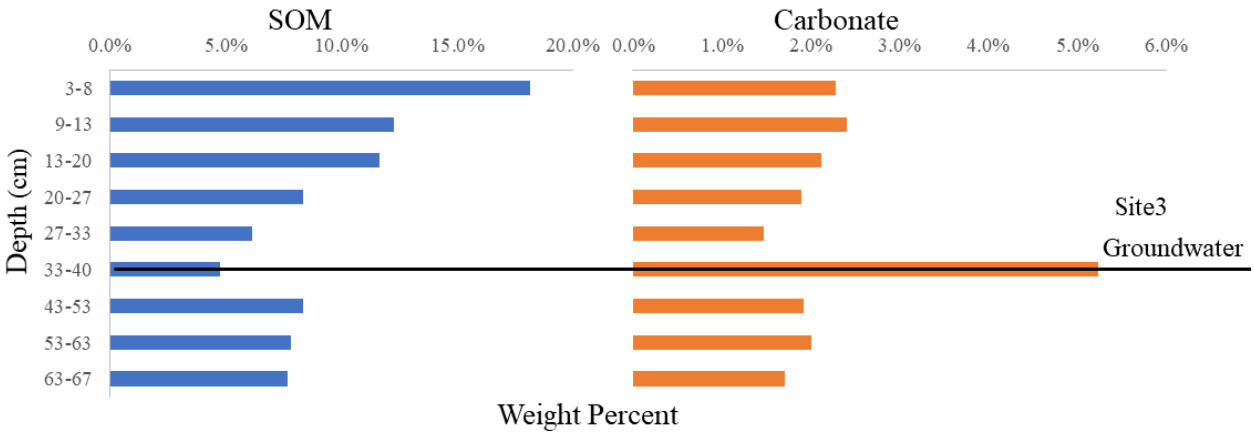

Figure 3. 4) SOM & Carbonate Material at Site3. Depth-resolved organic and carbonate fraction of sample Site3. Groundwater was reached between a depth of 33 and 40 cm and is indicated with the black horizontal bar.

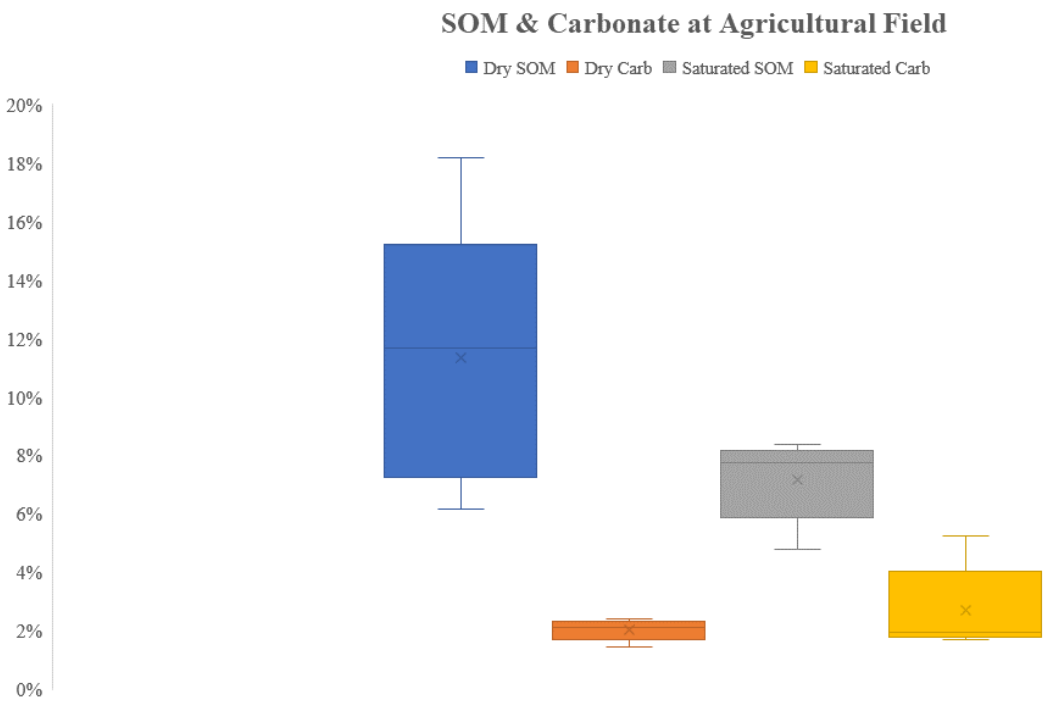

Figure 3. 5) Error on SOM and Carbonate Material at Agricultural Field. The boxplot gives the five-number summary for SOM and carbonate material. The separation of data points is determined by SOM and carbonate material above and below groundwater.

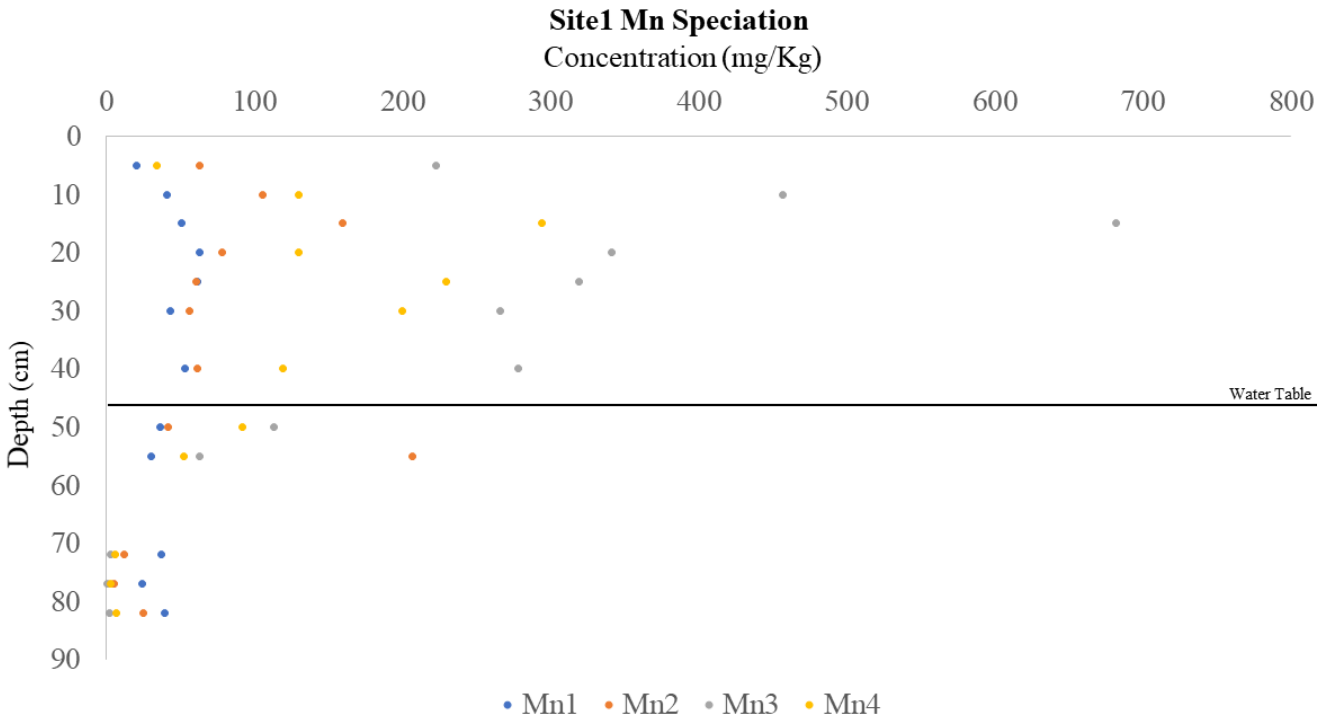

Figure 3. 6) Mn concentrations at Site1. Depth-resolved Mn speciation at Site1. Water-table is between 45-50 cm below surface and is indicated with the black horizontal bar.

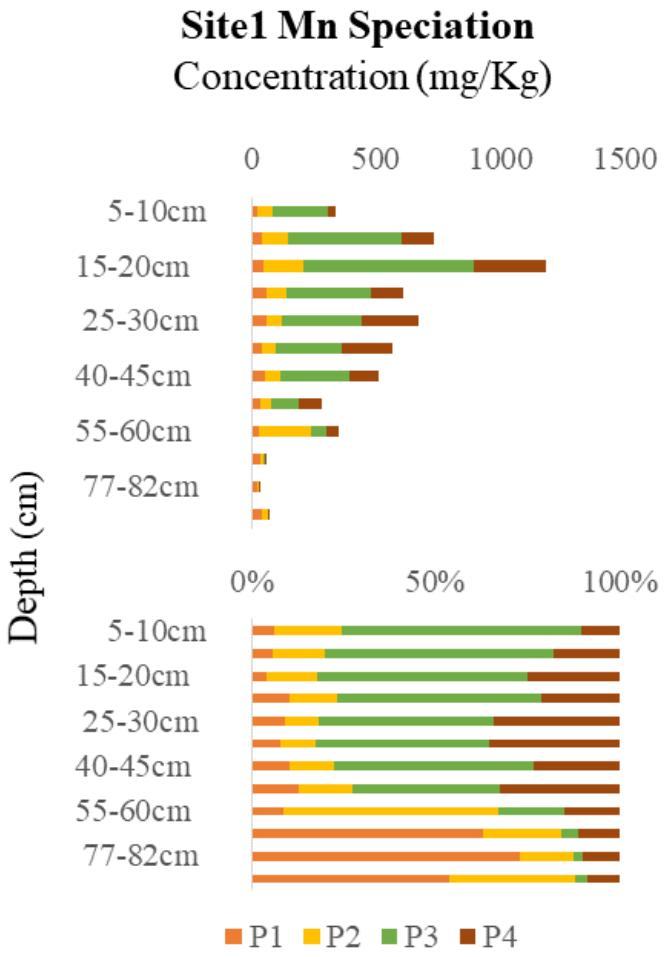

Figure 3. 7) Mn speciation at Site1. The top panel shows the total concentration of manganese species with depth. The bottom panel describes the percentage of manganese species with depth.

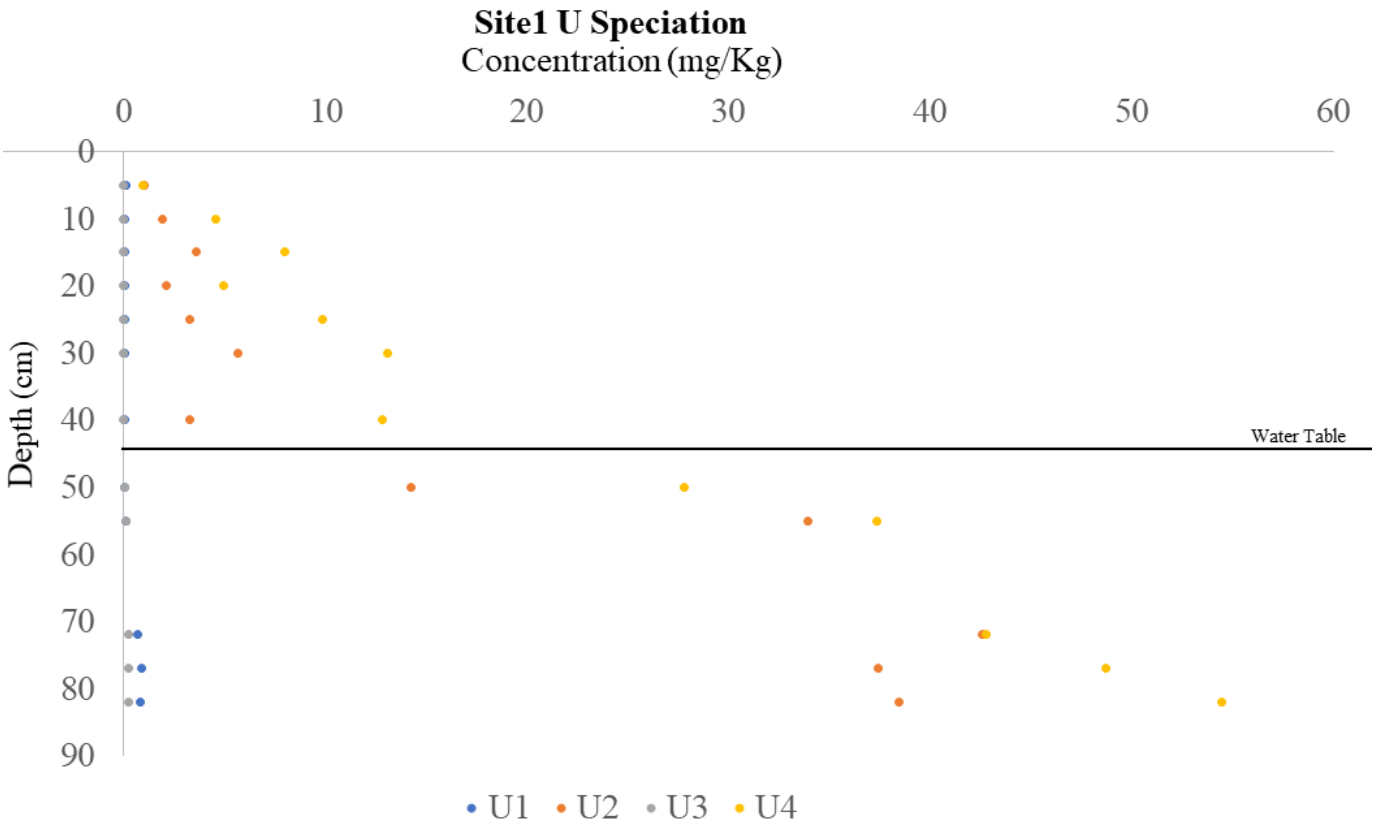

Figure 3. 8) U concentrations at Site1. Depth resolve uranium speciation at Site1. Water-table is between 45-50 cm below surface and is indicated with the black horizontal bar.

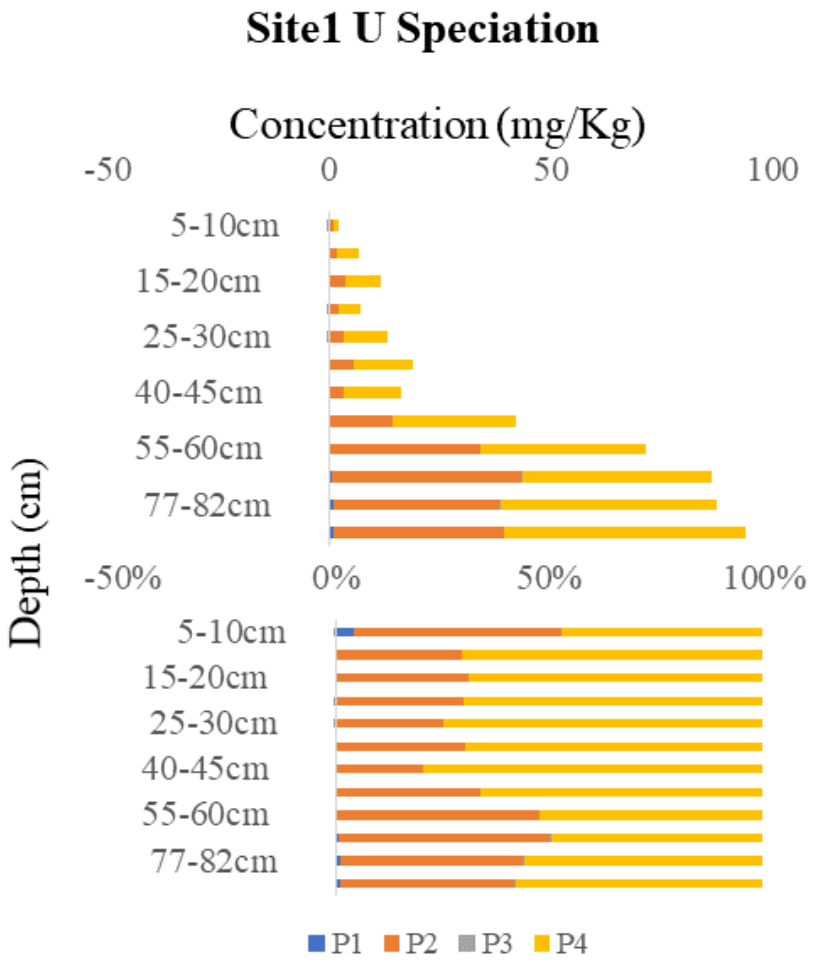

Figure 3. 9) U Speciation at Site1. The top panel shows the total concentration of uranium species with depth. The bottom panel describes the percentage of uranium species with depth.

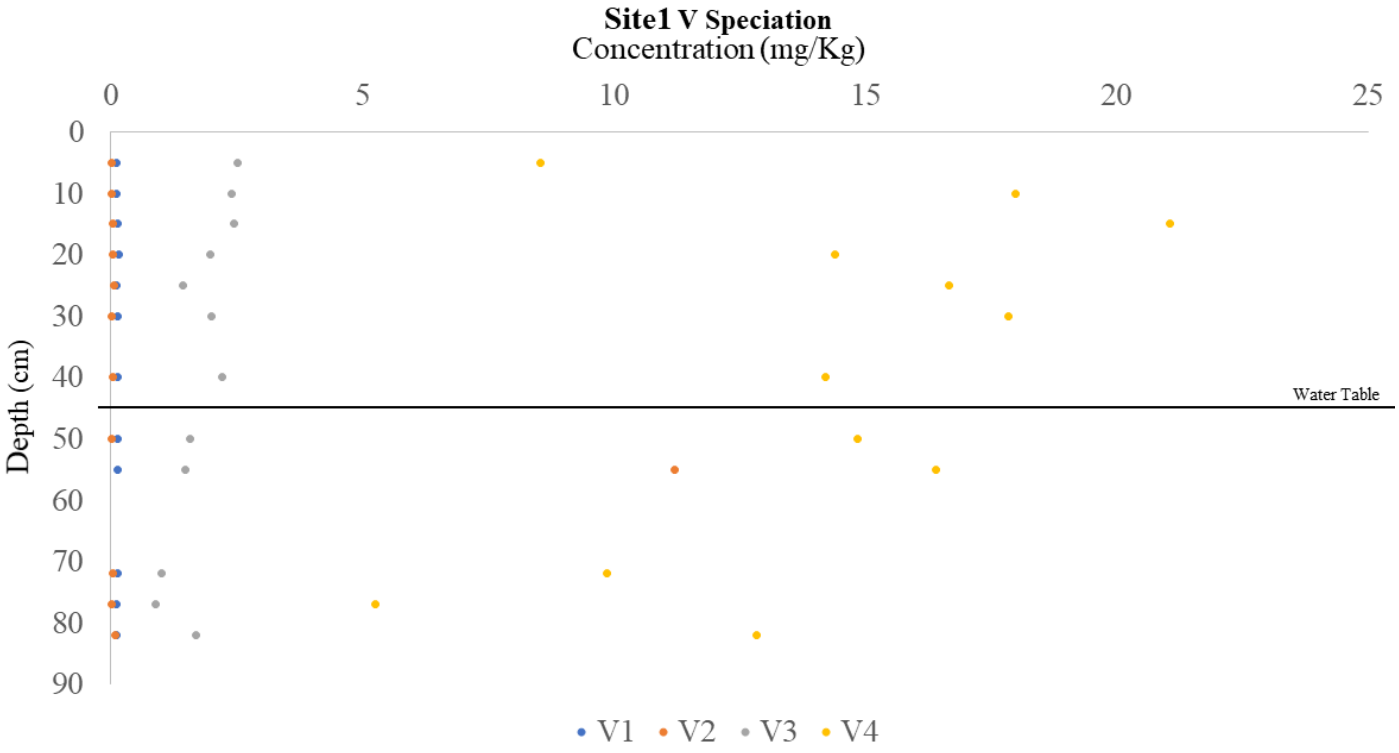

Figure 3. 10) V concentrations at Site1. Depth resolve vanadium speciation at Site1. Groundwater is between 45-50 cm below surface and is indicated with the black horizontal bar.

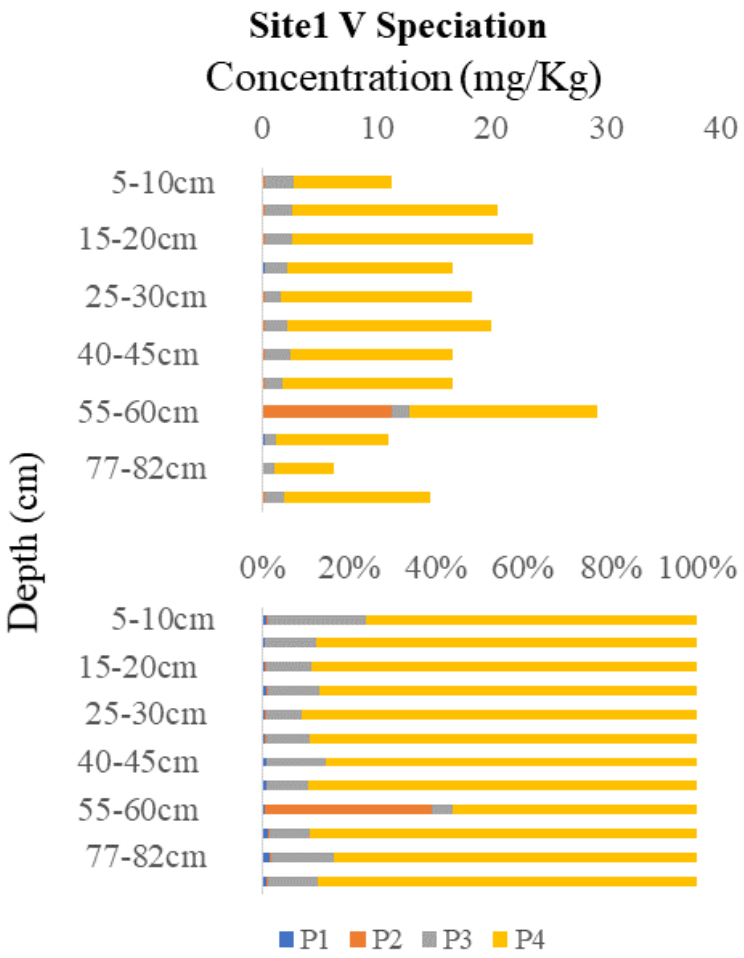

Figure 3. 11) V speciation at Site1. The top panel shows the total concentration of vanadium species with depth. The bottom panel describes the percentage of vanadium species with depth.

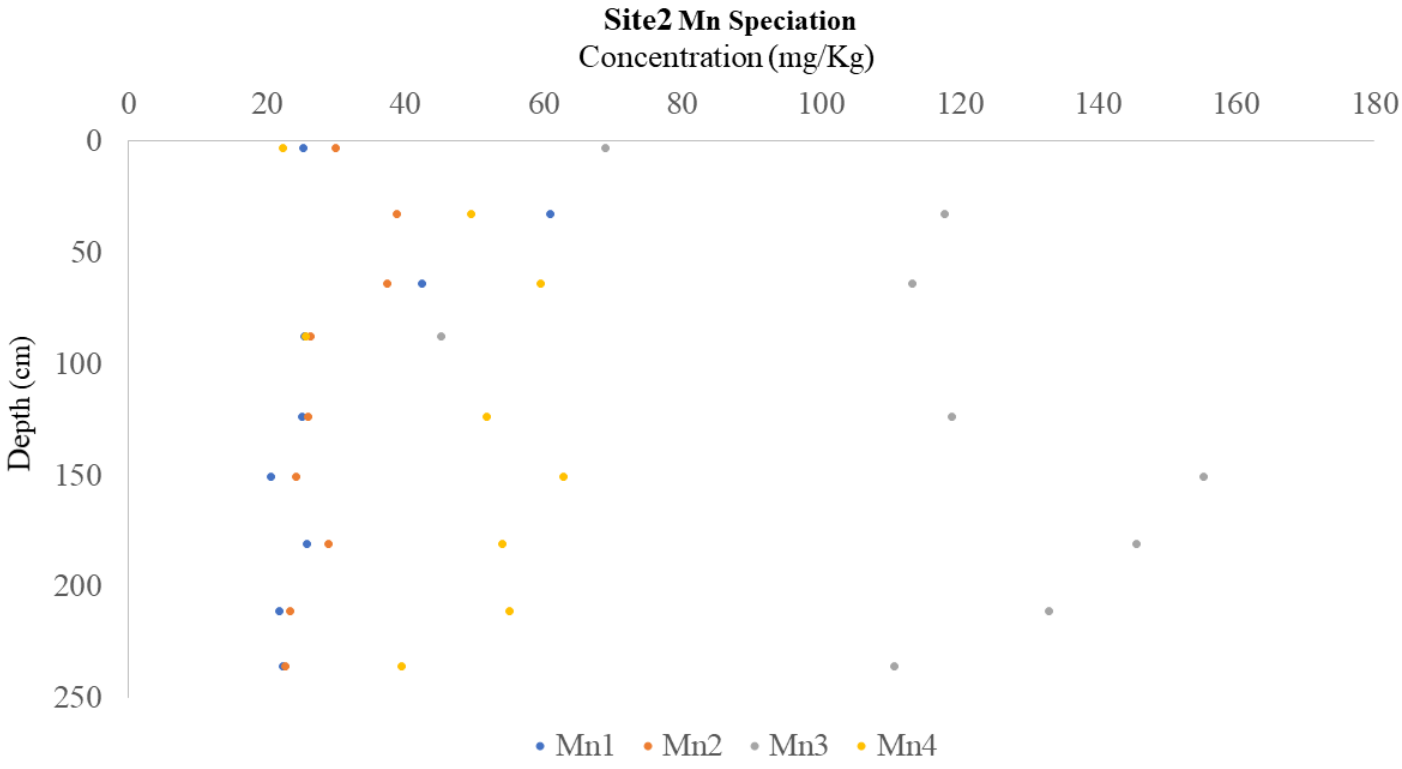

Figure 3. 12) Manganese concentrations at Site2. Depth-resolved manganese speciation for sample Site2. Water-table was not found during sampling.

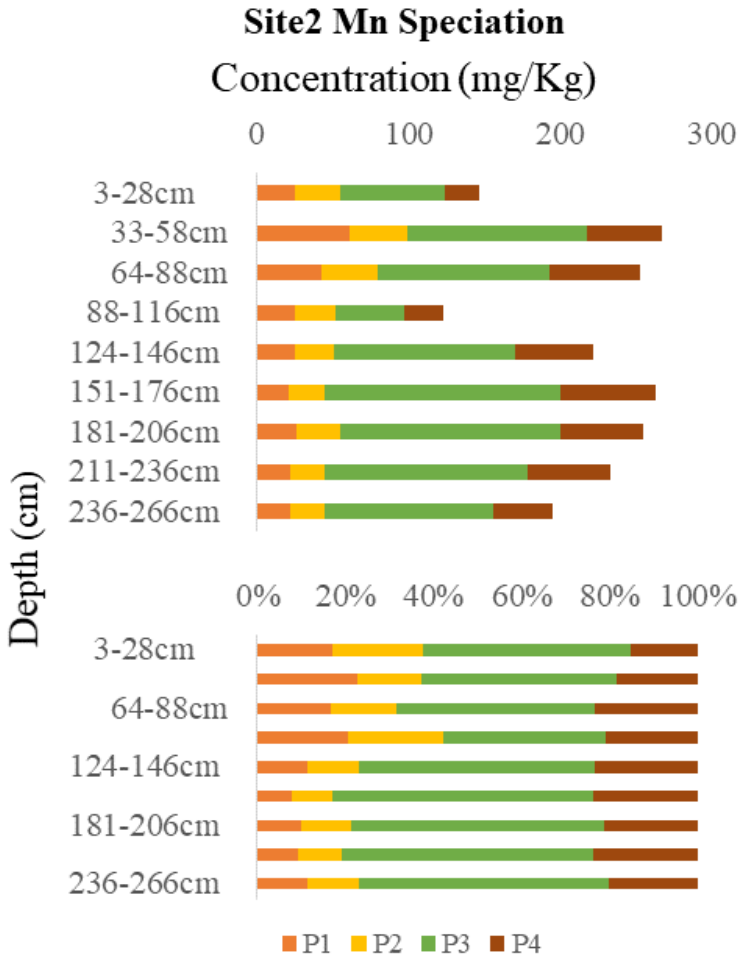

Figure 3. 13) Mn speciation at Site2. The top panel shows the total concentration of manganese species with depth. The bottom panel describes the percentage of manganese species with depth.

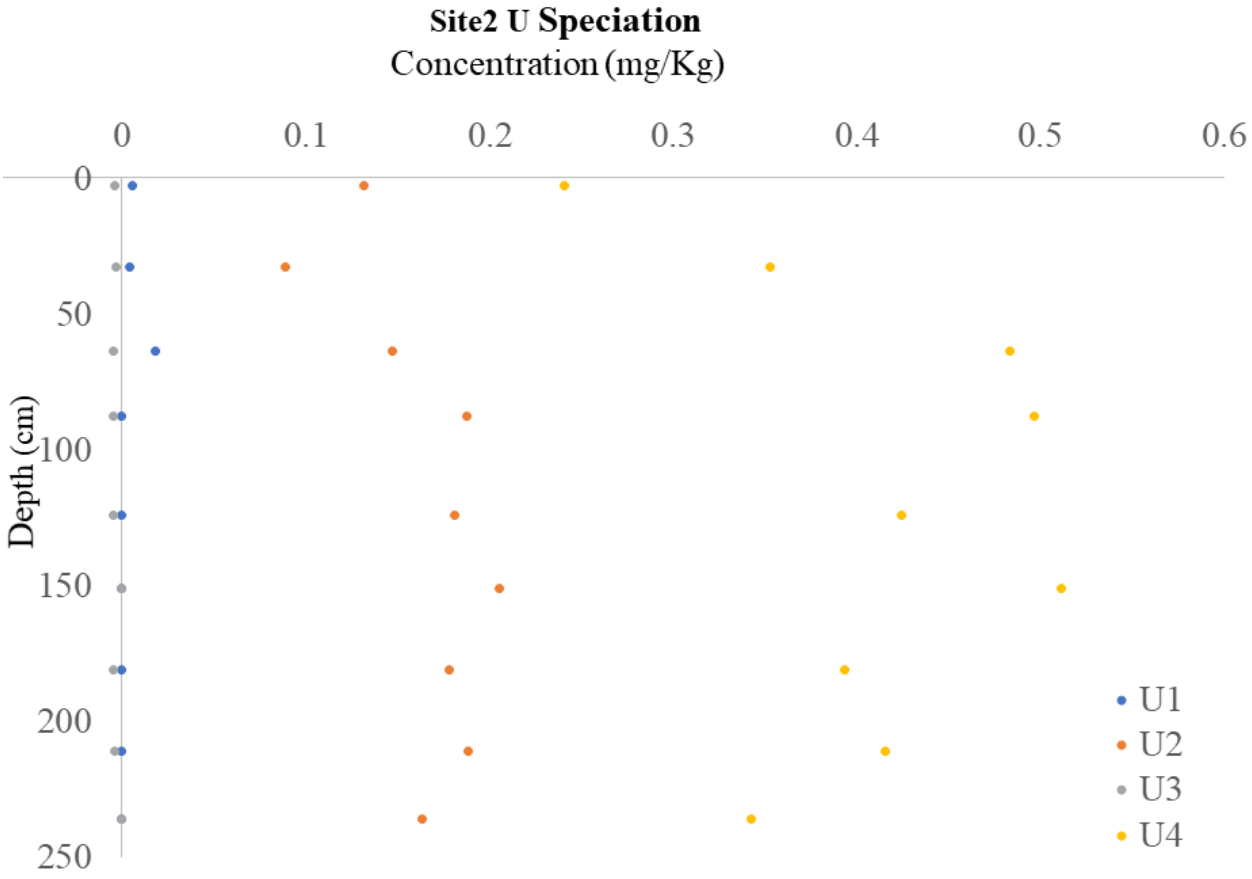

Figure 3. 14) U concentrations at Site2.Depth-resolved uranium speciation for sample Site2. Water-table was not found during sampling.

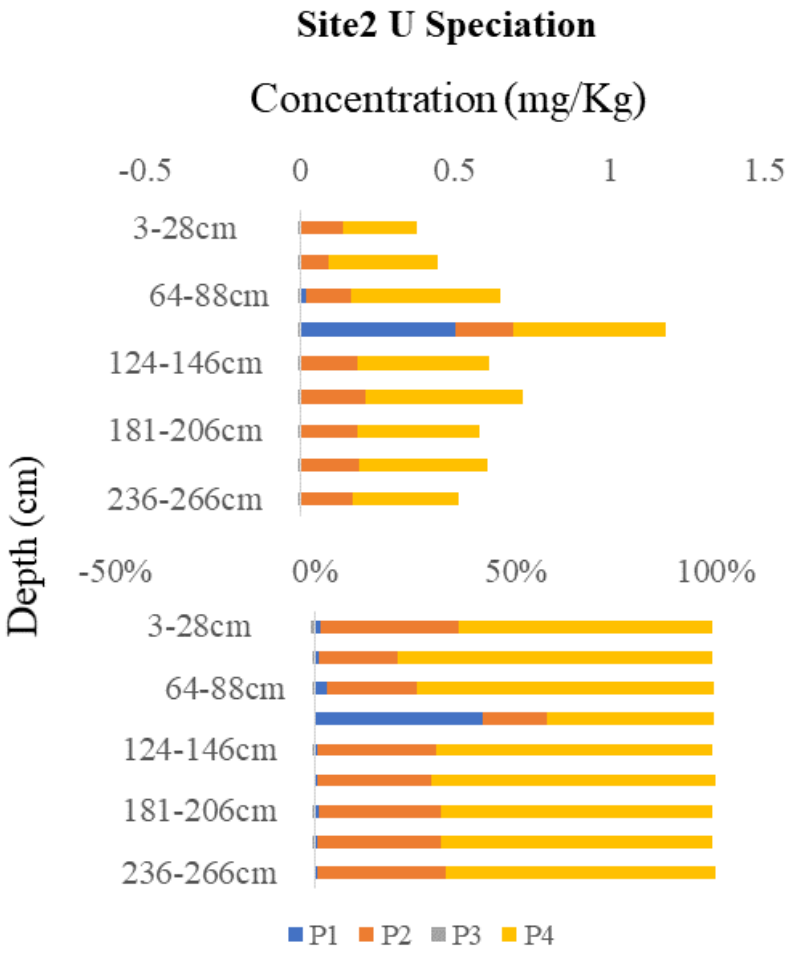

Figure 3. 15) U speciation at Site2. The top panel shows the total concentration of uranium species with depth. The bottom panel describes the percentage of uranium species with depth.

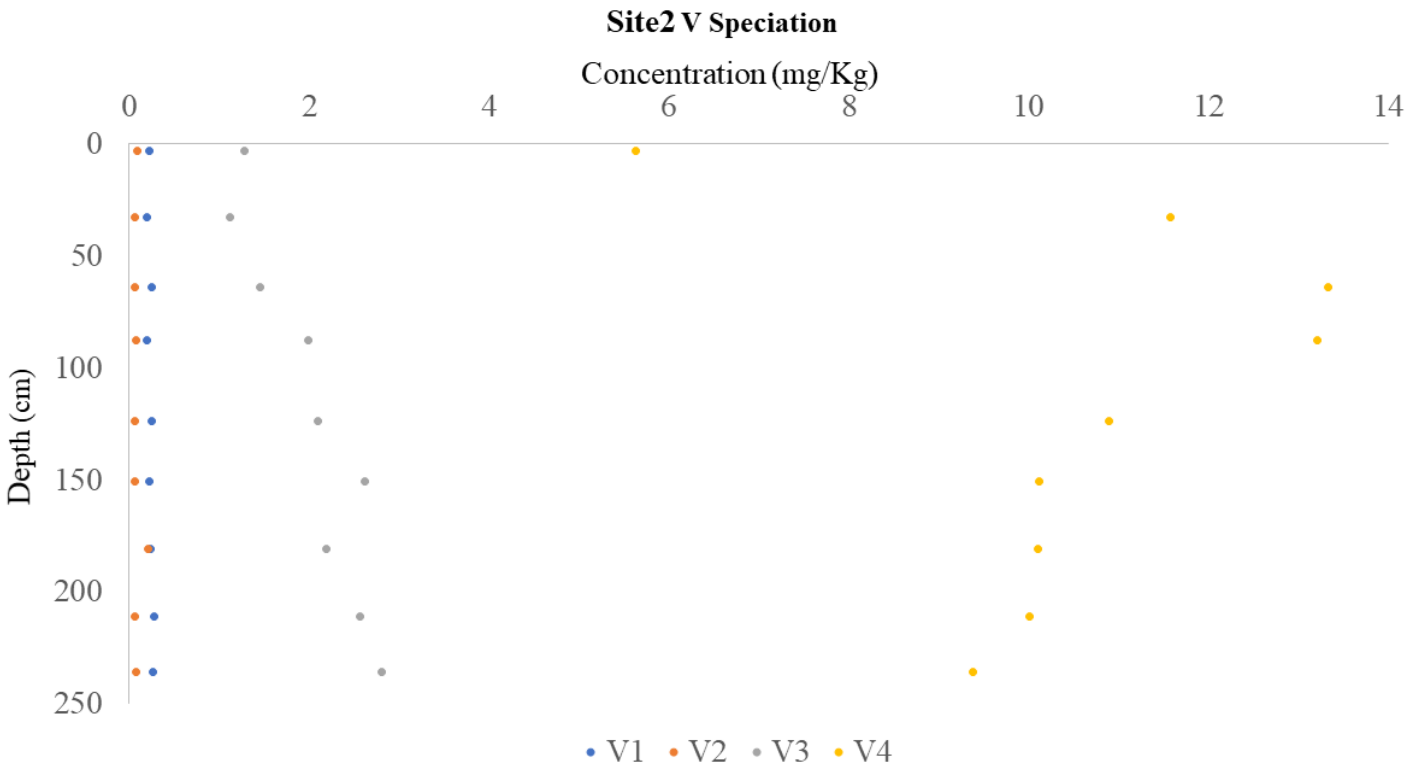

Figure 3. 16) V concentrations at Site2. Depth-resolved vanadium speciation for sample Site2. Water-table was not found during sampling.

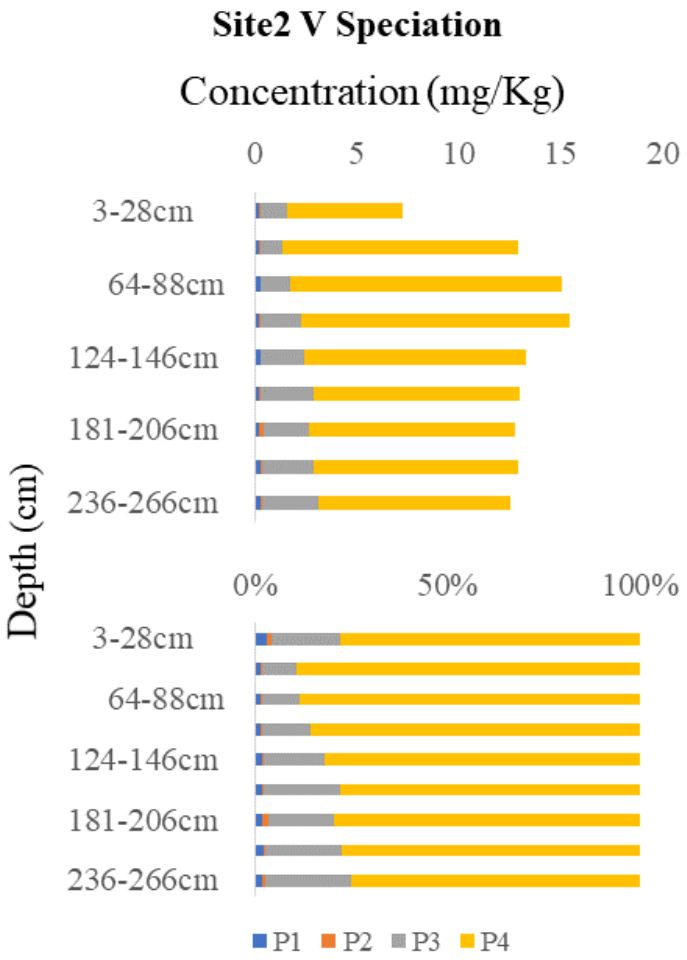

Figure 3. 17) V speciation at Site2. The top panel shows the total concentration of vanadium species with depth. The bottom panel describes the percentage of vanadium species with depth.

Figure 3. 18) Mn concentrations at Site3. Depth-resolved manganese speciation at Site3. Water-table was measured between 33-40 cm below surface and is indicated with the black horizontal bar.

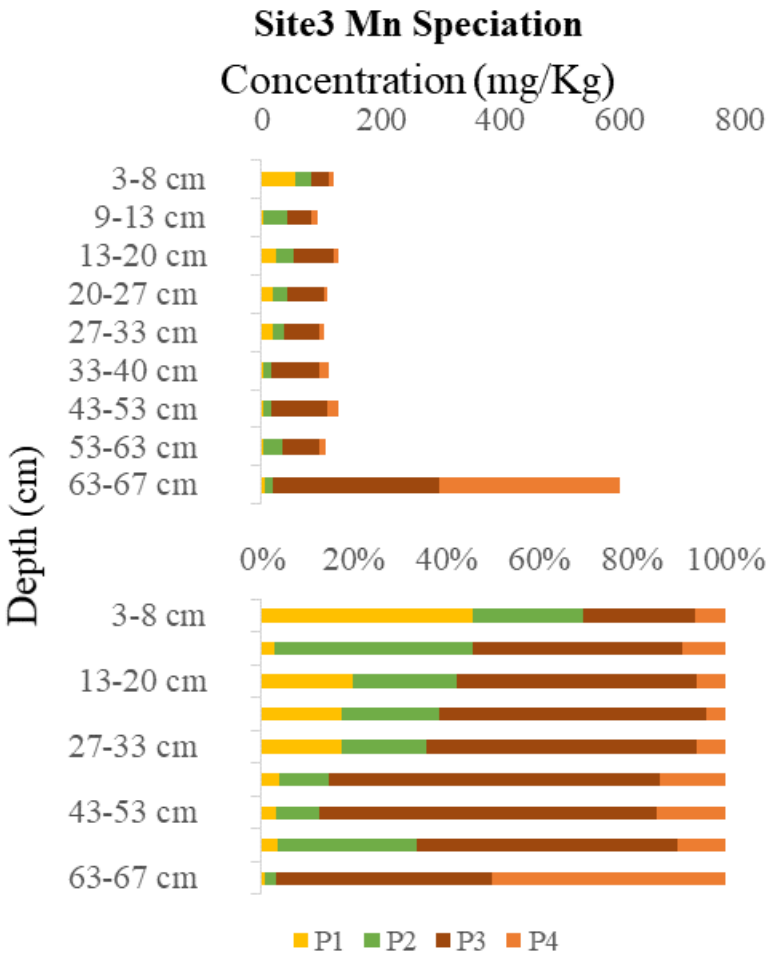

Figure 3. 19) Mn speciation at Site3. The top panel shows the total concentration of manganese species with depth. The bottom panel describes the percentage of manganese species with depth.

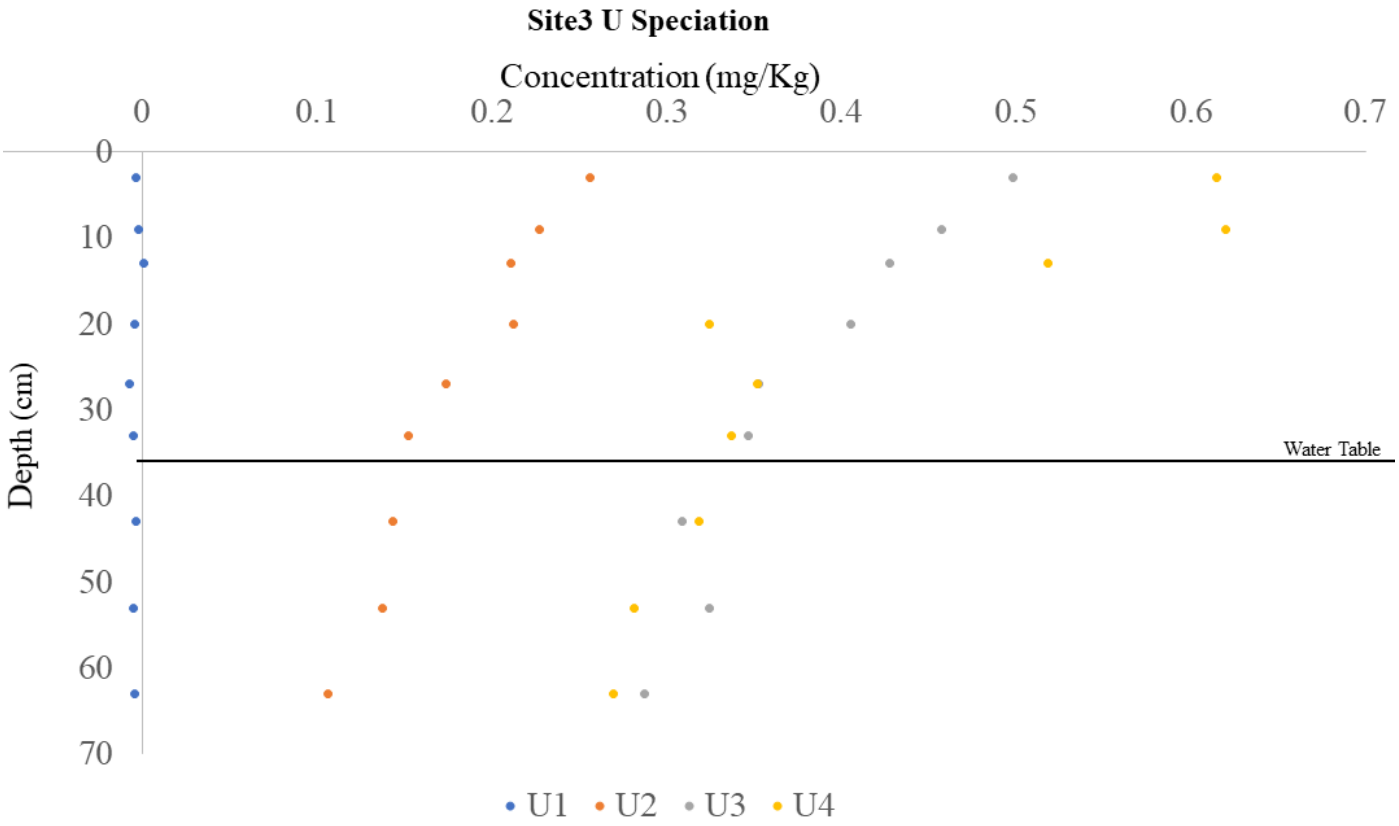

Figure 3. 20) U concentrations at Site3. Depth-resolved uranium speciation at Site3. Water-table was measured between 33-40 cm below surface and is indicated with the black horizontal bar.

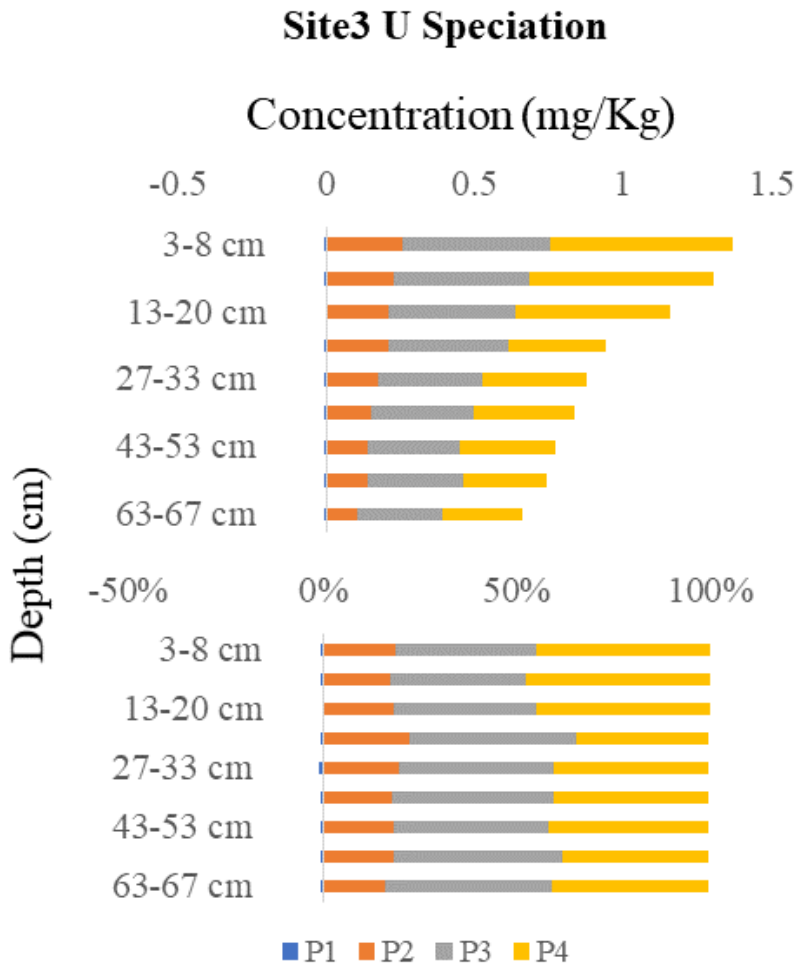

Figure 3. 21) U speciation at Site3. The top panel shows the total concentration of uranium species with depth. The bottom panel describes the percentage of uranium species with depth.

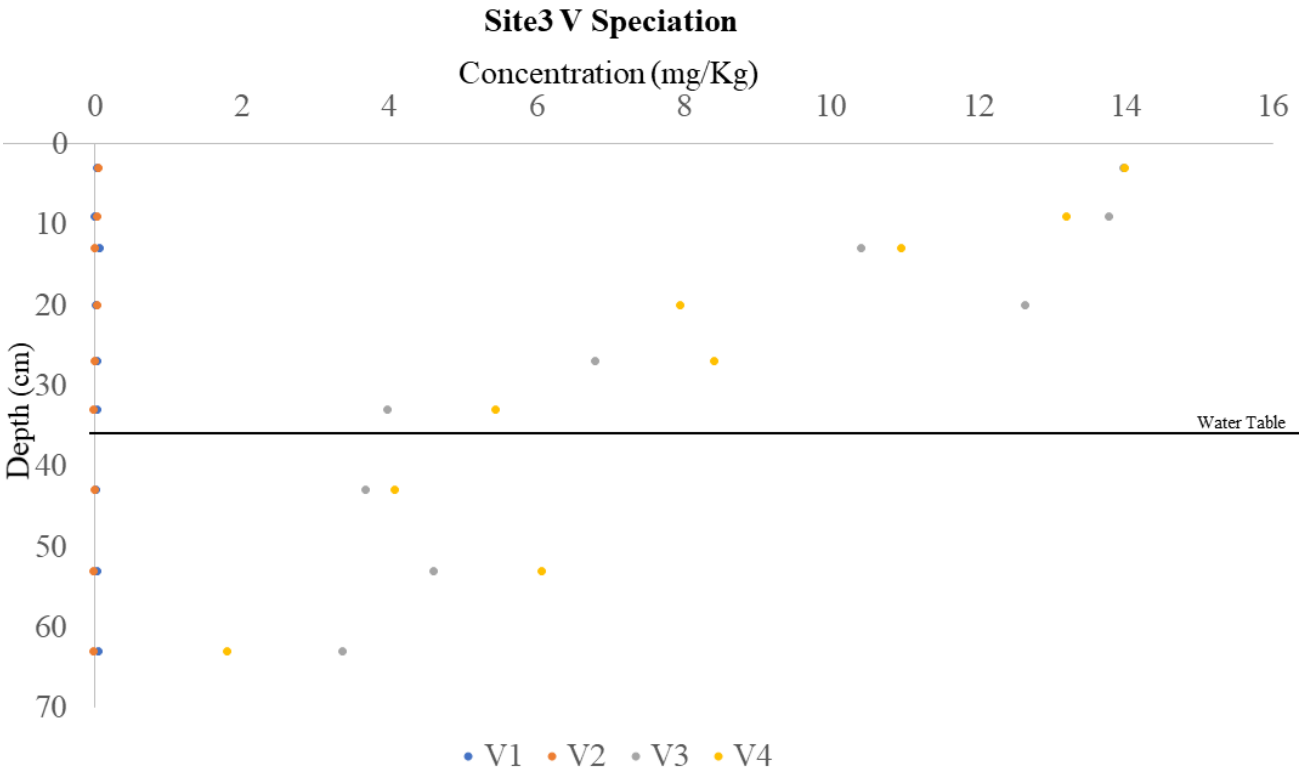

Figure 3. 22) V concentrations at Site3Depth-resolved vanadium speciation at Site3. Water-table was measured between 33-40 cm below surface and is indicated with the black horizontal bar.

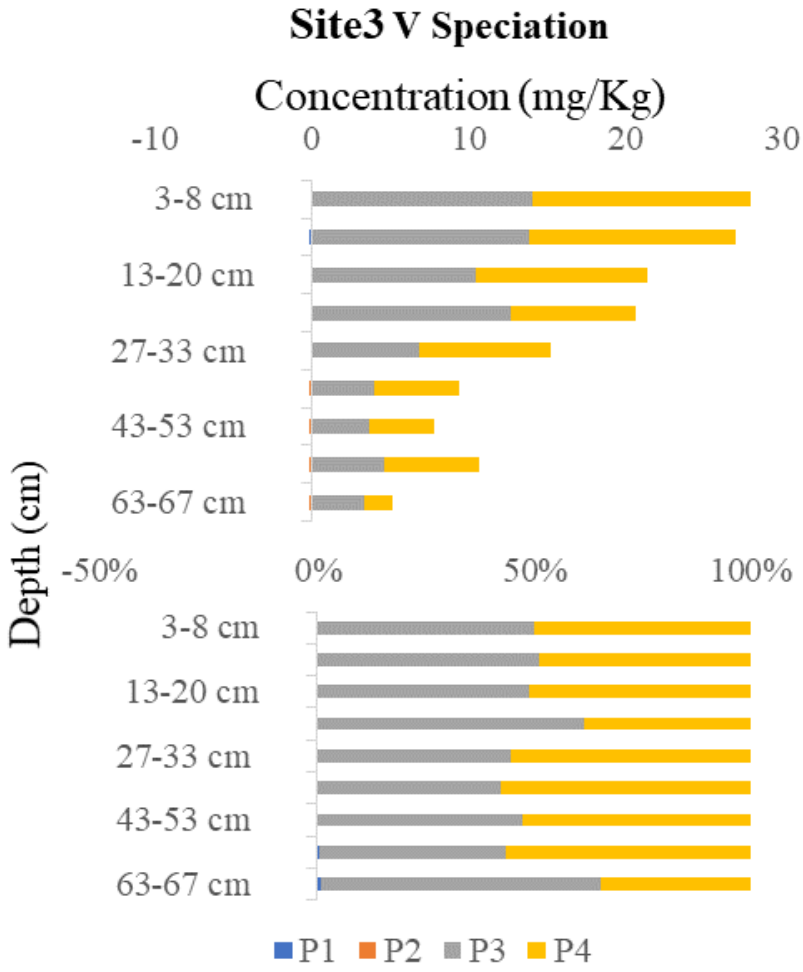

Figure 3. 23) V speciation at Site3. The top panel shows the total concentration of vanadium species with depth. The bottom panel describes the percentage of vanadium species with depth.

CHAPTER 4

Inherent Toxicity Through Dispersion of Sized Determined Dust Particles in Bugesera, Rwanda

To Be Submitted to *The Journal of Environmental Pollution*

Abstract

Soils from tropical environments have a noticeably greater ability to collect, retain, and concentrate heavy metals compared to soils from more temperate environments (Naidu et al., 1998). Indeed, natural weathering commonly associated with tropical soils leaves behind soils concentrated with trace and heavy metals (Rieuwerts, 2007). Therefore, either from naturally occurring or anthropogenic sources, tropical soils are a vast potential source for contamination release into the surrounding environment. Exposure pathways include, amongst others, dispersion of contaminated particles.

Though metal concentration levels are a concern, those concentrations do not assess the complete ecological or environmental risk of the associated metals. Ecological risk indices, described by Hakanson (1980) and Tomlinson et al. (1980) among others, provide a more accurate indication of the ecological risk presented by each metal and the combined contamination risk from the comprehensive metal load. Contamination factor (C_f), Pollution Load Index (PLI), and Potential Ecological Risk Index (RI) are typical indices used to determine the extent of heavy metal contamination in sediments.

Rwanda's Bugesera district hosts a variety of distinct weathered soils capable of producing fine sized dust particles. With these airborne particles, there is the possibility of widespread contamination to the environment and public health. Two distinct sites from the Bugesera region were sampled, collected, and subsampled for fine size particles (sub 75 μm).

Particles were analyzed for heavy metal concentrations. Ecological risk indices were then applied to the metal concentrations to fully evaluate potential hazardous risk. It was found that sub 75μm particles present the highest level of potential ecological risk. The largest potential risk, from a lowland marsh with cyclically saturated redox soil, is associated with Cu and Pb. While Cu, Pb, and Cd dominate the risk exposure found from an area with a deep vadose zone that is near consistently dry. This study not only highlights known problematic metal contaminations in the sediment, but also uncover lesser-known sediment contamination issues. In doing so, it highlights the dangers of fine size airborne particulate matter.

4.1 Introduction

Metal contamination and toxicity is a concern for communities in the process of modernization. Soils from tropical areas of the world experience higher levels of heavy metal availability attributable to the nature of tropical soils (Rieuwerts, 2007). Several factors influence the availability of trace and heavy metals in these soils. Weathering leaves behind aluminum and iron hydroxides with associated trace metals. This weathering process often drives soil pH change. Specifically, tropical oxisol formation is often coincident with acidic soils and varying amounts of organic material.

Release of heavy metals into environmental systems poses a potential hazardous risk, both ecological and from a public health perspective. However, total concentration is not a complete indication of metal contamination risk. A variety of ecological risk indices are used to evaluate and determine the potential hazard metal contamination poses on an ecological setting, and, by virtue, local populations. Ecological risk indices help determine the risk from a singular metal concertation as well as the combined risk of contamination.

Pathways for pollution exposure include groundwater contamination, contamination uptake by biota via the food chain, and contamination exposure via small particles, among others. Fine size particles, like dust particles, are a viable pathway for exposure and themselves contain a disproportionally higher concentration of heavy metals (Carpi, 1997; Kim et al., 2011). This study focuses on risk and exposure of heavy metal dust contamination from two locations in the Bugesera region of Rwanda.

Rwanda hosts diverse terrain, thus there are numerous regions for particulate study with expected varying results. The locations used in this study, were determined from previous groundwater studies. Site1 is a lowland wet marsh with initially elevated levels of manganese. Sediment at this location is seasonally inundated with groundwater. Site2 is an elevated albeit still lowland region. Surface sediment is substantially higher than the groundwater. A loose, rocky, dry sediment profile describes this sample spot. Site2 was also determined from previous groundwater sampling with elevated levels of uranium found at a nearby decommissioned borehole.

Representative samples from each sampling locale illustrate the difference of environmental risk associated with small particle sizes from variable sediment profiles. The first from a location of cyclical wetting versus the second from an area of particulate fractions from an empty vadose zone. Samples thus represent locales with different governing subsurface processes. These subsurface processes, in turn, are controlling and leading to varying geochemical and physical properties.

4.2 Methods

4.2.1 Field Site

Samples were collected at two different sites in the Bugesera district of Rwanda. As previously stated, collection sites were predetermined from prior groundwater analysis. Site1 was selected due to the suspicion of elevated manganese in the surrounding groundwater. Site1 is a lowland marsh with seasonal groundwater saturation. This inundation leads to seasonally-driven cyclical redox transformations at the near-surface.

Site2 was chosen for its approximate location near a groundwater source elevated with uranium. Site2 is a drier location with looser sediments. The site experienced a yearlong, deep dry vadose zone.

4.2.2 Particle Distribution

Particle distribution was completed using a set of 12 different standard test sieves, ASTM E-11 specification. Sieve sizes ranged from 9mm to 75µm. Size distributions were generated for particles of 9mm, 4.75 mm, 2.36mm, 1.18 mm, 850 µm, 600µm, 425 µm, 300 µm, 180 µm, 150 µm, 75 µm, and sub75 µm. Size distributions were collected and stored in a sufficient voluminous container.

4.2.3 Loss On Ignition

A modified loss on ignition (LOI) analysis was taken from Methods of Soil Analysis part 3(Reed and Martens, 1996). LOI determined the organic fraction of the samples. Homogenized samples, from each particle size fraction, were dried in an oven around 100°C for 1 hour, driving off any surface water. Samples were then massed to gain the dry mass. Samples were placed in a pre-massed ceramic crucible. Following measurement, each sample was placed in the furnace at a temperature of 550 °C for 1 hour to oxidize organic matter to CO_2. Each crucible was then removed and allowed to cool in a desiccator until room temperature was reached. Once cooled, the crucible containing the sample was massed again. The differential mass loss can be attributed to the amount of organic material in each sample (Walter E. Dean, Jr., 1974). An equation for LOI is given by (Heiri et al., 2001):

$$\mathrm{LOI_{SOM}} = \frac{(M_{dry} - M_{550})}{M_{dry}} \times 100$$

Where,

LOI_{SOM} = the mass differential of organic material.

M_{dry} = the mass of the dried solid at 100°C

M_{550} = the mass of the solid at 550 °C

4.2.4 Calcination

A modified calcination analysis, from *Methods of Soil Analysis Part 3*, was used to determine the carbonate fraction(Reed and Martens, 1996). Samples previously measured in the

LOI experiment were then placed in the furnace at temperatures of 1000 °C for one hour. After ignition, the crucibles were carefully cooled to room temperature in a desiccator. Once the crucible containing the sample reaches ambient temperature, the mass was taken again. Mass loss from 550-1000°C is considered mass loss attributed to carbonate conversion to CO_2 (Walter E. Dean, Jr., 1974). Modified equations for calculating calcination is given by (Heiri et al., 2001):

$$\mathrm{LOI_{Carb}} = \frac{(M_{1000} - M_{550})}{M_{dry}} \times 100$$

$$\text{Carbonate \%} = \mathrm{LOI_{Carb}} \times 1.36$$

Where,

LOI_{Carb} = The mass differential of the loss of carbonate material.

$M_{1,000}$ = The mass of solid at 1000°C

M_{550} = The mass of solid at 550°C

M_{dry} = The mass of solid at 100°C

4.2.5 Soil Acidity

A modified method for soil pH determination is taken from *Methods of Soil Analysis part 3- Chemical Methods* (*Methods Soil Anal. Part 3—Chemical Methods*, 1996). Soil acidity

analysis determines pH using a 1M KCL solution. 2 g of sample, from each sampled depth, was massed out and placed in a 15ml centrifuge tube. 2 ml of 1M KCL was added to the sample and mixed. The mixture was rested for ten-minutes then measured with a Mettler Toledo Five Easy Plus meter and pH probe. The pH is recorded as pH_{KCl} (*Methods Soil Anal. Part 3—Chemical Methods*, 1996).

4.2.6 Heavy Acid Digestion

Small-sized particles (850 µM, 600 µM, 425 µM, 300 µM, 180 µM, 150 µM, 75 µM, <75 µM) were subsampled for heavy digestion analysis. Each particle subset was massed in 30 mL PFA vials. Reverse *aqua regia* was determined as the most appropriate method for digestion. The method involved using three-parts concentrated nitric acid with one-part hydrochloric acid. Digestion was performed until dryness and repeated in triplicate. Digested sediment is pickup in 10 mL of a known amount of 5% HNO_3. The 5% supernatant was siphoned off from teflon tubes into a plastic centrifuge tube and used as sample stock. Dilutions are sampled from the sample stock and prepared for elemental analysis. All acids used were ACS grade concentrated mineral acids from Fisher Chemical.

4.2.7 Elemental Analysis

A methodology used for sediment metal concentration determination via inductively coupled plasma mass spectrometry (ICP-MS) was taken from Al-Mur et al. (2017). Briefly, the method involved used a 5% HNO_3 matrix, prepared from trace metal grade concentrated 65-70%

nitric acid and 18.2 mΩ water. Samples were diluted with and the same 5% HNO_3 matrix described above to adhere to a calibration concentration range of 0.5 µg/L to 50 µg/L. Sediment samples were analyzed in collision cell technology with kinetic exclusion discrimination (CCT-KED) analytical mode. Blank 5% matrix samples, used to verify background concentrations, were measured every sample cycle. Blanks were also used as a safety check for sufficient washout between samples. Analytical calibration curves, r^2 values of .999 or higher, were used to verify mass spectrometry measurement of analytes. Standard solution preparations, used for ICP-MS calibration, were formulated from SPEX CertiPrep trace metal grade standards.

4.2.8 Statistical Analysis for Environmental Risk Assessment

Total metal concentration, while important, does not discriminately recognize the bioavailability and environmental risk associated with metal contamination. Statistical analysis and other environmental indices can more accurately assess heavy metal concentration and their potential ecological hazards. In this study, four related indices are used.

4.2.8.1 Contamination Factor

A contamination factor is the ratio of an analyte's sediment concentration against the background concentration of the analyte in question. Hakanson gives a simple equation for the contamination factor (1980):

$$C_f^i = C_s^i / C_b^i$$

Where,

C_s^i = the concentration of the specific metal

C_b^i = the background value for the metal in question

Background values are metal-specific, and are described by Turekian and Wedepohl, 1961. For this study, C_b^i are sedimentary mg/kg values where: V=130, Cr=90, Mn=850, Ni =68, Cu =45, Zn=95, Mo= 2.6, Cd=0.3, Pb=20, and U= 3.7. Terminology, from Hakanson, is used to qualify and categorize calculated C_f^i values. A contamination factor <1equates to low contamination of the sediment. $1 \leq C_f^i < 3$ refers to a moderate contaminated sediment. When $3 \geq C_f^i < 6$ is a considerably contaminated sediment, and when $C_f^i \geq 6$ is a very high contamination factor for a given element (1980).

4.2.8.2 Pollution Load Index (PLI)

The Pollution Load Index gives an overall summation of contamination-weighted concentrations for all analytes of interest in a given site or sample (Rabee. A, et al., 2011). In this study, PLI is calculated per particle size for each location to find the total pollution potential a particular fraction size produces. An equation for determining PLI is given by (Tomlinson et al., 1980):

$$PLI = \left(C_f^1 \times C_f^2 \times \ldots \times C_f^n\right)^{\frac{1}{n}}$$

Where,

C_f = the contamination factor

n = the number metals used to determine PLI

4.2.8.3 Potential Ecological Risk Index

The potential ecological risk index (E_r) is a method used to evaluate environmental risk a sediment heavy metal presents to a location (Zhu et al., 2012). Hakanson provides an equation for finding the risk index (RI):

$$E_r = C_f^i * T_f^i$$

Where, C_f^i = the contamination factor

T_f^i = the coefficient of toxicity for a given element

E_r = the potential risk an individual sediment analyte presents

T_f^i values are given as Zn=Mn= 1, Cr=V= 2, Cu=Ni=Pb= 5, and Cd= 30 (Hakanson, 1980).

T_f^i values for Mo and U were not found, thus they were not included in PERI or RI calculations. To further evaluate, E_r values are described according to their potential ecological risk associated with studied elements. An E_r<40 has a low potential risk. 40≥ E_r <80 has moderate potential risk. 80≥ E_r <160 has considerable potential risk. 160≥ E_r <320 has a high potential risk, and when E_r <320, there is a very high potential risk (Hakanson, 1980).

To completely and thoroughly establish the ecological risk of a sediment, the Risk Index (RI) must be calculated. In this study, RIs evaluate the complete heavy metal contamination of individual particle size fractions for given locations and their potential impact on the local environment (Hakanson, 1980; Zhu et al., 2012). Hakanson establishes the equation for the determination of RI values (1980):

$$RI = \sum E_r$$

Where, the risk index (RI) is the sum of the ecological risk by individual metals.

Given categories for RI values are as follows: RI <150 equates to a low risk; 150≥RI<300 leads to a moderate risk; 300≥RI <600 is a considerable risk; RI ≥600 is a very high-risk factor.

4.3 Results

Particle size distribution was investigated near-surface sediment of collected grab samples, representing two different sites of interest. Samples were collected from sites previously verified for high concentrations of transition and heavy metals, including Mn, U, V, and Cr. Size fractionation of near-surface sediment, of samples collected from the marshland, is shown in Figures 4.1 & 4.2. There is not a noticeably large discrepancy of particle fractionation between samples A & B. Both samples mimic each other in terms of size distribution. Specifically, particulate masses of both samples are concentrated in the larger fractions, mostly sizes of 4.75mm and 2.76mm, with minor amounts in the smaller fractions (Figures 4.1 & 4.2).

Figures 4.3 & 4.4 present the size distribution data of near-surface particles sampled at site BG2-4. While sampled identically and simultaneously, fractionation from sample A to B differs enormously (Figures 4.3 & 4.4). Sample A is shown to have ample of mass in nearly all size fractions, with large mass percentages in the fine fractions of 300μm and 180μm (Figure 4.3). Sample B exhibits a far different fractionation. Particle mass, from sample B, is concentrated in the 180μm and 300μm fraction sizes (Figure 4.4). Discrepancy between the two samples is attributed to field variance within the BG2-4 sampling location.

Following size fractionation, soil acidity was tested on all four samples separately. Figure 4.5 describes the soil acidity of each sample for fractionation sizes down to 75μm. pH testing indicated that there is a high degree of pH variability between the two sampled locations. Variance amongst A & B samples is near-constant for samples coming from location BG2-4. A pH unit difference is observed between samples A & B regardless of particle size. Samples from location BG2-3 display low pH variance across all particle sizes, however, smaller particle sizes do exhibit larger pH changes between samples A & B.

Elemental analysis is the starting point for determining ecological risk. Metal concentrations are determined per particle size for all four samples. For both site locations, the average concentrations for heavy metal analysis of the two samples is presented and used for multiple ecological indices (Table 4.1). Particle contamination factors (C_f^i) for V, Cr, Mn, Ni, Cu, Zn, Mo, Cd, Pb, and U are presented in Table 4. 2.

Contamination factors quantify the degree of toxicity an element or substance has on its environment. From Table 4.3, elemental contamination factors vary greatly in their pollution of sediment fractions. However, small fractions below 75μm exhibit higher contamination than other sizes. This is seen in both average fraction sets. Cd exhibits the highest contamination risk, independent of particle size and site location, with a very high contamination factor. Other analytes, Mo and U both express contamination factors with moderate to considerable contamination, depending on fraction size. Low contamination is exhibited on the fraction by many of the metals studied; however, even among the metals exhibiting a low contamination, the sub 75μm fraction is relatively elevated.

The average pollution load index (PLI) of each fraction is given in Figure 4.7. The PLIs, are determined by the equation from Tomlinson (1980). Across both sites, the highest average PLI of each average sample was the sub 75μm fraction size. This confirms pollution potential levels to be size-dependent.

Table 4.3 presents the potential ecological risk factor (Er) for individual heavy metals at the particulate sizes examined. Er is described as the potential risk of an individual metal at a certain location (Zhu et al., 2012). Hakanson similarly classifies Ers to the previous contamination factors. Most of the E_r values present low ecological risk. Cu, at sub75 μm for Site1, does show a moderate ecological risk. On average, the heavy metals studied present higher Er values at sub 75 μm even though they are considered low risk.

Figure 4.8 illustrates the average calculated Risk Index (RI) for each fraction size at each location. The RIs calculated here are the sum of each metal's ecological risk for a given fraction size. Using the defined terminology from Hakanson, RIs record low ecological risk; however, sub 75μm fractions still present a higher ecological risk over larger particle sizes.

4.4 Discussion

Soil particle size distribution amongst the respective samples, is not ubiquitous at each site location. Figures 4.1-4.4 detail the particle distribution differences between each sample. Figures 4.1 & 4.2 show that samples A & B, collected from Site1, show similarities in their distributions. However, Figures 4.3 & 4.4 reveal significant differences between samples A & B collected from Site2. It is understandable to see a difference between the samples from one site to the other. Topography of Site1 differs from Site2. Site1 being a lowland swampy region and

Site2 a hilly region with a looser and rockier sediment profile. The large distinction between Site2's A & B samples is related to regional *in situ* field variance. Sediment profiles from this region vary in terms of particle size distribution as well as organic material, and soil acidity.

The soil acidity profile details similar pH distinctions between particle distributions and site locations. There is a larger pH discrepancy between Site2's A & B samples versus the samples taken from Site1; however, there is no differential pH trend between distribution and particle size. The soil pH has a strong influence on metal concentrations and helps to explain why metal concentrations are higher at Site1 versus Site2.

Soil pH only presents a partial answer to metal concentrations and the association with particle size. It has been well documented that small particle sizes have an affinity for metal sorption (Hamilton-Taylor et al., 1997; Nnaji and Emefu, 2017). As observed, particle sizes under 75 μm have a higher metal concentration. While soil pH is a factor in this phenomenon, it is mainly due to the increased soil organic matter in these fraction sizes. Figure 6 contrasts the organic and carbonate material present in bulk versus sub 75μm particles. Organic material is more abundant in the subfractions than the bulk material, especially Site1's B sample. Organic matter in this fraction is substantial and provides rationale, along with observed acidic pH values, as to why metal concentrations are higher in this fraction than any other. It is well documented that organic material sequesters many metals (Schijf and Zoll, 2011; Wen et al., 1997). Furthermore, the metals found to be elevated on sub 75μm particles are commonly, and strongly bound to organic material (Weng et al., 2002). With the available organic matter and pH conditions, sub 75μm particles are suitable for fostering high metal concentrations.

While small particle sizes do hold higher metal concentrations, that does not necessarily mean they present an environmental or ecological risk. Ecological risk is assessed on particle distributions and evaluated for their ecological impact. Particle distributions are first evaluated for their contamination factors (C_f^i). C_f^i values are categorized according to terminology developed by Hakanson (1980). From Table 4.2 it is observed that the C_f^i for most of the elements presents low contamination of the sediment, with the highest contamination factors nominally being distributed on fine size particles. Uranium (U) is evaluated for having moderate soil contamination in most distributions, while Molybdenum (Mo) expresses considerable contamination in every distribution from Site1. Mo is evaluated for moderate contamination amongst all distributions in Site2. Copper (Cu) presents the highest contamination factor for fine-sized particles.

The PLI indicates a similar trend of fine size particles containing higher levels of pollution than larger masses. However, this trend is observed most noticeably on particles obtained from Site1. While the trend holds for particles from Site2, the pollution differential does not indicate a severe difference in particle size. PLI not only illustrates the pollution levels over particle distributions but also from the variance per site. PLI confirms that larger particles and sub 75 μm particles, from Site2, are consistent with natural metal abundance. All PLI's for these particles fall under a value of 0.5. However, the fine fractions related to Site1 show a PLI greater than 1. A PLI greater than 1 indicates contamination within the local area. Whether that is natural or anthropogenic is yet unknown within the scope of this study.

E_r and RI values demonstrate that particle size does factor into available ecological risk, at both site locations. Cu and Pb are the dominant hazards in small particle sizes. At Site1, Cu on sub 75μm is given as a moderate potential risk while Pb, though elevated, is seen as low

ecological potential risk. At Site2, Cu and Pb again are the major elements of concern, along with Cd. E_r and RIs for Site2 present a lower potential risk than particles from Site1, however fine sub 75μm particles still have a greater potential risk than other, larger sizes.

4.5 Conclusion

This study found that small particle sizes produce more hazardous levels of contamination leading to higher levels of ecological risk. Factors contributing to this phenomenon include soil acidity and the amount of organic material found on sub 75μm fractions. While areas of interest sampled are significantly different in terms of their topology and subsurface environment, observable trends still held. Geochemical factors control the differential in metal concentration between the Site1 and Site2. Site2's deeper groundwater level and larger vadose zone means less available environmental material in contrast to Site1's cyclical inundation by groundwater, with constant and shallow redox reactions, which leads to an abundant amount of available organic material.

It is essential to note that particle size is the key factor in determining ecological risk. Individual contaminants, such as Cu and Pb produce higher elevated contamination, though at moderate and low risk, for fine size particles. However low the potential ecological risk maybe, sub 75μm particles contain higher associated risk. Results from ecological risk studies prove this notion making it necessary to recognize and account for the ecological risk brought about by contamination of small particle fractions. The varying geochemical soil processes regulate the differing levels of metal contamination, at the lowland marsh location. A constant cycling of the water table inundating the topsoils catalyzes local redox reactions. These redox reactions supply lower soil pH values, suitable for metal mobility. However, a yearly dry vadose locale is

constantly oxidized. The locale may be subjected to harsher weathering, on the topsoil, resulting in a larger number of finer particles, including sub 75 µm as supported by Figures 1-4. However, the oxidized environment does not promote the subsurface conditions allowing for major metal mobility.

Ultimately, this study looks at most likely naturally occurring toxic metals. Thorough investigation of both sites indicate subsurface processes encouraging higher metal concentrations at Site1 versus Site2. While this investigation centered on naturally occurring metals, there are indications of potential anthropogenic toxicity as well. The PLI values, Figure 4.7, suggest anthropogenic pollution is affecting Bugesera heterogeneously. Lead abundances most heavily contribute to PLI values for all particle sizes at both locales. The PLI expression, therefore, suggests anthropogenic lead likely from an atmospheric source. Further studies can verify this claim and further determine the sourcing of Pb. All these findings play into the safety and public health of current populations in the region. Future development in the region should also note the potential risk of mobilization of not just dust fractions but the heavy metal load therein.

4.6 Figures & Tables

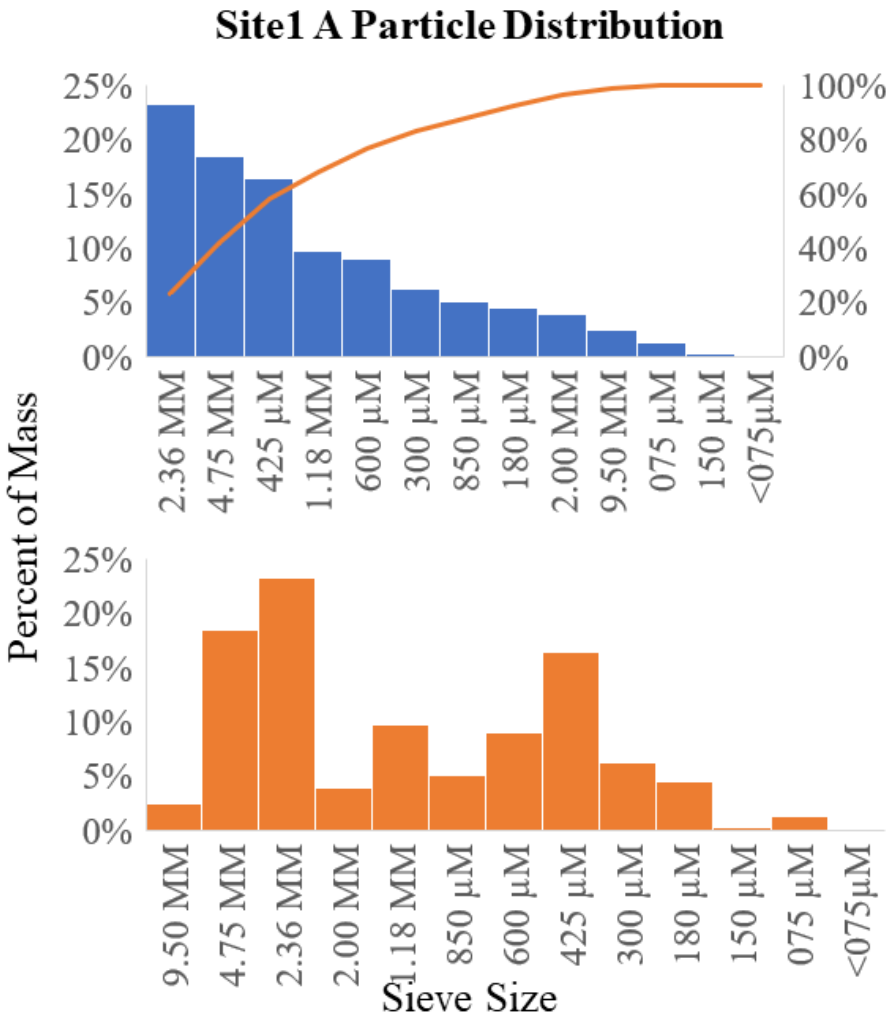

Figure 4. 1) Site1 A's Particle Size Distribution. The top panel illustrates the mass of particle sizes in descending order. The left y-axis shows each size distribution's percentage of the total sampled mass.X-axis displays particle size distribution. The bottom chart illustrates the mass percent of each particle distribution in descending size order.

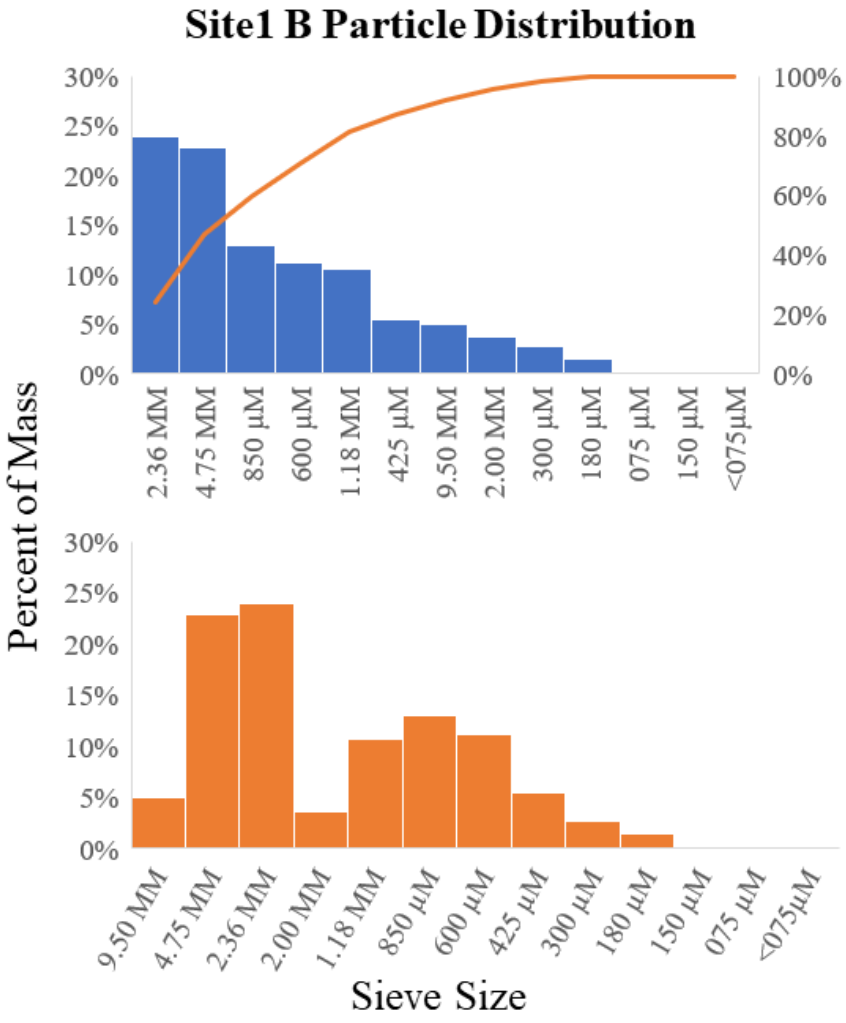

Figure 4. 2) Site1 B's Particle Size Distribution. The top panel illustrates the mass of particle sizes in descending order. The X-axis displays particle size distribution. Y-axis shows each size distribution's percentage of the total sampled mass. The bottom chart illustrates the mass percent of each particle distribution, in descending size order.

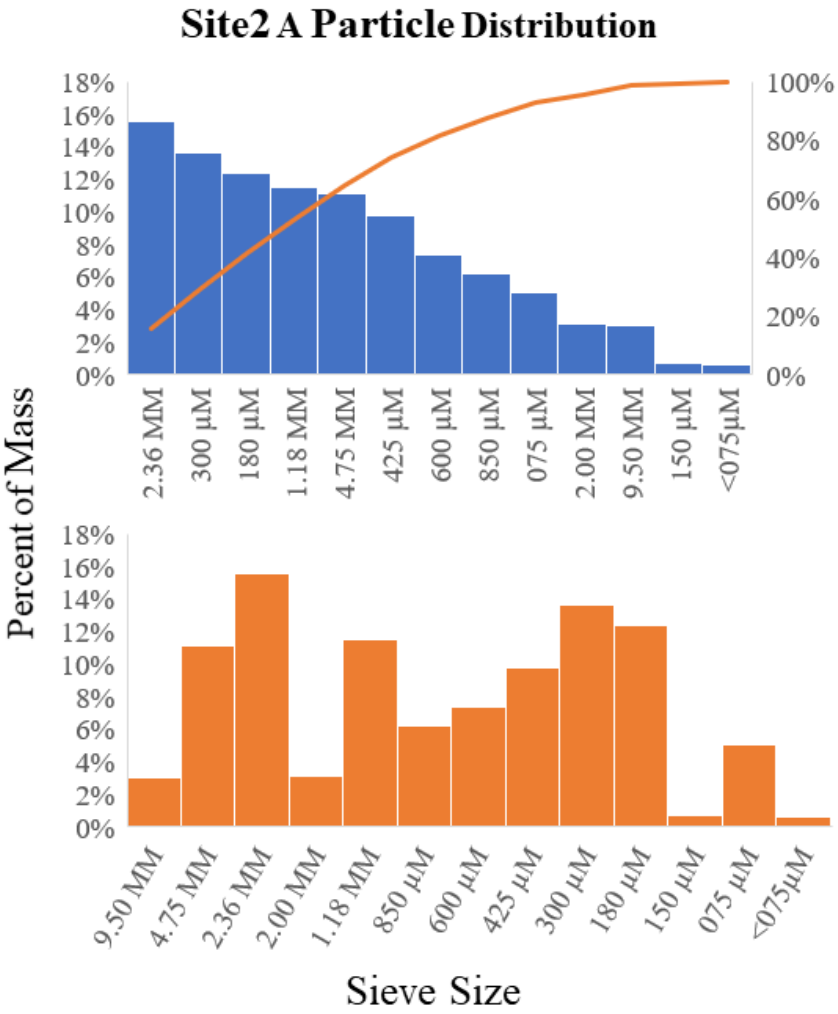

Figure 4. 3) Site2 A's Particle Size Distribution. The top panel illustrates the mass of particle sizes in descending order. The left y-axis shows each size distribution's percentage of the total sampled mass. The X-axis displays particle size distribution. The bottom chart illustrates the mass percent of each particle distribution, in descending size order.

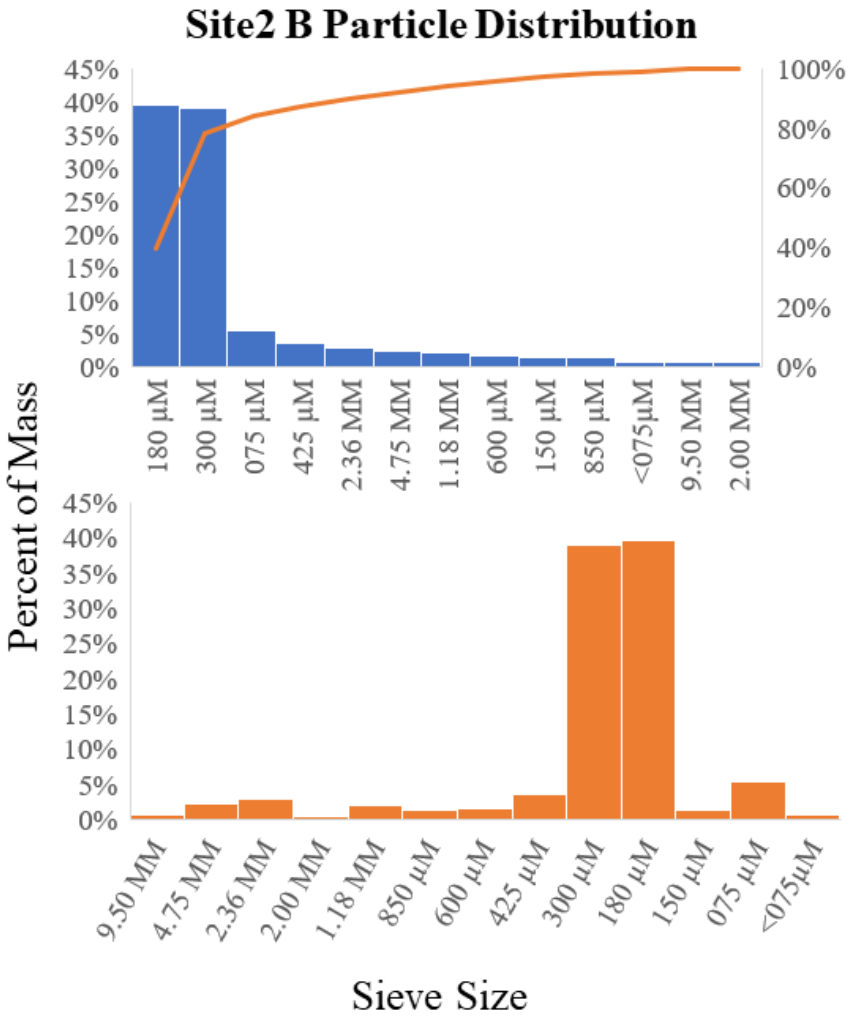

Figure 4. 4)Site2 B's Particle Size Distribution. The top panel illustrates the mass of particle sizes in descending order. The left y-axis shows each size distribution's percentage of the total sampled mass. The X-axis displays particle size distribution. The bottom chart illustrates the mass percent of each particle distribution, in descending size order.

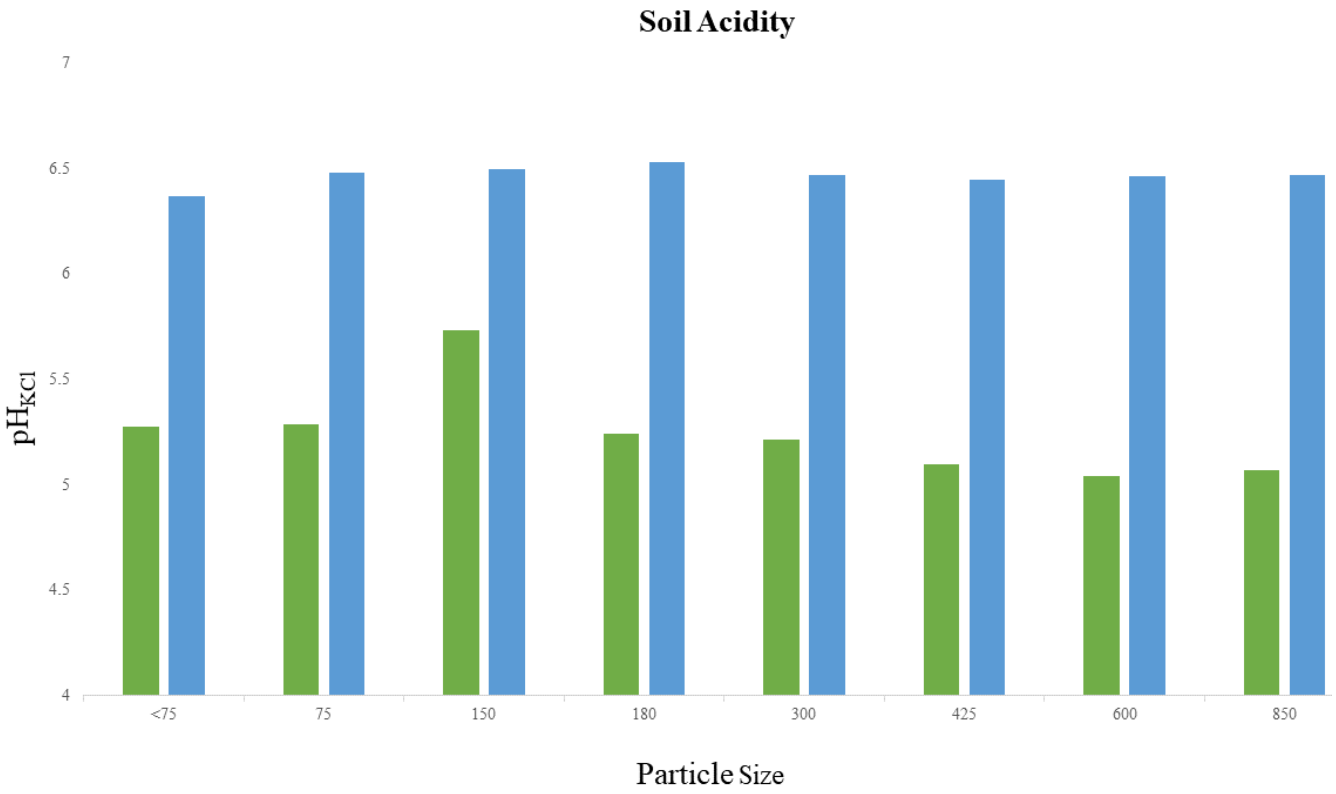

Figure 4. 5) Soil Acidity for Sites1 & 2. The average pH_{kcl} values of each particle size from Site1 and Site2. The more acidic green bars indicate soil pH at Site1. Site2 soil pH values, shown in blue, are near circumneutral levels.

Table 4. 1) t-test results Comparing Average pH from Site1 and Site2

t-Test: Paired Two Sample for Means

	Variable 1	Variable 2
Mean	5.2	6.5
Variance	0.0	0.0
Observations	8	8
Pearson Correlation	0.2	
Hypothesized Mean Difference	0	
df	7	
t Stat	-16.1	
P(T<=t) one-tail	4.3E-07	
t Critical one-tail	1.9	
P(T<=t) two-tail	8.5E-07	
t Critical two-tail	2.4	

Table 4. 2) Average Concentrations. The average concentration of elevated metals for each size distribution from Site1 and Site2.

Concentrations (mg/Kg)

Sample	51V	52Cr	55Mn	60Ni	65Cu	66Zn	96Mo	111Cd	208Pb	238U
$BG2\text{-}3_{avg}$ <075	86.0	76.1	140.3	23.6	402.1	83.4	14.4	0.0	59.0	19.6
$BG2\text{-}3_{avg}$ 075	58.4	53.6	101.8	23.2	25.6	10.0	9.2	0.0	19.3	10.3
$BG2\text{-}3_{avg}$ 150	53.4	46.3	90.0	9.2	23.9	10.9	7.9	0.0	18.6	10.0
$BG2\text{-}3_{avg}$ 180	54.1	47.0	101.6	12.8	21.9	9.0	7.9	0.0	17.6	8.4
$BG2\text{-}3_{avg}$ 300	56.7	50.3	123.3	10.2	21.3	6.8	8.6	0.0	17.1	10.5
$BG2\text{-}3_{avg}$ 425	58.0	55.3	115.4	10.1	18.9	6.2	7.8	0.0	16.3	9.7
$BG2\text{-}3_{avg}$ 600	67.2	60.7	106.4	9.8	20.6	7.4	9.4	0.0	15.0	9.2
$BG2\text{-}3_{avg}$ 850	84.8	100.4	118.9	11.1	22.2	9.8	10.9	0.0	16.1	9.4
$BG2\text{-}4_{avg}$ <075	31.3	24.7	284.4	9.4	52.6	17.3	6.7	0.1	25.4	9.5
$BG2\text{-}4_{avg}$ 075	25.4	21.1	205.2	8.5	16.0	4.4	6.4	0.1	14.9	9.7
$BG2\text{-}4_{avg}$ 150	22.0	19.0	182.2	8.3	14.3	4.8	6.0	0.1	13.4	8.7
$BG2\text{-}4_{avg}$ 180	25.2	21.0	214.8	10.3	13.8	5.0	6.3	0.1	14.1	9.8
$BG2\text{-}4_{avg}$ 300	26.5	22.9	230.0	10.2	14.2	5.1	6.9	0.1	14.9	10.3
$BG24\text{-}_{avg}$ 425	32.3	27.7	283.6	11.1	15.7	11.5	7.2	0.1	16.5	10.6
$BG2\text{-}4_{avg}$ 600	30.3	25.6	296.8	9.3	13.8	10.2	6.5	0.1	15.4	9.0
$BG2\text{-}4_{avg}$ 850	31.2	32.5	298.5	8.7	13.2	12.7	6.6	0.1	13.7	7.2

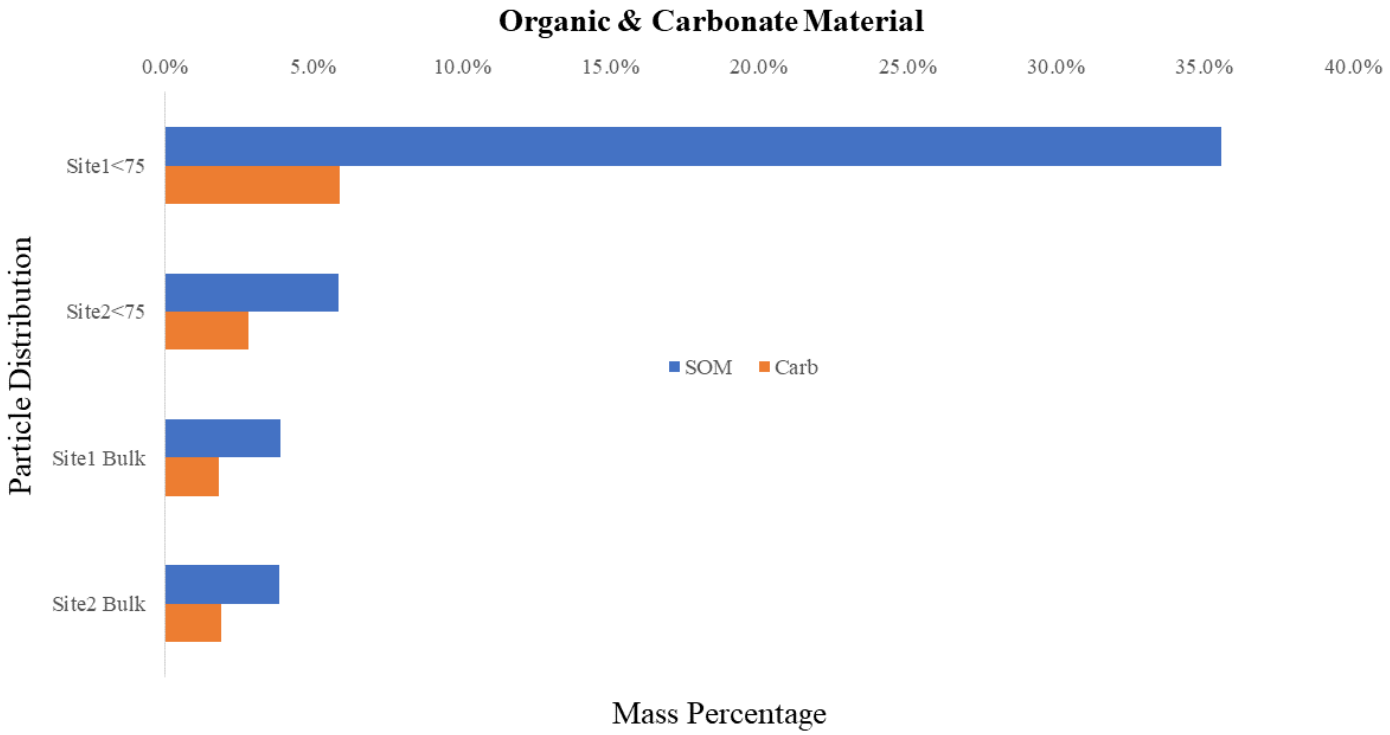

Figure 4. 6) The SOM and carbonate material measured on sub 75 um particles and bulk material. Error from LOI and calcination measurements are calculated into the analysis and are at a minimum

Table 4. 3) The average contamination factor, C_f, of measured metals. C_fs are applied to each particle from both Site1 and Site2.

	Contamiation Factor(C_f^i)									
Sample	**51V**	**52Cr**	**55Mn**	**60Ni**	**65Cu**	**66Zn**	**96Mo**	**111Cd**	**208Pb**	**238U**
$Site1_{avg}$ <075	0.7	0.8	0.2	0.3	8.9	0.9	5.6	0.1	2.9	5.3
$Site1_{avg}$ 075	0.4	0.6	0.1	0.3	0.6	0.1	3.5	0.1	1.0	2.8
$Site1_{avg}$ 150	0.4	0.5	0.1	0.1	0.5	0.1	3.0	0.1	0.9	2.7
$Site1_{avg}$ 180	0.4	0.5	0.1	0.2	0.5	0.1	3.0	0.1	0.9	2.3
$Site1_{avg}$ 300	0.4	0.6	0.1	0.2	0.5	0.1	3.3	0.1	0.9	2.8
$Site1_{avg}$ 425	0.4	0.6	0.1	0.1	0.4	0.1	3.0	0.1	0.8	2.6
$Site1_{avg}$ 600	0.5	0.7	0.1	0.1	0.5	0.1	3.6	0.1	0.8	2.5
$Site1_{avg}$ 850	0.7	1.1	0.1	0.2	0.5	0.1	4.2	0.1	0.8	2.5
$Site2_{avg}$ <075	0.2	0.3	0.3	0.1	1.2	0.2	2.6	0.2	1.3	2.6
$Site2_{avg}$ 075	0.2	0.2	0.2	0.1	0.4	0.0	2.5	0.2	0.7	2.6
$Site2_{avg}$ 150	0.2	0.2	0.2	0.1	0.3	0.1	2.3	0.2	0.7	2.4
$Site2_{avg}$ 180	0.2	0.2	0.3	0.2	0.3	0.1	2.4	0.2	0.7	2.6
$Site2_{avg}$ 300	0.2	0.3	0.3	0.1	0.3	0.1	2.6	0.2	0.7	2.8
$Site2_{avg}$ 425	0.2	0.3	0.3	0.2	0.3	0.1	2.8	0.3	0.8	2.9
$Site2_{avg}$ 600	0.2	0.3	0.3	0.1	0.3	0.1	2.5	0.3	0.8	2.4
$Site2_{avg}$ 850	0.2	0.4	0.4	0.1	0.3	0.1	2.5	0.4	0.7	1.9

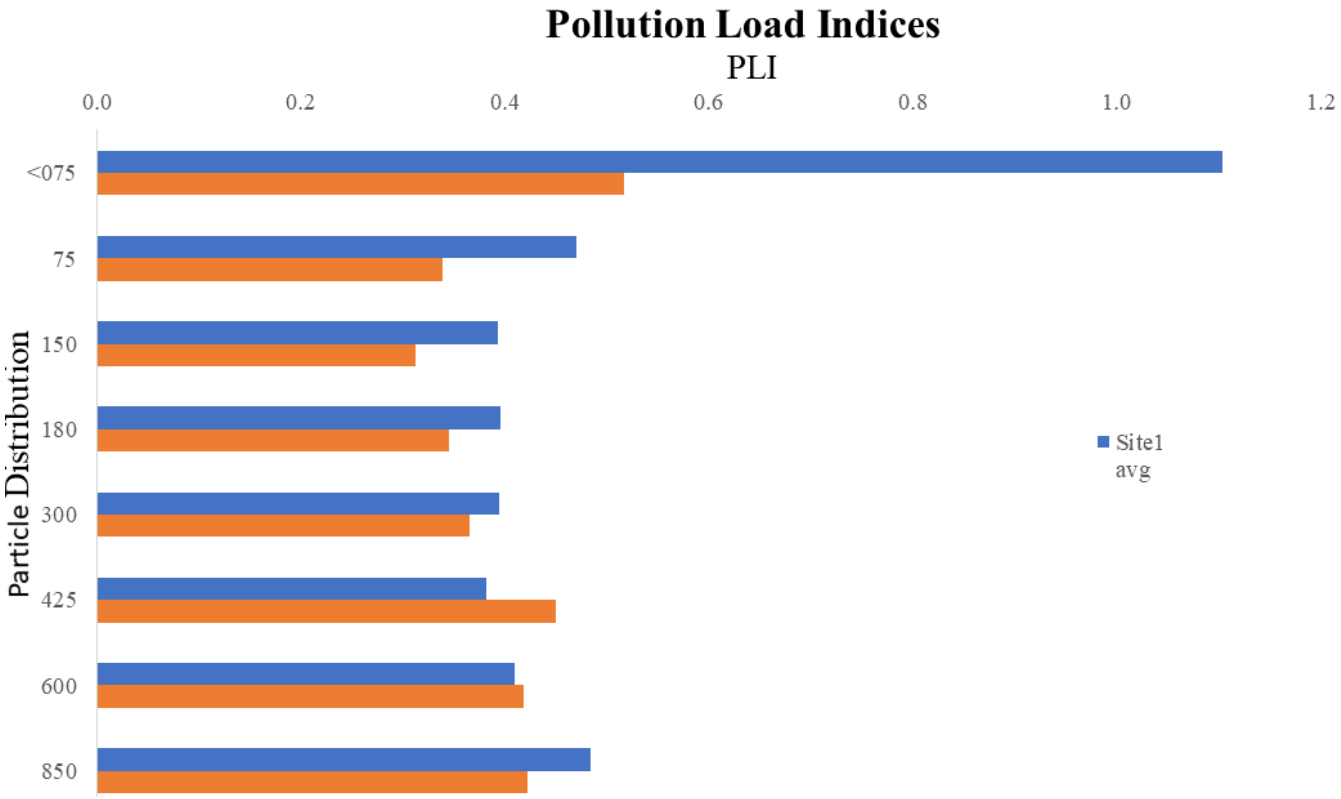

Figure 4. 7) The average PLI per particle size for both Site1 and Site2. As shown, PLIs indicate that there is higher contamination on sub 75µm particles particularly for Site1.

Table 4. 4) Table of E_R values; the potential risk exhibited by each metal. Sub 75µm from both sites show a higher environmental contamination than larger counterparts.

E_R

Sample	51V	52Cr	55Mn	60Ni	65Cu	66Zn	111Cd	208Pb
$Site1_{avg}$ <075	1.3	1.7	0.2	1.7	44.7	0.9	3.7	14.7
$Site1_{avg}$ 075	0.9	1.2	0.1	1.7	2.8	0.1	2.6	4.8
$Site1_{avg}$ 150	0.8	1.0	0.1	0.7	2.7	0.1	1.9	4.6
$Site1_{avg}$ 180	0.8	1.0	0.1	0.9	2.4	0.1	2.0	4.4
$Site1_{avg}$ 300	0.9	1.1	0.1	0.8	2.4	0.1	1.9	4.3
$Site1_{avg}$ 425	0.9	1.2	0.1	0.7	2.1	0.1	2.0	4.1
$Site1_{avg}$ 600	1.0	1.3	0.1	0.7	2.3	0.1	2.6	3.8
$Site1_{avg}$ 850	1.3	2.2	0.1	0.8	2.5	0.1	2.9	4.0
$Site2_{avg}$ <075	0.5	0.5	0.3	0.7	5.8	0.2	7.4	6.4
$Site2_{avg}$ 075	0.4	0.5	0.2	0.6	1.8	0.0	5.6	3.7
$Site2_{avg}$ 150	0.3	0.4	0.2	0.6	1.6	0.1	5.0	3.3
$Site2_{avg}$ g 180	0.4	0.5	0.3	0.8	1.5	0.1	5.7	3.5
$Site2_{avg}$ 300	0.4	0.5	0.3	0.7	1.6	0.1	6.4	3.7
$Site2_{avg}$ 425	0.5	0.6	0.3	0.8	1.7	0.1	8.9	4.1
$Site2_{avg}$ 600	0.5	0.6	0.3	0.7	1.5	0.1	10.1	3.8
$Site2_{avg}$ 850	0.5	0.7	0.4	0.6	1.5	0.1	10.5	3.4

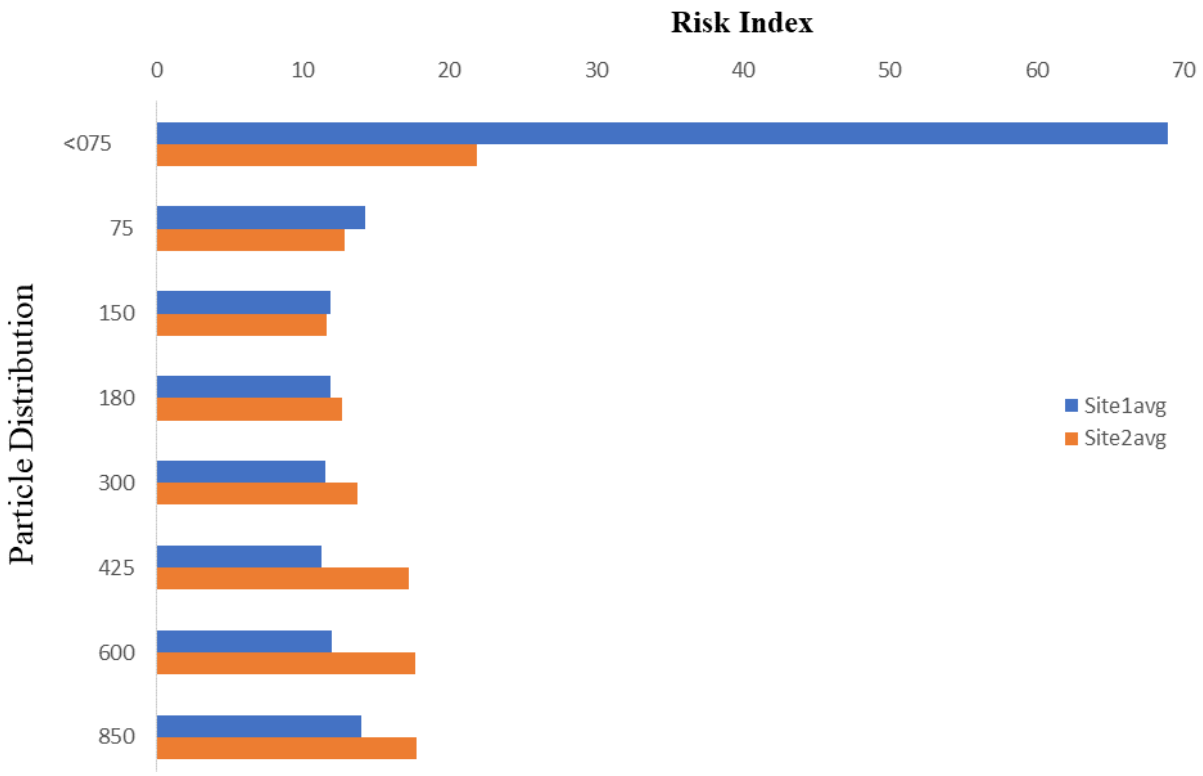

Figure 4. 8) The Risk Index of each particle size for Site1 and Site2. The Risk Index illustrates the contamination difference between sub 75µm particles and lager particle masses. Also illustrated are the differences in contamination between and area with cyclical redox against a yearly dry vadose zone. Fine particle masses, regardless of site location, poses the greatest threat to the surrounding environment and the public health.

CHAPTER 5

Conclusion

5.1 Summarization

This dissertation demonstrates that understanding the geochemical processes involved with the release of naturally occurring metals is an essential initial phase for mitigation. Chapter 2 examines Pb contamination in Bangladeshi refugee camp drinking water wells. Naturally occurring Pb is found to be elevated throughout the Kutupalong settlement. Further examination of the matter revealed that Pb release was controlled by a series of biogeochemical processes. Nutrient loading, via fertilization and animal waste, drives nitrogen dynamics causing shifts in the groundwater pH. The pH swings thus dictate Pb sorption and solubility of Pb containing Fe and Mn hydroxide particles. Instead of an *in situ* method for mitigating Pb, risk assessment maps were designed to manage contamination through avoidance as well as provide strategic planning for the implementation of future wells and the closure of currently contaminated ones.

Chapter 3 assesses elevated levels of multiple trace and heavy metal contaminants in near-surface sediments of Bugesera, Rwanda. Three different sites were cored to evaluate Mn, U, and V in subsurface sediment. Sequential extractions determined the speciation of subsurface metal contaminants. Phase determination, in combination with soil acidity, LOI, and calcination measurements yielded an evaluation of the mobility and potential bioavailability of Mn, U, and V. This study ultimately contrasts locales with cyclical redox changes, due to groundwater oscillation, to a yearly vadose region. Different mechanisms of potential metal release were identified at each site. The specific locale within Bugesera will often dictate the geochemical processes associated with metal release. Ideally, understanding many of these complex

geochemical processes should be used to help further the subsurface awareness of contamination risk in Bugesera. Thus, allowing for safe, sustainable growth in the region.

Chapter 4 of this dissertation investigates potential airborne contamination of fine size dust particles in Bugesera. Surface particle size distribution was measured and evaluated for trace and heavy metals. Though complete elemental breakdown is assessed, it alone is inadequate to determine total hazardous potential dust particles pose on the surrounding environment. Ecological risk indices were applied to establish environmental risk. Risk indices determine that the highest level of risk came from Site1, with Cu and Pb presenting the greatest risk. The highest risk assessment from Site2 was found to come from Pb, Cd, and Cu contamination. As asserted, particle size does influence the risk level in calculated ecological indices. However, Cd ecological risk is noticeably higher on larger particle sizes at site2. While Cd does not change the ecological trend of smaller particle sizes producing higher risk, it is worth noting that there is a higher ecological risk for Cd among larger particles. From the independently calculated RIs, it is determined that while ecological risk is low, there is a larger risk with fine particles, especially from Site1.

This dissertation examines mechanisms for trace and heavy metal release, chiefly through the soil-water interface of tropical soil profiles. The findings from this dissertation attain to emphasize the vulnerability of communities, in these two regions, to metal contamination exposure. In Bangladesh, the uses of risk assessment maps as a mitigation technique that is used for current and potential contamination avoidance. The use of risk maps, in Kutupalong, is a way to avoid Pb contaminated and potentially contaminated areas. Also, they are to be used in strategic development and site planning, for the influx of future settlement inhabitants. Risk maps apply to every world region, provided adequate data has been collected. Using a GIS tool

for mapping purposes is a cost-effective and ecologically conservative method for mitigating risk. Globally, there are numerous different functions for risk maps and assessments. While the maps provided in this dissertation do not directly correlate to any other region beyond their intended use, variations and multilayer GIS maps dedicated to specific locations can provide an accurate assessment of ecological exposure and public health risk.

Chapters 3 and 4 present assessments rather than outlined mitigation strategies. These evaluations apply to other parts of the world. Sampling was completed in the East African Rift Valley. It is reasonable to presume that similar geochemical processes take place in other rift valleys, especially in the global south with similar tropical soil profiles.

Findings from chapters 3 and 4 from this dissertation may not layout concrete planning of mitigation or remediation. However, results do indicate that extensive care should be placed in the Bugesera region during development. Rwanda is in the process of developing Bugesera, including the construction of the country's largest international airport. If consideration is not taken during development, it is quite plausible for the community to be susceptible to high-risk exposure. Subsurface contamination and inhalation are factors that contribute to environmental exposure and public health risk.

Part of engineering is gathering all available data to make the most informed decision possible. Data collection is never truly complete as more can always be collected and processed, as is the case for this dissertation. Further study of the spatial extent of geochemical processes at each studied locale would build an extensive foundation in each location's subsurface chemistry in conjunction with comprehensive depth modeling. Building a near-complete model of the region's subsurface geochemistry and the local geochemical processes will greatly help in the ecological and environmental development aspects of Bugesera. Furthermore, initiating a

geologic control study would help to compare sediment on granite bedrock in Bugesera to that of shale bedrock found in other Rwandan regions. This should show the variance in naturally occurring metals and indicate the differing soil expression across contrasting Rwandan regions.

In addition to previously sampled sub 75μm particles, it would be beneficial to further fractionate these masses into soil particulates of PM_{10} and $PM_{2.5}$. The current sub 75μm mass is a combination of fine size and particulate matter including PM_{10} and PM2.5. Analysis of particulate matter falling into these two fractions will further demonstrate the hazards presented by airborne particles. These two particle sizes alone can be considered carcinogenic (Kim et al., 2019). Collecting PM_{10} and $PM_{2.5}$ would allow for in-depth dispersion modeling. Using the climatic setting of Bugesera and considering the source of PM being highly weathered sediments, a dispersion model can identify the extent of PM travel. As different particle sizes travel at different rates, the model would identify locations where expected PM fractions would be expected to cluster.

Continued elemental analysis on different particles would advantageously increase the understanding of potential risk association. Sequential extraction experiments, applied to fine particle sizes, will further determine the speciation of trace and heavy metals. Knowing phase or speciation is a key component in assessing public health risk. Phase will help determine potential environmental release and potential bioavailability. Finally, adding Pb isotope analysis, and combining it with elemental regressions will be able to source Pb and, indirectly, other major associated contaminants. The ultimate culmination of the techniques from this dissertation would use a multi-layered GIS map, consisting of multiple analytes paired with corresponding toxicity factors, to appropriately weight mapping algorithms. Risk maps applied to the water quality problem found in Kutupalong are unique. They were also the recommended solution

provided to the UNHCR as a mitigation strategy to the Pb issues in Kutupalong. This strategy helps the UNHCR and settlement leaders solve their drinking water issue without the economic and environmental strains of implementing a massive project. Combining and pairing these techniques will create a map illustrating the regional scale of toxic metal risk providing a useful regional tool like the small-scale tool constructed in the Kutapalong refugee settlement.

Appendix A Supplemental Statistics

Appendix Table 1)

Lowland Marsh	Above Groundwater				Below Groundwater			
55 Mn	P1	P2	P3	P4	P1	P2	P3	P4
Minimum	20.7	56.1	223.1	34.4	24.3	4.9	0.9	3.3
Quartile 1	42.3	61.4	271.8	124.5	30.7	12.3	2.6	6.4
Median	50.7	63.0	319.1	130.2	36.4	25.3	2.8	6.4
Quartile 3	57.2	91.9	399.1	214.7	36.9	41.8	62.7	52.3
Max	63.4	159.5	682.1	294.4	39.8	206.6	113.1	92.2
Mean	47.7	83.6	366.6	162.5	33.6	58.2	36.4	32.1
Range	42.7	103.4	459.0	260.0	15.5	201.7	112.2	88.9
SD	14.5	37.5	157.7	85.3	6.2	84.1	50.3	39.3
SEM	5.5	14.2	59.6	32.2	2.8	37.6	22.5	17.6

Appendix Table 2)

Lowland Marsh	Above Groundwater				Below Groundwater			
238U	P1	P2	P3	P4	P1	P2	P3	P4
Minimum	0.0	1.0	0.0	0.9	0.0	14.2	0.0	27.8
Quartile 1	0.0	2.0	0.0	4.8	0.1	33.9	0.1	37.3
Median	0.0	3.3	0.0	8.0	0.7	37.4	0.2	42.8
Quartile 3	0.0	3.5	0.0	11.3	0.8	38.4	0.2	48.7
Max	0.1	5.6	0.0	13.1	0.9	42.6	0.3	54.4
Mean	0.0	3.0	0.0	7.7	0.5	33.3	0.2	42.2
Range	0.1	4.7	0.0	12.2	0.8	28.4	0.2	26.6
SD	0.0	1.5	0.0	4.5	0.4	11.1	0.1	10.3
SEM	0.0	0.6	0.0	1.7	0.2	5.0	0.0	4.6

Appendix Table 3)

Lowland Marsh	Above Groundwater				Below Groundwater			
51V	P1	P2	P3	P4	P1	P2	P3	P4
Minimum	0.1	0.0	1.4	8.6	0.1	0.0	0.9	5.3
Quatrile 1	0.1	0.0	2.0	14.3	0.1	0.0	1.0	9.9
Median	0.1	0.0	2.2	16.7	0.1	0.0	1.5	12.8
Quartile 3	0.1	0.0	2.4	17.9	0.1	0.1	1.6	14.9
Max	0.2	0.1	2.5	21.1	0.1	11.2	1.7	16.4
Mean	0.1	0.0	2.1	15.8	0.1	2.3	1.3	11.8
Range	0.1	0.0	1.1	12.5	0.0	11.2	0.8	11.1
SD	0.0	0.0	0.4	4.0	0.0	5.0	0.4	4.4
SEM	0.0	0.0	0.1	1.5	0.0	2.2	0.2	2.0

Appendix Table 4)

Mining Hill	Top Half				Bottom Half			
55Mn	P1	P2	P3	P4	P1	P2	P3	P4
Minimum	25.3	26.3	45.1	22.4	20.6	6.0	35.3	18.1
Quartile 1	25.4	28.9	63.0	24.8	21.8	23.3	118.9	51.8
Median	34.0	33.6	91.1	37.5	22.2	24.1	133.0	53.9
Quartile 3	47.0	37.7	114.5	52.0	25.1	25.8	145.6	55.1
Max	60.8	38.8	118.0	59.5	25.8	28.9	155.4	62.9
Mean	38.5	33.1	86.4	39.2	23.1	25.0	132.7	52.6
Range	35.6	12.5	72.9	37.1	5.2	22.9	120.1	44.8
SD	16.9	6.0	35.3	18.1	2.3	2.5	18.4	8.5
SEM	8.5	3.0	17.6	9.1	1.0	1.1	8.2	3.8

Appendix Table 5)

Mining Hill	Top Half				Bottom Half			
238U	P1	P2	P3	P4	P1	P2	P3	P4
Minimum	0.0	0.1	0.0	0.2	0.0	0.2	0.0	0.3
Quartile 1	0.0	0.1	0.0	0.3	0.0	0.2	0.0	0.4
Median	0.0	0.1	0.0	0.4	0.0	0.2	0.0	0.4
Quartile 3	0.1	0.2	0.0	0.5	0.0	0.2	0.0	0.4
Max	0.5	0.2	0.0	0.5	0.0	0.2	0.0	0.5
Mean	0.1	0.1	0.0	0.4	0.0	0.2	0.0	0.4
Range	0.5	0.1	0.0	0.3	0.0	0.0	0.0	0.2
SD	0.2	0.0	0.0	0.1	0.0	0.0	0.0	0.1
SEM	0.1	0.0	0.0	0.1	0.0	0.0	0.0	0.0

Appendix Table 6)

Mining Hill	Top Half				Bottom Half			
52 V	P1	P2	P3	P4	P1	P2	P3	P4
Minimum	0.2	0.1	1.1	5.6	0.2	0.1	2.1	9.4
Quartile 1	0.2	0.1	1.2	10.1	0.2	0.1	2.2	10.0
Median	0.2	0.1	1.4	12.4	0.3	0.1	2.6	10.1
Quartile 3	0.2	0.1	1.6	13.2	0.3	0.1	2.6	10.1
Max	0.2	0.1	2.0	13.3	0.3	0.2	2.8	10.9
Mean	0.2	0.1	1.5	10.9	0.2	0.1	2.5	10.1
Range	0.1	0.0	0.9	7.7	0.0	0.2	0.7	1.5
SD	0.0	0.0	0.4	3.6	0.0	0.1	0.3	0.5
SEM	0.0	0.0	0.2	1.8	0.0	0.0	0.1	0.2

Appendix Table 7)

Agricultural Field	Above Groundwater				Below Groundwater			
55Mn	P1	P2	P3	P4	P1	P2	P3	P4
Minimum	2.7	19.0	29.3	4.6	3.7	19.0	29.3	4.0
Quartile 1	17.9	23.4	42.1	6.5	3.9	12.1	75.4	14.8
Median	18.9	28.6	60.4	7.9	4.2	12.6	86.6	17.4
Quartile 3	25.1	28.9	63.0	7.9	4.6	17.9	139.4	89.7
Max	55.4	39.9	66.0	8.6	5.1	32.3	279.0	302.6
Mean	24.0	28.0	52.2	7.1	4.3	17.4	128.2	87.1
Range	52.7	20.9	36.7	4.0	1.4	13.4	249.6	298.6
SD	19.4	7.8	15.8	1.6	0.6	10.0	101.4	143.7
SEM	8.7	3.5	7.1	0.7	0.3	5.0	50.7	71.8

Appendix Table 8)

Agricultural Field	Above Groundwater				Below Groundwater			
238U	P1	P2	P3	P4	P1	P2	P3	P4
Minimum	0.0	0.2	0.4	0.3	0.0	0.1	0.3	0.3
Quartile 1	0.0	0.2	0.4	0.4	0.0	0.1	0.3	0.3
Median	0.0	0.2	0.4	0.5	0.0	0.1	0.3	0.3
Quartile 3	0.0	0.2	0.5	0.6	0.0	0.1	0.3	0.3
Max	0.0	0.3	0.5	0.6	0.0	0.2	0.3	0.3
Mean	0.0	0.2	0.4	0.5	0.0	0.1	0.3	0.3
Range	0.0	0.1	0.1	0.3	0.0	0.0	0.1	0.1
SD	0.0	0.0	0.1	0.1	0.0	0.0	0.0	0.0
SEM	0.0	0.0	0.0	0.1	0.0	0.0	0.0	0.0

Appendix Table 9)

Agricultural Field	Above Groundwater				Below Groundwater			
51V	P1	P2	P3	P4	P1	P2	P3	P4
Minimum	0.0	0.0	6.8	8.0	0.0	0.0	3.4	1.8
Quartile 1	0.0	0.0	10.4	8.4	0.0	0.0	3.6	3.5
Median	0.0	0.0	12.6	11.0	0.0	0.0	3.8	4.8
Quartile 3	0.0	0.0	13.8	13.2	0.0	0.0	4.1	5.6
Max	0.1	0.0	14.0	14.0	0.0	0.0	4.6	6.1
Mean	0.0	0.0	11.5	10.9	0.0	0.0	3.9	4.3
Range	0.1	0.0	7.2	6.0	0.0	0.0	1.2	4.3
SD	0.0	0.0	3.0	2.7	0.0	0.0	0.5	1.9
SEM	0.0	0.0	1.3	1.2	0.0	0.0	0.3	0.9

t-Test Comparing Analytes Above and Below Groundwater

Lowland Marsh

Appendix Table 10)

t-Test: Two-Sample Assuming Unequal Variances		
55Mn	P1 above	P1 below
Mean	47.7	33.6
Variance	209.8	38.2
Observations	7	5
Hypothesized Mean Difference	0	
df	9	
t Stat	2.3	
P(T<=t) one-tail	0.0	
t Critical one-tail	1.8	
P(T<=t) two-tail	0.0	
t Critical two-tail	2.3	

Appendix Table 11)

t-Test: Two-Sample Assuming Unequal Variances		
55Mn		
	P2above	P2 below
Mean	83.6	58.2
Variance	1407.8	7079.2
Observations	7	5
Hypothesized Mean Difference	0	
df	5	
t Stat	0.6	
P(T<=t) one-tail	0.3	
t Critical one-tail	2.0	
P(T<=t) two-tail	0.6	
t Critical two-tail	2.6	

Appendix Table 12)

t-Test: Two-Sample Assuming Unequal Variances		
55Mn		
	P3above	P3 below
Mean	366.6	36.4
Variance	24872.9	2526.9
Observations	7	5
Hypothesized Mean Difference	0	
df	8	
t Stat	5.2	
P(T<=t) one-tail	0.0	
t Critical one-tail	1.9	
P(T<=t) two-tail	0.0	
t Critical two-tail	2.3	

Appendix Table 13)

t-Test: Two-Sample Assuming Unequal Variances

55Mn	P4above	P4 below
Mean	162.5	32.1
Variance	7279.3	1541.5
Observations	7	5
Hypothesized Mean Difference	0	
df	9	
t Stat	3.6	
P(T<=t) one-tail	0.0	
t Critical one-tail	1.8	
P(T<=t) two-tail	0.0	
t Critical two-tail	2.3	

Appendix Table 14)

t-Test: Two-Sample Assuming Unequal Variances

238U

	P1 Top	P1 Bot
Mean	0.0	0.6
Variance	0.0	0.1
Observations	6	4
Hypothesized Mean Difference	0	
df	3	
t Stat	-3.3	
P(T<=t) one-tail	0.0	
t Critical one-tail	2.4	
P(T<=t) two-tail	0.0	
t Critical two-tail	3.2	

Appendix Table 15)

t-Test: Two-Sample Assuming Unequal Variances		
238U		
	P2 Top	P2 Bot
Mean	3.3	38.1
Variance	1.8	12.8
Observations	6	4
Hypothesized Mean Difference	0	
df	4	
t Stat	-18.6	
P(T<=t) one-tail	0.0	
t Critical one-tail	2.1	
P(T<=t) two-tail	0.0	
t Critical two-tail	2.8	

Appendix Table 16)

t-Test: Two-Sample Assuming Unequal Variances		
238U		
	P3 Top	P3 Bot
Mean	0.0	0.2
Variance	0.0	0.0
Observations	6	4
Hypothesized Mean Difference	0	
df	3	
t Stat	-4.6	
P(T<=t) one-tail	0.0	
t Critical one-tail	2.4	
P(T<=t) two-tail	0.0	
t Critical two-tail	3.2	

Appendix Table 17)

t-Test: Two-Sample Assuming Unequal Variances		
238U		
	P4 Top	P4 Bot
Mean	8.9	45.8
Variance	13.7	54.6
Observations	6	4
Hypothesized Mean Difference	0	
df	4	
t Stat	-9.3	
P(T<=t) one-tail	0.0	
t Critical one-tail	2.1	
P(T<=t) two-tail	0.0	
t Critical two-tail	2.8	

Appendix Table 18)

t-Test: Two-Sample Assuming Unequal Variances		
51V		
	P1 above	P1 below
Mean	0.1	0.1
Variance	0.0	0.0
Observations	7	5
Hypothesized Mean Difference	0	
df	10	
t Stat	0.7	
P(T<=t) one-tail	0.2	
t Critical one-tail	1.8	
P(T<=t) two-tail	0.5	
t Critical two-tail	2.2	

Appendix Table 19)

51V		
	P2above	P2 below
Mean	0.0	2.3
Variance	0.0	25.0
Observations	7	5
Hypothesized Mean Difference	0	
df	4	
t Stat	-1.0	
P(T<=t) one-tail	0.2	
t Critical one-tail	2.1	
P(T<=t) two-tail	0.4	
t Critical two-tail	2.8	

Appendix Table 20)

t-Test: Two-Sample Assuming Unequal Variances		
51V		
	P3above	P3 below
Mean	2.1	1.3
Variance	0.1	0.1
Observations	7	5
Hypothesized Mean Difference	0	
df	9	
t Stat	3.8	
P(T<=t) one-tail	0.0	
t Critical one-tail	1.8	
P(T<=t) two-tail	0.0	
t Critical two-tail	2.3	

Appendix Table 21)

t-Test: Two-Sample Assuming Unequal Variances		
51V		
	P4above	P4 below
Mean	15.8	11.8
Variance	15.7	19.5
Observations	7	5
Hypothesized Mean Difference	0	
df	8	
t Stat	1.6	
P(T<=t) one-tail	0.1	
t Critical one-tail	1.9	
P(T<=t) two-tail	0.1	
t Critical two-tail	2.3	

Lowland Marsh Contrasted with Agricultural Field

Appendix Table 22)

t-Test: Two-Sample Assuming Unequal Variances		
55 Mn		
	P1 above	P1 above
Mean	41.8	15.2
Variance	180.9	295.5
Observations	12	9
Hypothesized Mean Difference	0	
df	15	
t Stat	3.8	
P(T<=t) one-tail	0.0	
t Critical one-tail	1.8	
P(T<=t) two-tail	0.0	
t Critical two-tail	2.1	

Appendix Table 23)

t-Test: Two-Sample Assuming Unequal Variances		
55 Mn		
	P2	P2
Mean	73.0	23.2
Variance	3513.7	99.3
Observations	12	9
Hypothesized Mean Difference	0	
df	12	
t Stat	2.9	
P(T<=t) one-tail	0.0	
t Critical one-tail	1.8	
P(T<=t) two-tail	0.0	
t Critical two-tail	2.2	

Appendix Table 24)

t-Test: Two-Sample Assuming Unequal Variances		
55 Mn		
	P3	P3
Mean	229.0	86.0
Variance	43393.2	5584.0
Observations	12	9
Hypothesized Mean Difference	0	
df	15	
t Stat	2.2	
P(T<=t) one-tail	0.0	
t Critical one-tail	1.8	
P(T<=t) two-tail	0.0	
t Critical two-tail	2.1	

Appendix Table 25)

t-Test: Two-Sample Assuming Unequal Variances		
55 Mn		
	P4	P4
Mean	108.2	42.7
Variance	9038.5	9521.1
Observations	12	9
Hypothesized Mean Difference	0	
df	17	
t Stat	1.5	
P(T<=t) one-tail	0.1	
t Critical one-tail	1.7	
P(T<=t) two-tail	0.1	
t Critical two-tail	2.1	

Appendix Table 26)

t-Test: Two-Sample Assuming Unequal Variances		
238 U		
	P1 above	P1 above
Mean	0.2	0.0
Variance	0.1	0.0
Observations	12	9
Hypothesized Mean Difference	0	
df	11	
t Stat	2.2	
P(T<=t) one-tail	0.0	
t Critical one-tail	1.8	
P(T<=t) two-tail	0.0	
t Critical two-tail	2.2	

Appendix Table 27)

t-Test: Two-Sample Assuming Unequal Variances		
238 U		
	P2above	P2above
Mean	15.6	0.2
Variance	290.2	0.0
Observations	12	9
Hypothesized Mean Difference	0	
df	11	
t Stat	3.1	
P(T<=t) one-tail	0.0	
t Critical one-tail	1.8	
P(T<=t) two-tail	0.0	
t Critical two-tail	2.2	

Appendix Table 28)

t-Test: Two-Sample Assuming Unequal Variances		
238 U		
	P3above	P3above
Mean	0.1	0.4
Variance	0.0	0.0
Observations	12	9
Hypothesized Mean Difference	0	
df	19	
t Stat	-8.0	
P(T<=t) one-tail	0.0	
t Critical one-tail	1.7	
P(T<=t) two-tail	0.0	
t Critical two-tail	2.1	

Appendix Table 29)

t-Test: Two-Sample Assuming Unequal Variances		
238 U		
	P4above	P4above
Mean	22.1	0.4
Variance	364.6	0.0
Observations	12	9
Hypothesized Mean Difference	0	
df	11	
t Stat	3.9	
P(T<=t) one-tail	0.0	
t Critical one-tail	1.8	
P(T<=t) two-tail	0.0	
t Critical two-tail	2.2	

Appendix Table 30)

t-Test: Two-Sample Assuming Unequal Variances		
52 V		
	P1 above	P1 above
Mean	0.1	0.0
Variance	0.0	0.0
Observations	12	9
Hypothesized Mean Difference	0	
df	16	
t Stat	13.5	
P(T<=t) one-tail	0.0	
t Critical one-tail	1.7	
P(T<=t) two-tail	0.0	
t Critical two-tail	2.1	

Appendix Table 31)

t-Test: Two-Sample Assuming Unequal Variances		
52 V		
	P2above	P2above
Mean	1.0	0.0
Variance	10.4	0.0
Observations	12	9
Hypothesized Mean Difference	0	
df	11	
t Stat	1.0	
P(T<=t) one-tail	0.2	
t Critical one-tail	1.8	
P(T<=t) two-tail	0.3	
t Critical two-tail	2.2	

Appendix Table 32)

t-Test: Two-Sample Assuming Unequal Variances		
52 V		
	P3above	P3above
Mean	1.8	8.1
Variance	0.3	20.7
Observations	12	9
Hypothesized Mean Difference	0	
df	8	
t Stat	-4.1	
P(T<=t) one-tail	0.0	
t Critical one-tail	1.9	
P(T<=t) two-tail	0.0	
t Critical two-tail	2.3	

Appendix Table 33)

t-Test: Two-Sample Assuming Unequal Variances		
52 V		
	P4above	P4above
Mean	14.2	8.0
Variance	19.9	17.0
Observations	12	9
Hypothesized Mean Difference	0	
df	18	
t Stat	3.3	
P(T<=t) one-tail	0.0	
t Critical one-tail	1.7	
P(T<=t) two-tail	0.0	
t Critical two-tail	2.1	

Works by Kenneth Hamilton II

Hamilton, KM*; Wilson, ME*; Grant, KE*; Aleto, DM*; Quicksall, AN**.** Groundwater Lead and Nitrate Mapping for Origination and Risk Assessment in Kutupalong, Bangladesh. *Water Research. (Under Review*).

Hamilton, KH*; Quicksall, AN. Inherent Toxicity Through Dispersion of Sized Determined Dust Particles in Bugesera, Rwanda.

Hamilton, KH*; Quicksall, AN. Spatial Resolution and Origination of Toxic elements in the Soil-Water Partitioning of Subsurface Bugesera (Working).

Bayan, MA*; Hamilton, KM*; Quicksall, AN. Lab Scale Assessment of Biological Filtration for Removal of Microconstituents in Drinking Water. *ACS 2014.*

Hamilton, KM*; Wilson, ME*; Aleto, DM*; Grant, KE*; Quicksall, AN. Mapping of Contaminants in Developing World Aquifers for Origination and Risk Assessment. *OU Water Conference 2015*

BIBLIOGRAPHY

Al-Mur, B.A., Quicksall, A.N., Al-Ansari, A.M.A., 2017. Spatial and temporal distribution of heavy metals in coastal core sediments from the Red Sea, Saudi Arabia. Oceanologia. https://doi.org/10.1016/j.oceano.2017.03.003

Bajwa, B.S., Kumar, S., Singh, S., Sahoo, S.K., Tripathi, R.M., 2017. Uranium and other heavy toxic elements distribution in the drinking water samples of SW-Punjab, India. J. Radiat. Res. Appl. Sci. https://doi.org/10.1016/j.jrras.2015.01.002

Bredberg, K., Karlsson, H.T., Holst, O., 2004. Reduction of vanadium(V) with Acidithiobacillus ferrooxidans and Acidithiobacillus thiooxidans. Bioresour. Technol. https://doi.org/10.1016/j.biortech.2003.08.004

Brettar, I., Sanchez-Perez, J.M., Trémolières, M., 2002. Nitrate elimination by denitrification in hardwood forest soils of the Upper Rhine floodplain - Correlation with redox potential and organic matter. Hydrobiologia 469, 11–21. https://doi.org/10.1023/A:1015527611350

Carpi, A., 1997. Mercury from combustion sources: A review of the chemical species emitted and their transport in the atmosphere. Water. Air. Soil Pollut. https://doi.org/10.1007/BF02047037

Carter, R.C., Tyrrel, S.F., Howsam, P., 1996. Strategies for handpump water supply programmes in less-developed countries. Water Environ. J. 10, 130–136. https://doi.org/10.1111/j.1747-6593.1996.tb00022.x

Chen, Z.S., Lee, G.J., Liu, J.C., 2000. The effects of chemical remediation treatments on the extractability and speciation of cadmium and lead in contaminated soils. Chemosphere 41,

235–242. https://doi.org/10.1016/S0045-6535(99)00416-6

Crossgrove, J., Zheng, W., 2004. Manganese toxicity upon overexposure. NMR Biomed. https://doi.org/10.1002/nbm.931

Das, B., Hazarika, P., Saikia, G., Kalita, H., Goswami, D.C., Das, H.B., Dube, S.N., Dutta, R.K., 2007. Removal of iron from groundwater by ash: A systematic study of a traditional method. J. Hazard. Mater. 141, 834–841. https://doi.org/10.1016/j.jhazmat.2006.07.052

Dewaele, S., De Clercq, F., Muchez, P., Schneider, J., Burgess, R., Boyce, A., Fernandez Alonso, M., 2010. Geology of the cassiterite mineralisation in the Rutongo area, Rwanda (Central Africa): Current state of knowledge. Geol. Belgica.

Domingo, J.L., 2001. Reproductive and developmental toxicity of natural and depleted uranium: A review. Reprod. Toxicol. https://doi.org/10.1016/S0890-6238(01)00181-2

Dong, D., Derry, L.A., Lion, L.W., 2003. Pb scavenging from a freshwater lake by Mn oxides in heterogeneous surface coating materials. Water Res. 37, 1662–1666.

Drever, J.I., 2002. The Geochemistry of Natural Waters, Third. ed. Prentice Hall, Upper saddle River.

Fan, A.M., Willhite, C.C., Book, S.A., 1987. Evaluation of the nitrate drinking water standard with reference to infant methemoglobinemia and potential reproductive toxicity. Regul. Toxicol. Pharmacol. 7, 135–148. https://doi.org/10.1016/0273-2300(87)90024-9

Flora, G., Gupta, D., Tiwari, A., 2012. Toxicity of lead: A review with recent updates. Interdiscip. Toxicol. https://doi.org/10.2478/v10102-012-0009-2

Frisbie, S.H., Mitchell, E.J., Dustin, H., Maynard, D.M., Sarkar, B., 2012. World health

organization discontinues its drinking-water guideline for manganese. Environ. Health Perspect. https://doi.org/10.1289/ehp.1104693

Gadde, R.R., Laitinen, H.A., 1974. Heavy metal adsorption by hydrous iron and manganese oxides. Anal. Chem. 46, 2022–2026. https://doi.org/10.1021/ac60349a004

Ghehi, N.G., Nemes, A., Verdoodt, A., Van Ranst, E., Cornelis, W.M., Boeckx, P., 2012. Nonparametric Techniques for Predicting Soil Bulk Density of Tropical Rainforest Topsoils in Rwanda. Soil Sci. Soc. Am. J. https://doi.org/10.2136/sssaj2011.0330

Gidlow, D.A., 2004. Lead toxicity. Occup. Med. (Lond). 65, 348–56. https://doi.org/10.1093/occmed/kqv018

Guagliardi, I., Cicchella, D., De Rosa, R., Ricca, N., Buttafuoco, G., 2018. Geochemical sources of vanadium in soils: Evidences in a southern Italy area. J. Geochemical Explor. https://doi.org/10.1016/j.gexplo.2016.11.017

Hakanson, L., 1980. An ecological risk index for aquatic pollution control.a sedimentological approach. Water Res. https://doi.org/10.1016/0043-1354(80)90143-8

Hamilton-Taylor, J., Giusti, L., Davison, W., Tych, W., Hewitt, C.N., 1997. Sorption of trace metals (Cu, Pb, Zn) by suspended lake particles in artificial (0.005 M NaNO3) and natural (Esthwaite Water) freshwaters. Colloids Surfaces A Physicochem. Eng. Asp. https://doi.org/10.1016/S0927-7757(96)03722-3

Heiri, O., Lotter, A.F., Lemcke, G., 2001. Loss on ignition as a method for estimating organic and carbonate content in sediments: Reproducibility and comparability of results. J. Paleolimnol. https://doi.org/10.1023/A:1008119611481

HEM, J., 1972. Chemical Factors that Influence the Availability of Iron and Manganese in Aqueous Systems. Geol. Soc. Am. Bull. 83, 443–450. https://doi.org/10.1130/0016-7606(1972)83[443:cftita]2.0.co;2

Herndon, E.M., Havig, J.R., Singer, D.M., McCormick, M.L., Kump, L.R., 2018. Manganese and iron geochemistry in sediments underlying the redox-stratified Fayetteville Green Lake. Geochim. Cosmochim. Acta. https://doi.org/10.1016/j.gca.2018.04.013

Hosoi, M., Sharhan, D. Al, 2018. Operational Update Bangladesh.

Huang, J.H., Huang, F., Evans, L., Glasauer, S., 2015. Vanadium: Global (bio)geochemistry. Chem. Geol. https://doi.org/10.1016/j.chemgeo.2015.09.019

Huerta-Diaz, M.A., Tessier, A., Carignan, R., 1998. Geochemistry of trace metals associated with reduced sulfur in freshwater sediments. Appl. Geochemistry 13, 213–233. https://doi.org/10.1016/S0883-2927(97)00060-7

Imtiaz, M., Rizwan, M.S., Xiong, S., Li, H., Ashraf, M., Shahzad, S.M., Shahzad, M., Rizwan, M., Tu, S., 2015. Vanadium, recent advancements and research prospects: A review. Environ. Int. https://doi.org/10.1016/j.envint.2015.03.018

Jean, G.E., Bancroft, G.M., 1986. Heavy metal adsorption by sulphide mineral surfaces. Geochim. Cosmochim. Acta 50, 1455–1463. https://doi.org/10.1016/0016-7037(86)90319-4

Jiang, X., Lu, W.X., Zhao, H.Q., Yang, Q.C., Yang, Z.P., 2014. Potential ecological risk assessment and prediction of soil heavy-metal pollution around coal gangue dump. Nat. Hazards Earth Syst. Sci. https://doi.org/10.5194/nhess-14-1599-2014

Kim, C.S., Wilson, K.M., Rytuba, J.J., 2011. Particle-size dependence on metal(loid)

distributions in mine wastes: Implications for water contamination and human exposure. Appl. Geochemistry. https://doi.org/10.1016/j.apgeochem.2011.01.007

Kim, K., Byun, Y.H., Lee, D., Park, N., 2019. Understanding the global status of particulate matter with respect to research topics and research networks. Sustain. https://doi.org/10.3390/su11205594

Kurttio, P., Komulainen, H., Leino, A., Salonen, L., Auvinen, A., Saha, H., 2005. Bone as a possible target of chemical toxicity of natural uranium in drinking water. Environ. Health Perspect. https://doi.org/10.1289/ehp.7475

Lanphear, B.P., Hornung, R., Khoury, J., Yolton, K., Baghurst, P., Bellinger, D.C., Canfield, R.L., Dietrich, K.N., Bornschein, R., Greene, T., Rothenberg, S.J., Needleman, H.L., Schnaas, L., Wasserman, G., Graziano, J., Roberts, R., 2005. Low-level environmental lead exposure and children's intellectual function: An international pooled analysis. Environ. Health Perspect. https://doi.org/10.1289/ehp.7688

Larsen, F.J., Schiffer, T.A., Borniquel, S., Sahlin, K., Ekblom, B., Lundberg, J.O., Weitzberg, E., 2011. Dietary inorganic nitrate improves mitochondrial efficiency in humans. Cell Metab. https://doi.org/10.1016/j.cmet.2011.01.004

Mason, L.H., Harp, J.P., Han, D.Y., 2014. Pb neurotoxicity: Neuropsychological effects of lead toxicity. Biomed Res. Int. https://doi.org/10.1155/2014/840547

McBride, M., Sauvé, S., Hendershot, W., 1997. Solubility control of Cu, Zn, Cd and Pb in contaminated soils. Eur. J. Soil Sci. https://doi.org/10.1111/j.1365-2389.1997.tb00554.x

McCasland, M. (Cornell U., 1985. Nitrate: Health Effects in Drinking Water. Cornell Coop. Ext.

https://doi.org/10.1016/j.bmc.2010.05.076

McKenzie, R.M., 1980. The adsorption of lead and other heavy metals on oxides of manganese and iron. Aust. J. Soil Res. 18, 61–73. https://doi.org/10.1071/SR9800061

McKenzie, R.M., 1978. The effect of two manganese dioxides on the uptake of lead, cobalt, nickel, copper and zinc by subterranean clover. Aust. J. Soil Res. 16, 209–214. https://doi.org/10.1071/SR9780209

Methods of Soil Analysis Part 3—Chemical Methods, 1996. https://doi.org/10.2136/sssabookser5.3

Morse, J.W., Luther, G.W., 1999. Chemical influences on trace metal-sulfide interactions in anoxic sediments. Geochim. Cosmochim. Acta 63, 3373–3378. https://doi.org/10.1016/S0016-7037(99)00258-6

Naidu, R., Sumner, M.E., Harter, R.D., 1998. Sorption of heavy metals in strongly weathered soils: An overview. Environ. Geochem. Health. https://doi.org/10.1023/A:1006519009465

National Toxicology Program, D. of H. and H.S., 2011. Report on Carcinogens, Twelfth Edition (2011) - Formaldehyde. Rep. Carcinog.

Needleman, H.L., Bellinger, D., 1991. The health effects of low level exposure to lead. Annu. Rev. Public Health. https://doi.org/10.1146/annurev.pu.02.050181.001425

Nnaji, C.C., Emefu, S.C., 2017. Effect of particle size on the sorption of lead from water by different species of sawdust: Equilibrium and kinetic study. BioResources. https://doi.org/10.15376/biores.12.2.4123-4145

Nriagu, J.O., 1992. Toxic metal pollution in Africa. Sci. Total Environ.

https://doi.org/10.1016/0048-9697(92)90304-B

O'Reilly, S.E., Hochella, M.F., 2003. Lead sorption efficiencies of natural and synthetic Mn and Fe-oxides. Geochim. Cosmochim. Acta 67, 4471–4487. https://doi.org/10.1016/S0016-7037(03)00413-7

Pourret, O., Dia, A., Gruau, G., Davranche, M., Bouhnik-Le Coz, M., 2012. Assessment of vanadium distribution in shallow groundwaters. Chem. Geol. https://doi.org/10.1016/j.chemgeo.2011.11.033

Rabee, A.M., Al-Fatlawy, Y.F., Abd, A.-A.-H.N., Nameer, M., 2011. Using Pollution Load Index (PLI) and Geoaccumulation Index (I-Geo) for the Assessment of Heavy Metals Pollution in Tigris River Sediment in Baghdad Region. J. Al-Nahrain Univ. Sci. https://doi.org/10.22401/jnus.14.4.14

Redmon, J.H., Gibson, J.M.D., Woodward, K.P., Aceituno, A.M., Levine, K.E., 2018. Safeguarding Children's Health: Time to Enact a Health-Based Standard and Comprehensive Testing, Mitigation, and Communication Protocol for Lead in Drinking Water. N. C. Med. J. https://doi.org/10.18043/ncm.79.5.313

Reed, S., Martens, D., 1996. Methods of Soil Analysis Part 3—Chemical Methods. Methods Soil Anal. Part 3—Chemical Methods. https://doi.org/10.2136/sssabookser5.3.frontmatter

Rehman, K., Fatima, F., Waheed, I., Akash, M.S.H., 2018. Prevalence of exposure of heavy metals and their impact on health consequences. J. Cell. Biochem. https://doi.org/10.1002/jcb.26234

Reijonen, I., Metzler, M., Hartikainen, H., 2016. Impact of soil pH and organic matter on the

chemical bioavailability of vanadium species: The underlying basis for risk assessment. Environ. Pollut. https://doi.org/10.1016/j.envpol.2015.12.046

Rieuwerts, J.S., 2007. The mobility and bioavailability of trace metals in tropical soils: A review. Chem. Speciat. Bioavailab. https://doi.org/10.3184/095422907X211918

Roy, S., Edwards, M.A., 2019. Preventing another lead (Pb) in drinking water crisis: Lessons from the Washington D.C. and Flint MI contamination events. Curr. Opin. Environ. Sci. Heal. https://doi.org/10.1016/j.coesh.2018.10.002

Roychoudhury, A.N., Starke, M.F., 2006. Partitioning and mobility of trace metals in the Blesbokspruit: Impact assessment of dewatering of mine waters in the East Rand, South Africa. Appl. Geochemistry. https://doi.org/10.1016/j.apgeochem.2006.02.024

Rwanyiziri, G., Rugema, J., 2013. Climate Change Effects on Food Security in Rwanda: Case Study of Wetland Rice Production in Bugesera District. Rwanda J. https://doi.org/10.4314/rj.v1i1.

Salazar, G.J.P., Alfaro-De la Torre, M.C., Aguirre, R.N.J., Briones-Gallardo, R., Cedeño, C.J., Peñuela, M.G.A., 2013. Geochemical fractionation of manganese in the Riogrande II reservoir, Antioquia, Colombia. Environ. Earth Sci. 69, 197–208. https://doi.org/10.1007/s12665-012-1947-x

Santamaria, A.B., Sulsky, S.I., 2010. Risk assessment of an essential element: Manganese, in: Journal of Toxicology and Environmental Health - Part A: Current Issues. https://doi.org/10.1080/15287390903337118

Sauvé, S., Hendershot, W., Allen, H.E., 2000. Solid-solution partitioning of metals in

contaminated soils: Dependence on pH, total metal burden, and organic matter. Environ. Sci. Technol. https://doi.org/10.1021/es9907764

Schijf, J., Zoll, A.M., 2011. When dissolved is not truly dissolved-The importance of colloids in studies of metal sorption on organic matter. J. Colloid Interface Sci. https://doi.org/10.1016/j.jcis.2011.05.029

Schroth, A.W., Bostick, B.C., Kaste, J.M., Friedland, A.J., 2008. Lead sequestration and species redistribution during soil organic matter decomposition. Environ. Sci. Technol. 42, 3627–3633. https://doi.org/10.1021/es703002b

Selvakumar, R., Ramadoss, G., Mridula, P.M., Rajendran, K., Thavamani, P., Ravi Naidu, Megharaj, M., 2018. Challenges and complexities in remediation of uranium contaminated soils: A review. J. Environ. Radioact. https://doi.org/10.1016/j.jenvrad.2018.02.018

Shuang Wang1 & Yonghong Ran1 & Binghui Lu1 & Juan Li1 & Hongrong Kuang2 & Li Gong2 & Yuhui Hao, 2019. A Review of Uranium-Induced Reproductive Toxicity. Biol. Trace Elem. Res.

Silbergeld, E.K., 2003. Facilitative mechanisms of lead as a carcinogen. Mutat. Res. - Fundam. Mol. Mech. Mutagen. https://doi.org/10.1016/j.mrfmmm.2003.07.010

Slikker, W., Wang, C., Paule, M.G., 2018. Handbook of developmental neurotoxicology, Handbook of Developmental Neurotoxicology. https://doi.org/10.1016/C2015-0-04830-4

Stamatis Kalogirou & Christos Chalkias, 2014. Mapping environmental risks: Quantitative and spatial modeling approaches. J. Maps 10, 183–185.

Steenland, K., Boffetta, P., 2000. Lead and cancer in humans: Where are we now?, in: American

Journal of Industrial Medicine. pp. 295–299. https://doi.org/10.1002/1097-0274(200009)38:3<295::AID-AJIM8>3.0.CO;2-L

Szalińska, E., Orlińska-Woźniak, P., Wilk, P., 2018. Nitrate vulnerable zones revision in Poland-assessment of environmental impact and land use conflicts. Sustain. https://doi.org/10.3390/su10093297

Takeda, A., 2003. Manganese action in brain function. Brain Res. Rev. https://doi.org/10.1016/S0165-0173(02)00234-5

Tessier, A., Campbell, P.G.C., Bisson, M., 1979. Sequential Extraction Procedure for the Speciation of Particulate Trace Metals. Anal. Chem. https://doi.org/10.1021/ac50043a017

Tomlinson, D.L., Wilson, J.G., Harris, C.R., Jeffrey, D.W., 1980. Problems in the assessment of heavy-metal levels in estuaries and the formation of a pollution index. Helgoländer Meeresuntersuchungen. https://doi.org/10.1007/BF02414780

Trueman, B.F., Gregory, B.S., McCormick, N.E., Gao, Y., Gora, S., Anaviapik-Soucie, T., L'Hérault, V., Gagnon, G.A., 2019. Manganese Increases Lead Release to Drinking Water. Environ. Sci. Technol. https://doi.org/10.1021/acs.est.9b00317

Turekian, K.K., Wedepohl, K.H., 1961. Distribution of the elements in some major units of the earth's crust. Bull. Geol. Soc. Am. https://doi.org/10.1130/0016-7606(1961)72[175:DOTEIS]2.0.CO;2

Venkataraman, B. V, Sudha, S., 2005. Vanadium Toxicity. Asian J. Exp. Sci.

Villalobos, M., Bargar, J., Sposito, G., 2005. Mechanisms of Pb(II) sorption on a biogenic manganese oxide. Environ. Sci. Technol. 39, 569–576. https://doi.org/10.1021/es049434a

Wakida, F.T., Lerner, D.N., 2005. Non-agricultural sources of groundwater nitrate: A review and case study. Water Res. https://doi.org/10.1016/j.watres.2004.07.026

Walter E. Dean, Jr., 1974. Determination of Carbonate and Organic Matter in Calcareous Sediments and Sedimentary Rocks by Loss on Ignition: Comparison With Other Methods. SEPM J. Sediment. Res. https://doi.org/10.1306/74D729D2-2B21-11D7-8648000102C1865D

Waskom, J.R.S. and R.M., 1991. Nitrates in drinking water: Fact Sheet No. 0.517, Gigiena i sanitariia.

Wen, L.S., Santschi, P.H., Tang, D., 1997. Interactions between radioactively labeled colloids and natural particles: Evidence for colloidal pumping. Geochim. Cosmochim. Acta. https://doi.org/10.1016/S0016-7037(97)00139-7

Weng, L., Temminghoff, E.J.M., Lofts, S., Tipping, E., Van Riemsdijk, W.H., 2002. Complexation with dissolved organic matter and solubility control of heavy metals in a sandy soil. Environ. Sci. Technol. https://doi.org/10.1021/es0200084

Winde, F., Brugge, D., Nidecker, A., Ruegg, U., 2017. Uranium from Africa – An overview on past and current mining activities: Re-appraising associated risks and chances in a global context. J. African Earth Sci. https://doi.org/10.1016/j.jafrearsci.2016.12.004

World Health Organisation, 2017. ROHINGYA REFUGEE CRISIS. Humanit. response plan Sept. 2017 – Febr. 2018.

World Health Organization, 2011. Manganese in Drinking-water [WWW Document]. Manganese Drink. Backgr. Doc. Dev. WHO Guidel. Drink. water Qual.

Wright, R.O., Lewander, W.J., Woolf, A.D., 1999. Methemoglobinemia: Etiology, pharmacology, and clinical management. Ann. Emerg. Med. https://doi.org/10.1016/S0196-0644(99)70167-8

Zavodska, L., Kosorinova, E., Scerbakova, L., Lesny, J., 2008. Environmental chemistry of uranium. Hungarian Electron. J. Sci. - Environ. Eng. Sect. https://doi.org/HU ISSN 1418-7108: HEJ Manuscript no: ENV-081221-A

Zhu, H.N., Yuan, X.Z., Zeng, G.M., Jiang, M., Liang, J., Zhang, C., Yin, J., Huang, H.J., Liu, Z.F., Jiang, H.W., 2012. Ecological risk assessment of heavy metals in sediments of Xiawan Port based on modified potential ecological risk index. Trans. Nonferrous Met. Soc. China (English Ed. https://doi.org/10.1016/S1003-6326(11)61343-5